

Molecular characterization of pathogen-triggered cell polarity

Inaugural-Dissertation
zur
Erlangung des Doktorgrades
der Mathematisch-Naturwissenschaftlichen Fakultät
der Universität zu Köln

vorgelegt von
Dorit Meyer
aus Emsdetten

Köln, April 2008

Die vorliegende Arbeit wurde am Max-Planck-Institut für Züchtungsforschung in Köln in der Abteilung für Molekulare Phytopathologie (Direktor: Prof. Dr. P. Schulze-Lefert) angefertigt.

Berichtersteller:

Prof. Dr. Paul Schulze-Lefert

Prof. Dr. Martin Hülskamp

Prüfungsvorsitzender: Prof. Dr. Ulf-Ingo Flügge

Prüfungstermin am 23. Juni 2008



MAX-PLANCK-GESELLSCHAFT



Max-Planck-Institut für
Züchtungsforschung

I Table of contents

I Table of contents	I
II Abbreviations	III
III Summary	VI
IV Zusammenfassung	VIII
1 Introduction	1
1.1 Pathogen associated molecular pattern (PAMP) triggered immunity	2
1.2 Resistance gene-mediated immunity or effector triggered immunity	4
1.3 Pathogen induced cell polarity is a common phenomenon in plant defence	5
1.4 SNARE proteins mediate vesicle traffic	6
1.5 SNARE proteins establish effective barriers against fungal ingress at the cell periphery	8
1.6 Papilla formation often correlates with failure of fungal ingress	10
1.7 Development of haustorial complexes and deposition of callose at haustorial complexes	12
1.8 Exocytosis in plants	14
1.9 Aim of the thesis	16
2 Material and Methods	17
2.1 Material	17
2.1.1 Plant Material	17
2.1.2 Plant Pathogens	18
2.1.3 Antibodies	19
2.1.4 Chemicals and reagents	19
2.1.5 Media	20
2.1.6 Buffer and Solutions	20
2.1.7 Microscopic Equipment	22
2.1.8 Software	23
2.2 Methods	24
2.2.1 Plant cultivation	24
2.2.2 Generation of Arabidopsis F ₁ and F ₂ progeny	24
2.2.3 Inoculation procedures	25
2.2.4 Staining procedures for co-localization studies	27
2.2.5 Assessing host entry rates	27
2.2.6 Quantification of haustorial encasements	28
2.2.7 Isolation of haustorial complexes	28
2.2.8 Fixing and embedding of haustoria for Immunocytochemistry	29
2.2.9 Poly-L Lysine coating of Multiwell Microscope Slides	30
2.2.10 Assembling of ultrathin sections	30
2.2.11 Immunofluorescence labeling of sections	31
2.2.12 EMS-Mutagenesis of <i>Arabidopsis</i> seeds	31
2.2.13 Confocal Laser scanning microscopy	32
2.2.14 Confocal high throughput imaging	32
2.2.15 Preparation of leaves for high throughput screening	32

Table of Contents

2. 2. 16 Processing of high throughput images.....	33
2. 2. 17 Image processing and automated analysis.....	35
3. Results.....	39
3.1 Specificity of GFP-PEN1 focal accumulation.....	39
3. 1. 1 Association of GFP-PEN1 focal accumulation with attempted host cell entry by adapted and non-adapted direct penetrating fungi.....	39
3. 1. 2 GFP fluorescence in papillae of GFP-PEN1 plants remains stable over time.....	45
3. 1. 3 The GFP-signal spatially coincides with the location of callose at haustorial structures.....	48
3. 1. 4 Haustoria become encased by structures containing GFP-PEN1 and membrane material.....	52
3. 1. 5 The haustorial encasement preferentially contains t-SNAREs.....	55
3. 1. 6 Deposition of callose into haustorial encasements depends on PMR4 (GSL5) callose synthase, but is independent of PEN1 syntaxin.....	61
3. 1. 7 Time-course study of haustorial encasements.....	64
3. 2 Screening a chemically mutagenised plant population for mutants with altered GFP-PEN1 focal accumulation.....	67
3. 2. 1 Chemical mutagenesis of an <i>Arabidopsis</i> line expressing GFP-PEN1.....	67
3.2.2 Evaluation of the efficiency of mutagenesis.....	67
3. 2. 3. Manual screen for mutants showing an aberrant GFP-PEN1 focal accumulation phenotype.....	67
3. 2. 4 Development of a fully automated confocal high-throughput imaging method to image living plant tissue at sub-cellular resolution.....	71
3. 2. 6 A fully automated screen for mutants showing aberrant GFP-PEN1 focal accumulation at <i>B. g. hordei</i> entry sites.....	78
3. 2. 7 Validation of candidate mutants identified in the manual screen in the M ₃ generation.....	85
4. Discussion.....	91
4. 1 PEN1 focal accumulation might be suppressed by adapted powdery mildews.....	91
4. 2 GFP-PEN1 FA is located inside papillae.....	94
4. 3 Mature haustorial complexes contain GFP-PEN1 and membranous material.....	97
4. 4 Haustorial complexes preferentially contain t-SNAREs.....	101
4. 5 Development of a high-throughput screening method for living plant tissue.....	103
4. 6 Multiparametric analysis of the GFP-PEN1 focal accumulation.....	104
4. 7 A number of juvenile lethal mutants were identified.....	105
4. 8 The <i>dfa1</i> mutant shows an altered GFP-PEN1 focal accumulation pattern.....	106
5. Supplementary data.....	108
6 References.....	111
V Acknowledgements.....	121
VI Erklärung.....	123

VII Curriculum Vitae..... 125

II Abbreviations

% (v/v)	volume percent
% (w/v)	weight/volume percent
μ	micro
aa	amino acid
APC	antigen presenting cell
ATP	adenosine triphosphate
<i>Avr</i>	avirulence gene
<i>A. thaliana</i>	<i>Arabidopsis thaliana</i>
Arabidopsis	<i>Arabidopsis thaliana</i>
°C	degrees Celsius
Ca ²⁺	calcium ions
CFP	cyan fluorescent protein
cDNA	copy DNA
Col-0	<i>Arabidopsis thaliana</i> ecotype Columbia-0
C-terminus	carboxy terminus
dH ₂ O	de-ionized water
DMSO	dimethyl sulfoxide
DNA	desoxy ribonucleic acid
dpi	days post inoculation
EHM	extrahaustorial membrane
EMS	ethyl methane sulfonate, or methane sulfonic acid ethyl ester
ER	endoplasmic reticulum
ET	ethylene
FA	focal accumulation
flg22	22 amino acid peptide of flagellin
FRET	Förster resonance energy transfer
f sp	forma specialis

g	gram
GFP	green fluorescent protein
h	hour
hpi	hours post inoculation
HR	hypersensitive response
<i>Hv</i>	<i>Hordeum vulgare</i>
JA	jasmonic acid
K	kilo
Kb	kilo base
kD	kilo Dalton
l	liter
LRR	leucine-rich repeat
m	milli
M	molar (mol/l)
min	minutes
<i>MLO</i>	mildew resistance locus o
MVB	multi vesicular body
mRNA	messenger RNA
mYFP	monomeric yellow fluorescent protein
n	nano
NASC	Nottingham <i>Arabidopsis</i> Stock Center
NBS	nucleotide binding site
nm	nano meter
NSF	<i>N</i> -ethylmaleimide sensitive factor
N-terminus	amino terminus
<i>P</i>	probability value
p35S	promoter of Cauliflower mosaic virus promoter 35S
PAMP	pathogen associated molecular pattern
pH	negative logarithm of proton concentration

Abbreviations

PRR	PAMP recognition receptor
PBS	phosphate buffered saline
<i>PEN1</i>	penetration 1
PM	plasma membrane
pPEN1	promoter of PEN1
R	resistance
RLK	receptor like kinase
<i>ROR2</i>	required for <i>mlo</i> base resistance
rpm	rounds per minute
s	seconds
SA	salicylic acid
α -SNAP	soluble NSF attachment protein
SNAP25	synaptosomal protein of 25kD
SNAP33	synaptosomal protein of 33kD
SNARE	soluble NSF attachment protein receptor
SM	Sec/Munc
<i>SYP</i>	syntaxin of plants
TCR	T-cell receptor
TLR	Toll like receptor
TTSS	type III secretion system
t-test	statistical hypothesis test by Student (1908)
v	volume
VAMP	vesicle associated membrane protein
w	weight
wt	wild type

III Summary

Cell polarity is a common response of single plant cells in response to bacterial or fungal attack, typically leading to a polar rearrangement of the cytoskeleton and directional movement of various organelles such as the nucleus and Golgi to pathogen contact sites at the cell surface. This process is accompanied by a re-localisation of a subset of proteins and directed vesicle trafficking that might contribute to focal deposition of *de novo* synthesized cell wall material (called papilla) between the preformed plant cell wall and the plasma membrane underneath pathogen contact sites. Secretory processes involving vesicles that release antimicrobial cargo and cell wall building blocks have been thought for a long time to contribute to plant defence. Recently, genetic evidence proved ‘soluble *N*-ethylmaleimide sensitive factor attachment protein receptors’ (SNARE) proteins, which are known to drive intracellular vesicle fusions in various eukaryotes, to be required for resistance responses. A ternary SNARE complex containing plasma membrane-resident PEN1 syntaxin, SNAP33 and endomembrane resident VAMP721/722 is essential to restrict entry of several tested powdery mildew fungi into leaf epidermal sites. Focal accumulation of each of these three proteins at incipient fungal entry sites implies the existence of a secretory machinery that targets and discharges vesicle-resident antimicrobial cargo towards the fungal intruder into the extracellular space. However, the exact mechanism underlying focal SNARE protein accumulation at incipient entry sites remains elusive. In addition, it remains to be shown whether SNARE proteins must be concentrated at these sites to confer effective disease resistance.

To reveal the specificity of focal PEN1 accumulation at the cell periphery diverse pathogenic interactions involving direct penetrating fungi were analysed using an *Arabidopsis* line expressing functional GFP-PEN1 driven by the 35S promoter in the *pen1-1* mutant background. Neither non-adapted *Magnaporthe grisea*, *Phakopsora pachyrhizi*, or *Colletotrichum destructivum* nor adapted *Hyaloperonospora parasitica* or *Colletotrichum higginsianum* ascomycetes/oomycetes triggered detectable GFP-PEN1 accumulation. However, GFP-PEN1 accumulated at interaction sites with both non-adapted and adapted powdery mildews *Erysiphe pisi*, *Blumeria graminis* f sp. *hordei*, and *Golovinomyces orontii*. This suggests that only powdery mildews trigger PEN1 focal accumulation or that the other tested fungi/oomycetes suppress or avoid PEN1 accumulation at entry sites. It is conceivable that in pathogenic interactions where PEN1 accumulation was undetectable other syntaxins might become concentrated. Since PEN1 accumulation was detectable during compatible

Summary

interactions with adapted and incompatible interactions with non-adapted powdery mildews, focal PEN1 concentration *per se* does not predict effective resistance responses. It is possible that the adapted powdery mildew fungi intercept the SNARE protein-dependent resistance response through inhibition of ternary SNARE complex formation or of other components in this secretory pathway. Alternatively, virulent powdery mildews might have the ability to detoxify PEN1-delivered antimicrobial cargo. Unexpectedly, GFP-PEN1 was also detected in the interior of haustorial encasements after fungal entry into epidermal cells in about 10% of *G. orontii* interaction sites containing a haustorial complex. Whilst haustoria are essential for pathogenesis and nutrient uptake, haustorial encasements are presumed to terminate fungal growth. Of eight additional tested transgenic lines, each expressing a different fluorochrome-tagged fusion protein known to accumulate at incipient powdery mildew entry sites, only YFP-SNAP33 accumulated at a higher incidence (~25%) at haustorial encasements. These findings support previous ideas that haustorial encasements might be an extension of cell wall-associated defense responses at the cell periphery.

In a second experimental approach, I have developed a novel method for confocal high-throughput imaging at subcellular resolution. I have generated a chemically mutagenized M₂ population of an Arabidopsis line expressing functional GFP-PEN1 driven by the 35S promoter in the *pen1-1* mutant background. Following inoculation with *B. g. hordei* conidiospores, I aimed to identify mutant lines showing an aberrant PEN1 focal accumulation pattern at attempted fungal entry sites. Of several identified M₂ candidates, one line, tentatively designated *defect in focal accumulation 1 (dfa1)*, was validated in selfed M₃ progeny. This line shows a reduced incidence of PEN1 accumulation beneath *B. g. hordei* appressoria. Further genetic and molecular characterization of this mutant line should provide deeper insights in mechanisms underlying the polar accumulation of PEN1 syntaxin upon powdery mildew attack.

IV Zusammenfassung

Zellpolarität ist eine übliche Reaktion einzelner Pflanzenzellen auf bakteriellen oder pilzlichen Befall, der typischerweise zu Reorganisation des Zytoskeletts und gerichteter Bewegung von verschiedenen Organellen, wie Zellkern oder Golgi Apparat in Richtung der Penetrationsstelle an der Zelloberfläche führt. Dieser Prozess wird begleitet von der Relokalisation verschiedener Proteine und gerichtetem Vesikeltransport. Diese führen möglicherweise zur fokalen Deposition von *de novo* synthetisiertem Zellwandmaterial (genannt Papille) zwischen Zellwand und Plasmamembran unter der Pathogen Kontaktstelle. Schon seit einiger Zeit wird angenommen, dass sekretorische Prozesse, bei denen Vesikelinhalte mit antimikrobiellem Inhalt und Zellwand-Bausteinen abgesondert werden, an pflanzlicher Abwehr beteiligt sind. Erst kürzlich wurde genetisch belegt, dass ‚soluble *N*-ethylmaleimide sensitive factor attachment protein receptors‘ (SNARE) Proteine, die an intrazellulären Vesikelfusionen in verschiedenen Eukaryoten beteiligt sind, für Resistenzreaktionen benötigt werden. Ein ternärer SNARE Komplex, der membrangebundenes PEN1 Syntaxin, SNAP33 und endomembrangebundenes VAMP721/722 enthält, ist essentiell für die Begrenzung des Eintritts verschiedener getesteter Mehltäupilze in Epidermiszellen von Blättern. Fokale Akkumulation jeder dieser drei Proteine an Pilzeintrittsstellen impliziert die Existenz eines sekretorischen Mechanismus welcher Vesikel mit antimikrobiellen Inhalt gezielt transportiert und an der Interaktionsstelle in den extrazellulären Raum entlässt. Jedoch bleibt der exakte Mechanismus, der der fokalen SNARE Protein Akkumulation an der Penetrationsstelle unterliegt, unklar. Außerdem bleibt zu zeigen, ob die Konzentration der SNARE Proteine an diesen Stellen für effektive Abwehr erhöht sein muss.

Um die Spezifität der fokalen PEN1 Akkumulation an der Zellperipherie zu untersuchen, wurden diverse Pathogeninteraktionen von direkt penetrierenden Pilzarten analysiert. Dabei wurde eine *Arabidopsis* Linie verwendet, die ein funktionelles GFP-PEN1 Fusionsprotein expremiert, welches unter der Kontrolle des 35S-Promotors im *pen1-1* Hintergrund steht. Weder die nichtadaptierten Ascomyceten *Magnaporthe grisea*, *Phakopsora pachyrhizi* oder *Colletotrichum destructivum* noch der adaptierte Oomycete *Hyaloperonospora parasitica* bzw. der Ascomycet *Colletotrichum higginsianum* lösten eine detektierbare GFP-PEN1 Akkumulation aus. Jedoch akkumulierte GFP-PEN1 an Interaktionsstellen von den nichtadaptierten und adaptierten Mehltäupilzen *Erysiphe pisi*, *Blumeria graminis* f. sp. *hordei*, und *Golovinomyces orontii*. Das deutet darauf hin, dass nur Mehltäupilze die fokale Akkumulation von PEN1 auslösen oder dass die anderen getesteten Pilze bzw. Oomyceten die

fokale Akkumulation von PEN1 unterdrücken oder verhindern. Es ist vorstellbar, dass an Pathogen Interaktionsstellen, an denen die PEN1 Akkumulation nicht detektierbar ist, andere Syntaxine konzentriert werden. Da PEN1 Akkumulation in kompatiblen und inkompatiblen Interaktionsstellen mit adaptiertem und nichtadaptiertem Mehltau detektiert wurde, bestimmt die fokale PEN1 Akkumulation nicht *per se* die effektive Resistenzreaktion. Möglicherweise unterbinden die adaptierten Mehltaupilze die SNARE Protein abhängige Resistenzreaktion durch Inhibierung der Ternärkomplexbildung oder anderer Komponenten dieses Sekretionsweges. Alternativ könnten virulente Mehltaupilze die Fähigkeit besitzen PEN1-ausgeschütteten antimikrobiellen Inhalt zu detoxifizieren. Unerwarteterweise konnte an 10% der Interaktionsstellen mit Haustorien GFP-PEN1 auch im Inneren der haustoriellen Ummantelung von *G. orontii* nachgewiesen werden. Haustorien sind essentiell für Pathogenese und Nährstoffaufnahme, daher wird vermutet, dass eine haustorielle Ummantelung das Pilzwachstum begrenzt. Es wurden acht weitere transgene Linien getestet, die jeweils unterschiedliche fluorochrom-markierte Fusionsproteine exprimieren, von denen bekannt ist, dass sie an Mehltau Interaktionsstellen akkumulieren. Nur YFP-SNAP33 akkumulierte zu einem höheren Prozentsatz (25%). Diese Ergebnisse unterstützen die bisherige Vermutung, dass die haustorielle Ummantelung eine Erweiterung der zellwandassoziierten Abwehrreaktion an der Zellperipherie ist.

In einem zweiten experimentellen Ansatz wurde eine neue Methode der konvokalen Hochdurchsatz Mikroskopie auf subzellulärer Ebene entwickelt. Es wurde eine chemisch mutagenisierte M₂ Population einer *Arabidopsis* Linie generiert, die funktionelles GFP-PEN1 unter der Kontrolle des 35S Promotors im *pen1-1* Hintergrund expremiert. Es sollten Mutanten Linien identifiziert werden, die eine abweichende fokale Akkumulation von PEN1 an der Penetrationsstelle nach *B.g. hordei* Infektion aufweisen. Diese Musterung resultierte in der Identifizierung der *dfal* Mutante (*defect in focal accumulation 1*), die in der nachfolgenden M₃ Generation bestätigt wurde. Die Linie zeigt eine reduzierte Häufigkeit von PEN1 Akkumulationen unterhalb von *B.g. hordei* Appressorien. Weitere genetische und molekulare Charakterisierungen sollten Erkenntnisse über die Mechanismen der fokalen Akkumulation des PEN1 Syntaxins nach Mehltau Befall liefern.

1 Introduction

Both animals and plants are exposed to microbes throughout their life. Therefore, they developed an immune system to defend themselves against pathogens. The vertebrate immune system comprises innate and adaptive immune system, which co-operate. A functional innate immune system has been shown to be a prerequisite for the activation of adaptive immunity that is mediated by T lymphocytes and B lymphocytes (Nurnberger et al., 2004). Unlike vertebrates, plants lack an adaptive immune system and rely on the innate immunity of each cell and on systemic signals originating at the infection sites (Jones and Dangl, 2006).

The plant immune system is a multilayered type of immunity and consists of both pre-formed barriers, such as the waxy cuticle and cell wall components, and of induced defence responses (Dangl and Jones, 2001). The basis for the activation of innate immune responses is the ability to discriminate between self and nonself (Nurnberger et al., 2004). This is generally mediated by cell surface receptors which can sense pathogen structures, referred to as pathogen associated molecular patterns or PAMPs (Robatzek, 2007). Through these general defence mechanisms entire plant species are resistant to all genetic variants of a specific pathogen. This kind of immunity is referred to as non-host resistance and is the most common form of disease resistance in plants (Thordal-Christensen et al., 2000; Nurnberger et al., 2004).

Nevertheless, some plant pathogens are able to avoid or suppress PAMP-triggered defence responses and can cause disease on particular plant species through the secretion of effector molecules. To cope with these parasites, plants have evolved a second defence system based on resistance proteins (R), which are able to specifically recognize these effectors and mount pathogen-specific responses (Jones and Dangl, 2006).

1.1 Pathogen associated molecular pattern (PAMP) triggered immunity

Both in the plant and animal system, PAMP perception is mediated by pattern recognition receptors (PRRs) (Robatzek, 2007). PRRs contain an extracellular leucine-rich repeat (LRR) domain, a transmembrane domain and an intracellular part involved in signal transduction (Robatzek, 2007). In animals, PRRs of the Toll-like receptor (TLR) family are known to stimulate inflammatory responses in innate immunity.

A key feature of PAMPs is that they are molecules unique to microbes and are not produced by potential eukaryotic hosts. In addition, PAMPs are molecular structures essential for the survival of the pathogen and, therefore, are not subject to natural variation (Robatzek, 2007). These features are absent in the host organism and their conservation is a prerequisite for nonself recognition. One of the best characterized PAMPs is the bacterial flagellin. Flagellin is a protein subunit that builds the flagellar filament, which is important for motility of bacterial microbes (Zipfel and Felix, 2005). By testing flagellin deletion mutants for their activation of the animal TLR5 receptor, it was possible to demonstrate that mammals detect a highly conserved amino acid sequence of flagellin (Jaenicke-Despres et al., 2003). Interestingly, the 22-amino-acid peptide (flg22) recognised by many plant species differs from the one detected by mammals (Felix et al., 1999). The *Arabidopsis* PRR FLS2 mediates flg22 perception and leads to a series of downstream events, including oxidative burst, mitogen associated protein kinase (MAPK) cascade activation, and callose deposition at site of penetration entry (Asai et al., 2002; Gomez-Gomez and Boller, 2002).

Another example for prominent PAMPs are lipopolysaccharides, which are principal components of the outer membrane of Gram-negative bacteria. A role for lipopolysaccharides in plant diseases has been suggested by the observation that bacterial mutants, defective in lipopolysaccharides, have reduced virulence (Dow et al., 2000). In addition, treatment of *Arabidopsis* plants with lipopolysaccharides resulted in activation of NO, a hallmark of innate immunity both in animals and plants (Zeidler et al., 2004).

To overcome PAMP-triggered immunity, pathogens evolved the ability to interfere and suppress PAMP-triggered defence by secretion of effector proteins. This phenomenon is referred to as effector triggered susceptibility (Jones and Dangl, 2006). Pathogens evolved different means to secrete effectors into host cells, among them the best characterised is the bacterial type III secretion system (TTSS). The TTSS generates a ‘molecular syringe’ upon contact with the host to transfer proteins or protein-DNA complexes into the host cell (Nomura et al., 2005). This process is essential for the development of disease symptoms and for bacterial multiplication (Staskawicz et al., 2001), as effector molecules are injected through the TTSS (Chisholm et al., 2006). Some effectors of the bacterial pathogen *Pseudomonas syringae* are known to contribute to pathogen virulence by mimicking or inhibiting eukaryotic cellular functions (Jones and Dangl, 2006), e.g. HopM or AvrE, which target host vesicle transport mechanism (DebRoy et al., 2004; Nomura et al., 2006). In a screen for virulence factors of *Pseudomonas* species, AvrPto and AvrPtoB were identified as suppressors of early-defence gene transcription and of MAP kinase signalling. Expression of avrPto in Arabidopsis plants prevents early PAMP-signalling events resulting in growth of normally non-adapted *P. syringae* (He et al., 2006).

In contrast to bacteria, the mechanisms of effector delivery in eukaryotic pathogens, such as fungi or oomycetes, are still poorly understood (Jones and Dangl, 2006; Whisson et al., 2007). The first evidence for an eukaryotic counterpart of the bacterial TTSS comes from the observation that proteins secreted by oomycetes share a common motif with the effectors of the human malaria parasite, *Plasmodium falciparum*. It transfers pathogenic proteins into the host, thereby altering host cell function and causing disease. The exported proteins contain a leader sequence with a host-targeting motif, RxLx, that is required for export (Bhattacharjee et al., 2006). Recently, Bhattacharjee et al. (2006) identified the conserved RxLR motif in secreted proteins of the oomycete *Phytophthora infestans* and in secreted proteins of diverse *Phytophthora* species. Furthermore, secretion was shown to depend on this motif (Bhattacharjee et al., 2006). These data suggest that eukaryotic pathogens share equivalent host-targeting signals to access host cells both in plant and animal kingdoms.

1. 2 Resistance gene-mediated immunity or effector triggered immunity

The evolution of secreted pathogenic effector proteins led to the establishment of plant resistance (R) genes that recognize these effectors (Chisholm et al., 2006). Consistently, the effectors are termed avirulence (avr) proteins. If an Avr-gene product and the corresponding R-gene product are present, resistance is usually activated by triggering a localized programmed cell death, referred to as hypersensitive reaction or HR. In contrast, the absence of one of the proteins results in plant susceptibility against the pathogen. The HR plays a central role in plant resistance responses against biotrophic pathogens that require living host tissue for growth and whose growth is, therefore, stopped by the HR due to prevention of nutrient gain.

R genes can be categorized into two main classes based on domain organization (Dangl and Jones, 2001). The largest class of R genes contains a nucleotide binding site (NBS) and leucine-rich repeats (LRRs) and are named NBS-LRR proteins. This class is presumably cytoplasmic and can be further subdivided based on the N-terminal structure: TIR-NBS-LRRs have a domain with homology to the intracellular signalling domains of the *Drosophila* Toll and mammalian interleukin (IL)-1 receptors, whereas CC-NBS-LRRs contain putative coiled-coil (CC) domains (Dangl and Jones, 2001). A second class encodes membrane resident protein containing N-terminal extracellular LRRs. According to their domain structure three subclasses have been defined, including receptor-like proteins (RLP), exhibiting an extracellular LRR and a transmembrane (TM) domain; receptor like kinases (RLK), exhibiting an extracellular LRR, a TM domain and a cytoplasmic kinase; and polygalacturonase-inhibiting proteins (PGIP), exhibiting a cell wall LRR (Chisholm et al., 2006).

The interaction between R gene product and Avr gene product can be either direct or indirect. A direct interaction between R proteins and the corresponding Avr proteins was the initial and simplest biochemical interpretation of the genetically defined “gene-for-gene” resistance (Flor, 1971). However, only few examples of direct interaction have been observed (Jia Y et

al., 2000; Dodds et al., 2006). Rice plants expressing the Pita R gene undergo HR when inoculated with the blast fungus *Magnaporthe grisea* expressing Avr-Pita. Transient expression of Avr-Pita inside rice cells resulted in Pita-dependent HR, suggesting that Avr-Pita alone is sufficient to trigger defence response. Furthermore, yeast-two-hybrid assays and *in vitro* binding experiments showed the direct interaction of Avr-Pita and Pita. Together, the data suggest a direct binding of the corresponding resistance protein and avirulence protein (Jia Y et al., 2000).

However, other examples point to indirect R-Avr interactions and this led to the ‘guard hypothesis’ (Jones and Dangl, 2006). The model suggests that the avirulence protein contacts its cognate pathogenicity target in the host in order to confer virulence. At the same time, an R protein guarding this target protein is activated upon modification of the pathogenicity target, thereby triggering resistance response (Dangl and Jones, 2001). One of the best characterised examples of indirect interaction is the *Arabidopsis* NB-LRR *Rpm1* gene that confers resistance against *P. syringae* strains expressing the type III effectors AvrRpm1 (Dangl et al., 1992). After delivery of AvrRpm1 through the TTSS, the avirulence protein interacts with RIN4, a plasma membrane associated protein, and induces phosphorylation of RIN4. This modification activates RPM1-mediated disease resistance, including HR (Mackey et al., 2002).

1. 3 Pathogen induced cell polarity is a common phenomenon in plant defence

Cell polarity is a fundamental feature of all eukaryotic cells (Dhonukshe et al., 2005). It plays an essential role in plant developmental processes, such as tip growth of pollen, root hairs and trichomes, but also in plant immune responses cell polarity appears to play an important role (Lipka and Panstruga, 2005). Plant cells attacked by pathogens undergo drastic morphological changes, including reorganization of the cytoskeleton, translocation of

cytoplasm and cell nucleus, vesicle trafficking, and relocalization of a subset of proteins towards attempted pathogen entry site (Schmelzer, 2002; Assaad et al., 2004; Bhat et al., 2005; Lipka and Panstruga, 2005; Kwon et al., 2008).

In the animal field, a subset of immune responses are conferred by the interaction between T cells and antigen-presenting cells (APC) (Bromley et al., 2001; Das et al., 2004; Billadeau et al., 2007). Before contact with the antigen, T cells are nonpolarized showing a uniform radial distribution of membrane domains and receptors on the cell surface (Sánchez-Madrid and Angel del Pozo, 1999). T cell recognition of an APC, mediated by the T cell receptor (TCR), leads to rapid polarization of the cytoskeleton and accumulation of signalling components into supramolecular activation clusters (Das et al., 2004). The exact mechanism controlling TCR-mediated polarization is unknown, however, the polarization process is essential for T cell function and results in the formation of the immunological synapse (Billadeau et al., 2007).

In plant immunity, PAMPs and the respective plant PRR receptors are required for the first line of defence. However, it remains to be shown whether these receptors accumulate at the attempted pathogen entry sites (Kwon et al. 2008). In addition, whether a plant receptor drives the polarization processes upon pathogen attack is still unknown. It is conceivable that such a receptor is also essential in developmental processes, suggesting that lethality of homozygous mutants will make it difficult to identify it in a mutational screen.

1. 4 SNARE proteins mediate vesicle traffic

A special feature of eukaryotic cells is the cellular compartmentalization. Communication among the compartments occurs through vesicle trafficking, a mechanism which includes endo- and exocytosis and which is typically mediated by soluble N-ethylmaleimide-sensitive factor adaptor protein receptors (SNAREs) (Sanderfoot and Raikhel, 2003). The SNARE superfamily is conserved throughout kingdoms (Sutton et al., 1998; Bock et al., 2001;

Bonifacino and Glick, 2004; Jahn and Scheller, 2006). Each vesicle-trafficking step requires a subset of proteins of the SNARE superfamily. The specificity derives from different members localized to distinct membrane compartments (Bock et al., 2001).

SNARE proteins are characterized by the presence of a special motif, the SNARE domain, which consists of a coiled-coil heptad repeat motif of 60-70 amino acids (Sutton et al., 1998; Jahn et al., 2003; Jahn and Scheller, 2006). SNAREs can be classified in Q- and R-SNAREs, depending on a conserved glutamine or arginine residue in the centre of the SNARE domain. Q-SNAREs can be further subdivided into Qa-, Qb-, and Qc-SNAREs (Fasshauer et al., 1998; Bock et al., 2001). Qa-SNAREs are also referred to as syntaxins, while SNAREs containing a Qb- or Qc-motif are known as SNAP-25 like proteins (Bennett et al., 1992). Finally, R-SNAREs are often designated as VAMPs, vesicle-associated membrane proteins (Uemura et al., 2004).

To drive membrane fusion, SNAREs of opposing membranes form a highly stable four-helix bundle, the so called ternary SNARE complex, that consists of one of each of the Qa-, Qb-, Qc- and R-SNAREs (Fasshauer et al., 1998; Sutton et al., 1998; Bonifacino and Glick, 2004). Since SNARE complexes are thermodynamically more stable than individual SNAREs, complex formation leads to release of free energy. Moreover, complex formation leads to a close connection of the membranes and both is suggested to contribute to membrane fusion (Fasshauer et al., 1997; Hanson et al., 1997; Fasshauer et al., 1998; Sutton et al., 1998). After fusion and release of the cargo, SNARE complexes are recycled to maintain a stable cellular architecture and continuous vesicle trafficking. Disassembly requires energy, which is provided by the soluble accessory proteins α -SNAP and the ATPase N-ethylmaleimide-sensitive factor NSF. Therefore NSF binds to the α -SNAP-SNARE complex and the NSF-dependent hydrolysis of ATP dissociates the complex (Söllner, 1993; May et al., 2001).

1. 5 SNARE proteins establish effective barriers against fungal ingress at the cell periphery

Secretory processes have been thought for a long time to contribute to plant defence against pathogen attack (Hückelhoven, 2007). Recently, a plant SNARE protein was identified, that is required for preinvasion resistance in *Arabidopsis* to pathogen attack by the non-adapted barley powdery mildew *Blumeria graminis* f. sp. *hordei* (*B. g. hordei*) (Collins et al., 2003). Loss-of-function alleles of *AtPEN1* syntaxin and its barley ortholog *HvROR2* revealed enhanced host cell entry rates by *B. g. hordei*. Barley MLO is a suppressor of resistance, and silencing of *HvSNAP34*, a SNAP25 homolog, led to elevated fungal entry in the resistant *mlo* genotype. Yeast-two-hybrid assays showed an interaction of *HvROR2* with *HvSNAP34*, demonstrating the formation of a binary complex and suggesting, that at least two SNAREs are involved in preinvasion resistance (Collins et al., 2003). The *Arabidopsis* genome reveals three SNAP25 homologues, SNAP29, -30, -33. However, RT-PCR proved exclusively SNAP33 transcripts in leaves, assuming it as possible candidate for a potential SNARE complex (Kwon et al., 2008). Binary SNARE complex formation in *Arabidopsis* was proven by Kwon et al. (2008) by detecting interactions between *AtPEN1* and *AtSNAP33*, a SNAP25 homolog and the ortholog of *HvSNAP34*, *in vitro* by immunoblot analysis. To identify the interacting partner of PEN1-SNAP33 binary complex, co-immunoprecipitation with various VAMP family members was carried out and revealed VAMP722 as interacting partner. The data demonstrate the first biochemical and genetic evidence for ternary SNARE complex function in plants (Kwon et al., 2008).

In *Arabidopsis*, the closest homolog to VAMP722 is VAMP721, therefore, a double homozygous mutant was generated. However, *vamp722/vamp721* double mutants are lethal, suggesting essential as well as redundant wild-type gene functions in development (Kwon et al., 2008). Ethanol-inducible co-silencing of VAMP721/VAMP722 revealed enhanced *B. g. hordei* entry rates, reminiscent of *pen1* mutant plants. This provided genetic evidence for a VAMP721/VAMP722 function in preinvasion resistance. Taken together, these data suggests

a PEN1-SNAP33-VAMP722 ternary SNARE mediated vesicle trafficking involved in pathogen defence (Kwon et al., 2008).

An *Arabidopsis* line expressing a functional GFP-PEN1 fusion protein revealed that GFP-PEN1 focally accumulates at attempted fungal entry sites (Assaad et al., 2004; Bhat et al., 2005). Optical sectioning by confocal microscopy showed the GFP-PEN1 in the interior of the papilla, a *de novo* synthesized cell wall apposition, at 17-24 hpi after treatment with the adapted powdery mildew *Erysiphe cichoracearum* (Assaad et al., 2004). Furthermore, a delay in papilla formation was demonstrated in *pen1-1* null mutant plants. The localization studies and the delay in papilla formation led the authors to the suggestion, that PEN1 plays a role in polarised secretion, thereby giving rise to papilla formation (Assaad et al., 2004). By contrast, Bhat et al. (2005) found that the GFP-PEN1 focal accumulation (FA) at attempted entry sites of *B. g. hordei* remained in the plasma membrane after plasmolysis at 12 hpi. Their data suggest that the GFP-PEN1 FA is separable from the papillae and may represent a pathogen-triggered plasma membrane microdomain. FRET experiments revealed no recovery of fluorescence at *B. g. hordei* entry after bleaching of the GFP-PEN1 FA, indicating that the process of protein polarization is triggered only once after attack (Bhat et al., 2005). A transient co-expression in barley epidermal cells of the actin depolymerising factor 3, a peroxysome tagged dsRed variant and YFP-*HvROR2*, revealed recruitment of *HvROR2* at *B.g. hordei* entry sites, suggesting that the accumulation is an actin cytoskeleton independent process (Bhat et al., 2005). Taken together, the authors suggest that PEN1 FA is localized to the plasma membrane and triggered only once upon pathogen attack. Since papillary callose deposition was shown to be actin cytoskeleton-dependent (Schmelzer, 2002) and PEN1 FA actin independent, it is possible that PEN1 FA and papillary callose deposition are independent processes.

Taken together, the data on PEN1 localization are differing. Possibly, the formation of PEN1 containing plasma membrane microdomains is only transient and at later time points PEN1 localizes to papillae. Furthermore, the mechanisms behind PEN1 FA and its function at penetration entry sites remain elusive.

Arabidopsis lines co-expressing fluorescently tagged SNAP33 and VAMP722 showed a focal accumulation of these SNARE proteins at fungal entry site (Kwon et al., 2008). The evidence of a functional ternary SNARE complex involved in disease resistance and the focal accumulation at attempted fungal entry sites suggests that focal secretion of potentially toxic cargo leads to termination of pathogenesis (Kwon et al., 2008). However, the localization of PEN1, SNAP33 and VAMP722 in the interior of the papilla needs to be further proven by other means than only through descriptive confocal light microscopy analyses. In particular, it will be of interest to understand whether these SNARE proteins are present at the papilla as soluble or vesicle-associated proteins.

1. 6 Papilla formation often correlates with failure of fungal ingress

In plant cells, de novo synthesized cell wall appositions at attempted fungal entry sites, also referred to as papilla, is a common finding. Papillae are deposited between the plasma membrane and the cell wall and are thought to locally reinforce the cell wall at sites of attempted pathogen penetration, thereby acting as a physical barrier to terminate microbial invasion (Aist, 1976; Kobayashi et al., 1995). Pharmacological and cytological experiments have suggested the papilla to be important for penetration resistance (Belanger and Bushnell, 2002). Callose, a β -1,3-glucan is one component of papillae and it is suggested to provide a scaffold for the deposition of antimicrobial compounds (Aist, 1976; Thordal-Christensen et al., 1997; Bolwell et al., 2002). Furthermore, also membranous structures, phenolics, reactive oxygen species, hydroxyproline-rich glycoproteins or peroxidases were detected at papillae (Aist, 1976; Snyder and Nicholson, 1990; Thordal-Christensen et al., 1997).

There is evidence for a fundamental role of the actin cytoskeleton in cellular defence, including papilla formation. Pharmacological experiments revealed upon treatment with actin inhibitors that several defence responses at the penetration site were abolished, including cytoplasmic aggregation, nuclear movement, papilla formation, callose deposition and HR-

like cell death. Interestingly, microtubule inhibitors had only a subtle impact (Kobayashi et al., 1997; Skalamera et al., 1997; Skalamera and Heath, 1998).

Apparently, more than one stimulus is required to induce papilla formation (Gus-Mayer et al., 1998). In parsley cell suspension, a mechanical treatment *via* a needle (comparable to penetration of a fungal hypha) was able to induce translocation of cytoplasm and nucleus and generation of reactive oxygen intermediates (ROI). Upon treatment with an elicitor, ROI accumulated and a subset of defence-related genes was activated, but no morphological changes were detectable. Upon co-stimulation with both mechanical and chemical triggers, a cytoplasmic aggregation, nuclear migration and ROI accumulation, but no papilla formation was detectable (Gus-Mayer et al., 1998), indicating that yet uncharacterised stimuli are required for induction of papilla formation.

Until recently, it was common belief that callose accumulation is required for plant defence against pathogens. However, analyses of plants lacking PMR4/GSL5 callose synthase, required for wound and papillary callose formation, revealed enhanced disease resistance against the normally virulent powdery mildew *Golovinomyces orontii* and against the oomycete *Hyaloperonospora parasitica* (Jacobs et al., 2003) (Nishimura et al., 2003). Several previous studies established a role for the signalling molecule salicylic acid in disease resistance responses (Thomma et al., 2001). After blocking the salicylic acid signalling pathway in *pmr4/gsl5* mutant plants, the susceptibility phenotype was restored (Nishimura et al., 2003). In addition, an upregulation of salicylic acid in the *pmr4/gsl5* mutant was detectable, that further increased after infection. These data demonstrate that PMR4/GSL5 not only plays a role in callose deposition, but also negatively regulates the SA signalling pathway (Nishimura et al., 2003).

Taken together, these data indicate that papilla formation *per se* does not necessarily terminate pathogen growth at attempted fungal entry sites. Furthermore, at least one protein that is necessary for papilla formation can also regulate other defence pathways. However, the genetic basis and the regulation of papilla formation are still unidentified (Schmelzer, 2002; Jacobs et al., 2003).

1. 7 Development of haustorial complexes and deposition of callose at haustorial complexes

In a successful penetration attempt, the tip of the so called penetration peg penetrates the host cell wall and grows to form a specialized feeding structure, termed haustorium (Bushnell, 1971; Bushnell, 1972; Belanger and Bushnell, 2002). The haustorium is a nucleate cell that is devoted to the uptake of nutrients from the host and is therefore fundamental for the establishment of disease and pathogen reproduction (Talbot, 2004).

Different pathogens developed different mechanisms to enter host cells and to develop haustoria. Among the biotrophic pathogens, most powdery mildew fungi and some downy mildew fungi penetrate directly the epidermal cells, whereas some other downy mildew fungi produce an infection hypha that forces its way into the leaf along the middle lamella between adjacent epidermal cells, producing haustoria laterally in those cells (Chou, 1970). Some rust fungi produce an infection hypha that penetrates an epidermal cell and grows throughout the cell before establishing an intercellular hypha, which generates a haustorium in a mesophyll cell (Koch et al., 1983). Most of the hemibiotrophic *Colletotrichum* species directly penetrate epidermal cells and generate an infection hypha in the cell lumen, subsequently switching to the necrotrophic phase and growing throughout the tissue (Perfect et al., 1999).

The host plasma membrane surrounds the fungal structures and it is termed extrahaustorial membrane (EHM) (Bushnell, 1971; Belanger and Bushnell, 2002). Compared to the host plasma membrane the EHM has different biochemical features (Gil and Gay, 1977; Spencer-Phillips and Gay, 1981; Gay et al., 1987; Belanger and Bushnell, 2002; Koh et al., 2005), however, its origin is still unknown. Owing to the use of diverse monoclonal antibodies, it was possible to show that the extrahaustorial membrane harbours specific components that are absent in the plant plasma membrane (Green et al., 1994). Confocal microscopy of different transgenic *Arabidopsis* lines, expressing fluorescently tagged plasma membrane markers and treated with the adapted powdery mildew *Erysiphe cichoracearum*, revealed an exclusion of all tested markers from the EHM, suggesting that the EHM is a unique membrane either originating *via* differentiation of the host plasma membrane or *via de novo* synthesis (Koh et

al., 2005). The EHM is separated from the haustorial wall by the extrahaustorial matrix, and collectively haustorium, extrahaustorial matrix and EHM comprise the haustorial complex (Gil and Gay, 1977).

The host deposits papillary callose at the site of attempted penetration (see 1.6). In case of further fungal growth, additional callose is deposited around the penetration peg, probably representing an extension of the papilla. This deposit forms a collar around the haustorial neck and can also fully encase the whole haustorial body (Bushnell, 1972). Electron microscopic studies in a resistant interaction of cowpea and the rust *Uromyces phaseoli* var. *vignae* revealed that the encasement is formed after the haustorium is fully developed and after haustorium formation either host cell death or haustorial encasement was observed, both terminating fungal growth (Heath and Heath, 1971). The formation of haustorial encasements has been reported for diverse adapted and non-adapted interactions (Chou, 1970; Skalamera et al., 1997; Donofrio and Delaney, 2001; Mellersh and Heath, 2003). However, little is known about haustorial encasements in the interaction between powdery mildew fungi and *Arabidopsis*.

The detection of membrane-like structures was detected inside papillae (Aist, 1976) but it was also reported for haustorial encasements (Heath and Heath, 1971). Electron microscopic studies in a resistant interaction between cowpea and the rust *Uromyces phaseoli* var. *vignae* revealed a highly convoluted plasma membrane adjacent to the encasement and irregular fractions of this membrane appeared to be trapped between the developing encasement and the haustorial wall (Heath and Heath, 1971). Callose encasements of the oomycete *Hyaloperonospora parasitica* haustoria were shown to contain vesicles via detection with electron microscopy (Davison, 1968).

In summary, the haustorial encasement appears to be an extension of the papilla and the encasement seems to originate from the same material as papilla. In addition, membranous material can be detected in both structures. Thus, it is conceivable that the processes leading to papilla formation and haustorial encasement are the same. It remains to be shown, however, whether encasements can be actively suppressed by the pathogen.

1. 8 Exocytosis in plants

Early plant defence appears to be regulated by polarised transport and secretion of vesicles with potential antimicrobial cargo towards attempted penetration entry sites of pathogens, as revealed by several microscopic studies (An et al., 2006a ;Thordal-Christensen et al., 1997; Collins et al., 2003; An et al., 2006b). As a response, pathogens might have either developed mechanisms to suppress secretion of defence proteins or alternatively to exploit the secretion to gain nutrients (Schulze-Lefert, 2004; An et al., 2006a). However, no example is known of successful change of the plant primary metabolism by pathogens to gain nutrients (Biemelt and Sonnewald, 2006).

Besides other endomembranes, large vesicle-like bodies of different sizes accumulate at attempted fungal entry sites (Collins et al., 2003; An et al., 2006b). Transmission electron microscopy (TEM) detected in the interaction between the resistant *mlo5* mutant barley plants and *B. g. hordei* three different kinds of vesicles. They were characterized as small cell wall appositions and paramural bodies (PMB), which were filled with small vesicles and accumulate between plasma membrane and cell wall. The third kind of vesicles was defined as multivesicular bodies (MVBs) (An et al., 2006a). MVBs are mainly present in the cytoplasm, and are believed to originate from inward budding of endosomal membranes (Geldner and Jurgens, 2006).

In addition, in *mlo5* barley upon infection with *B. g. hordei*, TEM analyses led to the detection of MVBs close to the papillae. Interestingly, their outer membrane seems to be attached to the plasma membrane (An et al., 2006a). Furthermore, cerium staining of MVBs led to the detection of H₂O₂, which is involved in modification of cell walls through peroxidase catalyzed cross linking of polymers (Brisson et al., 1994). A vacuolar peroxidase, PRX7, was detected by immunogold labelling in MVBs, PMBs and the apoplast, indicating that MVBs release their internal vesicles into the apoplast (An et al., 2006a). The release of vesicles into the apoplast by MVBs is reminiscent of animal exosome delivery (An et al., 2006b). Animal MVBs fuse with the plasma membrane to release exosomes into the extracellular environment. Exosomes function in elimination of obsolete proteins, mediation of

intracellular communication and in immune response, e.g. in suppression of inflammatory and autoimmune responses in dendritic cells (Stoorvogel et al., 2002; Kim et al., 2005; Li et al., 2006; van Niel et al., 2006). Taken together, these data suggest that MVB are potential candidates for polarised secretion of antimicrobial compounds or compounds for papilla formation (An et al., 2006a).

An additional secretory pathway may involve the *Arabidopsis* proteins PEN2 and PEN3. Like PEN1, PEN2 and PEN3 were identified in a genetic screen for *Arabidopsis* mutants impaired in preinvasion resistance to the non-adapted *B. g. hordei* (Collins et al., 2003). Notably, fluorescent protein-fusion lines of all three PEN genes revealed a focal accumulation at attempted fungal entry site (Assaad et al., 2004; Bhat et al., 2005; Lipka et al., 2005; Stein et al., 2006). PEN2 encodes a glycosyl hydrolase and is localized to peroxisomes. It shows a broader spectrum of biological activity compared to PEN1. Furthermore, an observed accumulative effect of invasive growth in the *pen1 pen2* double mutant led to the suggestion that PEN1 and PEN2 act in different pathways (Lipka et al., 2005). PEN3 encodes a putative PDR-like ABC transporter, also known as PDR8 (Stein et al., 2006). The role of PEN3 in preinvasion resistance, its localization to haustorial complexes, and the finding of homologous ABC transporter in tobacco, which might function in export of toxic compounds and/or in detoxification of fungal toxins, led to the suggestion that PEN3 export toxic metabolites at sites of attempted pathogen invasion (Jasinski et al., 2001; Sasabe et al., 2002; Stein et al., 2006). Analysis of *pen2 pen3* double mutants suggests that the corresponding proteins act in the same pathway (Lipka et al., 2005). Thus, there are at least two pathways acting in preinvasion resistance, one is PEN1-dependent, the other one is PEN2- and PEN3-dependent. Intriguingly, both pathways involve potential focal secretion at fungal entry sites. Taken together, there are several potential secretion pathways, which could be involved in defence reactions. However, direct evidence that plant defence acts through vesicles containing antimicrobial compounds that are focally secreted at fungal entry site is still missing.

1. 9 Aim of the thesis

Cell polarity and papilla formation are a common response in plant defence; nevertheless the genetic basis and the trigger of these responses remain elusive (Schmelzer, 2002). The *Arabidopsis* syntaxin PEN1 is known to play a role in non-host resistance and to focally accumulate at attempted fungal entry sites of the non-adapted *B. g. hordei* (Collins et al., 2003; Assaad et al., 2004; Bhat et al., 2005). PEN1 was found to build a ternary SNARE complex with SNAP33 and VAMP722 and is presumed to be involved in a SNARE mediated focal secretion of antimicrobial compounds (Kwon et al., 2008); however, the mechanism behind focal accumulation of PEN1 is still unknown.

During my Ph.D. work, I intended to characterize the PEN1 focal accumulation at penetration entry sites and analyse its relevance and specificity in defence reactions. Furthermore, I aimed to detect the mechanism(s) behind focal accumulation of PEN1, thus also to better characterise the cell polarity phenomenon upon pathogen attack. Towards this end, I employed both microscopic and genetic approaches. To gain knowledge on the importance and the specificity of PEN1 focal accumulation, I challenged a GFP-PEN1 fusion line using diverse pathogens and I qualitatively and quantitatively analysed attempted pathogen entry sites by confocal microscopy. I have also developed a new confocal high-throughput imaging system. In a second approach, I screened an EMS-mutagenised line expressing GFP-PEN1 to identify mutants showing an altered GFP-PEN1 focal accumulation pattern. Characterization of the identified mutants will help to unravel the mechanisms behind cell polarity.

2 Material and Methods

2.1 Material

2. 1. 1 Plant Material

The transgenic *Arabidopsis* plants used in this study were in the genetic background of the *Arabidopsis thaliana* accession Columbia-0 (Col-0), as it is listed in Table 1.

Table 1. *Arabidopsis thaliana* wild type and mutants used in this study.

<i>Arabidopsis</i> genotype	protein	protein function	Source
Col-0	-	-	Nottingham Arabidopsis Stock Center (NASC)
<i>pen1-1</i> in Col-0	-	-	Collins et al., 2003
<i>pmr4-1</i> in Col-0	-	-	Vogel and Somerville, 2000
pnat::mYFP-PEN1 in <i>pen1-1</i>	mYFP-PEN1	functional syntaxin	S. Pajonk, pers communication
p35S::GFP-PEN1 in <i>pen1-1</i>	GFP-PEN1	functional syntaxin	Collins et al., 2003
p35S::mYFP-SNAP33 in <i>snp33</i>	mYFP-SNAP33	functional syntaxin	S. Pajonk, pers communication
pnat::GFP-VAMP722 in <i>vmp722</i>	GFP-VAMP722	functional syntaxin	S. Pajonk, pers communication
p35S::CFP-SYP122 in <i>pen1-1</i>	CFP-SYP122	functional syntaxin	Assaad et al., 2004
pnat::PEN3-GFP in <i>pen1-3</i>	PEN3-GFP	functional ABC-transporter	Stein et al., 2006
p35S::GFP-SIMIP in Col-0	GFP-SIMIP	aquaporin	Cutler et al., 2000
p35S::GFP-D41 in Col-0	GFP-AtVAMP3	truncated VAMP	Cutler et al., 2000
p35S::GFP-PIP2a in Col-0	GFP-PIP2a	aquaporin	Cutler et al., 2000
p35S::GFP-29-1 in Col-0	GFP-LTI6b	low temperature induced protein	Cutler et al., 2000

2. 1. 2 Plant Pathogens

The barley powdery mildew *Blumeria graminis* forma specialis *hordei* isolate K1 was propagated on seven day old barley seedlings Ingrid 10. Inoculated *A. thaliana* plants were kept at 20 °C, 60% relative humidity, and 16 h light/8 h darkness in a protected environment.

The pea powdery mildew *Erysiphe pisi* isolate *Birmingham* was propagated on 3 week old pea plants, cultivar Linga. Pea and inoculated *A. thaliana* plants were kept at 22 °C, 70% humidity, and 12h light/12 h darkness in a protected environment.

The *Arabidopsis* powdery mildew *Golovinomyces orontii* was maintained on *A. thaliana* Col-0 plants cultivated at 20 °C and 16 h light/ 8 h darkness, 80% humidity in a protected environment.

Hyaloperonospora parasitica isolate Noco2 was maintained by weekly subculturing on susceptible plants as described previously (Dangl et al., 1992).

Magnaporthe grisea, strain Haku 1-007 was cultivated on potato dextrose agar in plates at 25°C in constant light.

Colletotrichum higginsianum strain IMI34906I and *Colletotrichum destructivum* stain LARS 202 were cultivated on Mathur's agar medium in conical (Erlenmeyer) flasks at 25°C in constant light.

Phakopsora pachyrhizi was maintained on *Glycine max* plants, cultivated at 22 °C, 60% humidity and 16 h light/ 8 h darkness.

2. 1. 3 Antibodies

Antibodies used are listed in table 2.

Table 2. Primary and secondary antibodies.

Name	Source	Conjugate	Dilution	Reference
PEN1-antiserum	rabbit, polyclonal	-	1:10, 1:50, 1:200, 1:500, 1:2000,1:5000	H.T-Christensen, KVL, DK
VAMP722- antiserum	rabbit, polyclonal	-	1:10, 1:50, 1:200, 1:500, 1:2000,1:5000	Kwon et al., 2008, Nature
anti-rabbit	goat, monoclonal	fluorescein	1:50	Sigma, Sterinheim, Germany

2. 1. 4 Chemicals and reagents

Laboratory grade chemicals and reagents used are listed in table 3.

Table 3. Laboratory grade chemicals and reagents.

Name	Specification	Source
Aniline Blue	-	Sigma, Sterinheim, Germany
Aniline Blue Fluorochrome	-	Biosupplies, Australia
bovine serum albumin	-	Sigma, Sterinheim, Germany
Coomassie	Coomassie® Brilliant Blue G250	Fluka, Buchs, Switzerland
Methanesulfonic acid ethyl ester (EMS)	-	Sigma, Sterinheim, Germany
FM® 4-64	-	Molecular Probes
goat serum	-	Sigma, Sterinheim, Germany
poly-L-lysine	-	Sigma, Sterinheim, Germany
Percoll	-	Sigma, Steinheim, Germany
Tween 20	Tween® 20	Sigma, Steinheim, Germany
Other laboratory grade chemicals	-	Duchefa, Haarlem, Netherlands Fluka, Buchs, Switzerland Serva, Heidelberg, Germany Sigma, Steinheim, Germany Merck, Darmstadt, Germany Roth, Karlsruhe, Germany

2. 1. 5 Media

Unless otherwise indicated all media were sterilised by autoclaving at 121°C for 20 minutes. Heat labile solutions were sterilised using filter sterilisation units prior to addition of autoclaved components. For the addition of antibiotics and other heat liable components the solution or media were cooled down to 55°C.

Colletotrichum medium: Mathur's agar medium

2,8 g	Glucose
1,22 g	MgSO ₄ ·7H ₂ O
2,72 g	KH ₂ PO ₄
2,8 g	Oxoid Mycological peptone
30 g	Agar
in 1 l H ₂ O	

Potato Dextrose Agar

20g	PDA
500ml	water

2. 1. 6 Buffer and Solutions

Aniline Blue staining solution

150 mM	KH ₂ PO ₄
0,01% (w/v)	Aniline Blue
in dH ₂ O	
pH 9,5 adjusted with KOH pellets	

Aniline Blue Fluorochrome (Sirofluor)

0,1 mg/ml Aniline Blue Fluorochrome
fresh 1:3 dilution with water was prepared before use

Coomassie staining solution, 0,25%

Coomassie Blue 0,25% (w/v) in ethanol

FM4-64 staining solution, 17 mM stock

100µg FM4-64
10µl DMSO
Prepare fresh dilution with H₂O to a working solution of 17µM

Sodium phosphate buffer for fixation of isolated haustoria

20 ml 10 % formaldehyde
1 ml 25 % glutaraldehyde
25 ml 0.1M phosphate buffer
4 ml water

Formaldehyde, 10% (w/v) stock solution for fixation of isolated haustoria

1. Add 2.5 g of *para*formaldehyde powder to 20 ml of dH₂O and heat to 70°C on a hot plate with continuous stirring.
2. Add a few drops of 10 M NaOH, until the solution changes from milky to clear.
3. Cool to RT, adjust to pH 7.2-7.4 with 1M HCl and make up to a final volume of 25 ml.

Phosphate buffered saline (PBS) for immunofluorescence labeling of sections

pH 7.4, 0.01M phosphate buffer containing 0.15M NaCl

Stock solution A: 3.121 g Na H₂ PO₄ in 100 ml H₂O

Stock solution B: 7.144 g Na₂ H PO₄ in 100 ml H₂O

9.5 ml solution A + 40.5 ml solution B + 8.76 g NaCl,

make up to 1000 ml with deionised water.

Adjust pH with 1M HCl or 1M NaOH.

Isolation buffer for haustoria isolation

4,186 g MOPS buffer

68,46 g sucrose

2. 1. 7 Microscopic Equipment

A Zeiss Axiophot microscope (Carl Zeiss Jena, Jena, Germany) was used for bright field and epifluorescent imaging.

Confocal laser scanning microscopy was performed with a Leica TCS SP2 AOBS microscope (Leica Microsystems, Bensheim, Germany).

Confocal high throughput analysis was performed with the Opera microscope (Perkin Elmer).

2. 1. 8 Software

For statistical analyses Excel was used to perform a two-sided heteroscedastic t-test to determine the statistical significance of the difference between two sample means.

For general picture processing Adobe PHOTOSHOP 7.0 (Adobe Systems Inc., San Jose, CA, USA) was used.

The Leica software 'Leica Confocal Software', Version 2.61 (Leica Microsystems Heidelberg GmbH, Germany) was used to process images taken with the Leica Confocal microscope.

The software 'Acapella' Version 2.0 (Perkin Elmer Cellular Technologies, Germany) was used to process the images taken with the Opera microscope.

2. 2 Methods

2. 2. 1 Plant cultivation

A. thaliana seeds were sown on turf substrate (Stender Substrate, Wesel-Scharmbeck, Germany) including 0,001% Confidor WG70 (Bayer, Leverkusen, Germany) for protection against white flies. Seeds were stratified for two to three days at 4°C in complete darkness. To induce germination under protected conditions the seeds were transferred to a Vötsch growth chamber with a 12 h light period and 60% humidity. The temperature was regulated to 22°C during light period and 20°C during darkness.

Barley *Hordeum vulgare* cultivar Ingrid 10, was grown at 20°C, 70% relative humidity and a photoperiod of 16h light in a growth chamber.

2. 2. 2 Generation of Arabidopsis F₁ and F₂ progeny

Fine tweezers and a magnifying-glass were used to emasculate individual flowers. To prevent self-pollination, only flowers that had a well-developed stigma but immature stamen were used for crossing. Fresh pollen from three to four independent donor stamens was dabbed onto each single stigma. Mature siliques containing F₁ seed were harvested and allowed to dry. Approximately five F₁ seeds per cross were grown as described above and allowed to self pollinate. Produced F₂ seeds were collected and stored.

2. 2. 3 Inoculation procedures

Plants were grown in a Vötsch growth chamber in protected pathogen-free conditions for two weeks.

2. 2. 3. 1 Powdery mildews

Conidiospores of *B. g. hordei* colonies were transferred to *Arabidopsis* plants by gentle shaking. The inoculation procedure was performed using a settling tower to obtain an even distribution of the spores on the leaf surface of the test plants.

Conidiospores of *E. pisi* or *G. orontii* were transferred to *Arabidopsis* plants by gently touching the leaves with heavily sporulating (inoculum plant) pea or *Arabidopsis* plants, respectively.

2. 2. 3. 2 *Magnaporthe grisea*

A spore suspension was prepared from two week old cultures grown on Potato Dextrose Agar plates, by adding 5 ml sterile water to the plate and rubbing the surface with a glass rod or wire loop. To remove mycelial fragments, the suspension of spores was filtered through Mira cloth into a 15 ml centrifuge tube. Next, the suspension was centrifuged at 3000 rpm for 5 min and resuspended to the desired concentration (e.g. 1×10^4 to 2×10^5 per ml) in sterile water using a haemocytometer to count the spores. For plant inoculation 5-10 μ l droplets were placed onto the leaves. Inoculated plants were incubated in a sealed propagator at 25°C. To maintain 100% humidity inside the propagator, water was sprayed into the propagator lid before inserting the plants.

2. 2. 3. 3 *Colletotrichum* species

3 ml of spore suspensions were dispersed over Mathur's agar medium (Mathur et al., 1950), dispensed in 250 ml Erlenmeyer flasks and cultured at 20-25°C (Sherriff et al., 1994). Conidia

could be harvested at any time from 6-30 days, but 7-10 days was optimum for sub-culturing. For the harvest of conidia, 5 ml of sterile water was added to each flask and the flasks were vigorously shaken to suspend the conidia. For plant inoculation a fungal spore suspension was prepared in 15 ml sterile water by vigorous shaking of the Erlenmeyer flask. Spore concentrations were determined by use of a haemocytometer and spore-suspensions were diluted to the desired concentrations (1×10^5 spores/ml) in sterile water. Plants were spray-inoculated using an atomiser or 1 μ l droplets were placed on the leaves and inoculated plants were sealed inside a plastic propagator. The lid of the propagator was sprayed with sterile water to provide 100 % relative humidity. The propagators were incubated at 25°C in a growth chamber with a 16 h photoperiod and a PPFR of 80 $\mu\text{mol m}^{-2} \text{s}^{-1}$ and 81 % relative humidity.

2. 2. 3. 4 *Phacopsora pachyrhizi*

The Urospores of heavily sporulating soybean leaves were harvested. *Arabidopsis* plants were inoculated with a urosporesuspension (1 mg/ml spores in 0,01% (v/v) Tween20 in deionised water) by spraying. Inoculated plants were sealed inside a plastic propagator and the lid of the propagator was sprayed with sterile water to provide 100 % relative humidity. After 24 h the lid was removed and plants were grown under normal conditions.

2. 2. 3. 5 *Hyaloperonospora parasitica*

H. parasitica isolates were maintained as mass conidiosporangia cultures on leaves of their genetically susceptible *Arabidopsis* ecotypes over a 7 day cycle. Leaf tissue from infected seedlings was harvested into a 50 ml Falcon tube 7 days after inoculation. Conidiospores were collected by vigorously vortexing harvested leaf material in sterile dH₂O for 15 sec and after the leaf material was removed by filtering through miracloth (Calbiochem) the spore suspension was adjusted to a concentration of 4×10^4 spores/ml dH₂O using a Neubauer counting cell chamber. Plants to be inoculated had been grown under short day conditions. *H.*

parasitica conidiospores were applied onto 2-week-old seedlings by spraying until imminent run-off using an aerosol-spray-gun. Inoculated seedlings were kept under a propagator lid to maintain a high humidity atmosphere and incubated in a growth chamber at 18°C and a 10 h light period.

2. 2. 4 Staining procedures for co-localization studies

To stain *Arabidopsis* leaves with FM4-64 or Sirofluor, the leaves were vacuum infiltrated three times for 5 - 10 minutes. To analyse callosic papillae in barley, the leaves were cut into pieces of 1 cm and vacuum infiltrated with Sirofluor three times for 10 minutes.

Leaves were subsequently imaged by confocal microscopy.

2. 2. 5 Assessing host entry rates

To score the host entry rate, *Arabidopsis* leaves were destained in 70% ethanol over night. Destained leaves were incubated overnight in Aniline blue staining solution for visualizing callose deposition. To visualize extracellular fungal structures, i.e. spores, leaves were dipped in 0,25% Coomassie Blue staining solution, rinsed in water twice and mounted on microscopic slides. Fungal entry was scored using GFP-filter settings at a Zeiss Axiophot instrument

2. 2. 6 Quantification of haustorial encasements

Two week old transgenic plants were inoculated with the adapted *G. orontii*. For every genotype tested, five plants were analysed at 24 hpi and 72 hpi. One cotyledon per plant was harvested to score haustoria encased by a particular fluorescent fusion protein by confocal microscopy. The remaining cotyledon was harvested to score the number of fungal penetration sites and callose-encased haustoria by light microscopy. For this purpose, the leaves were cleared and then stained with Aniline blue.

To score fluorescent fusion protein containing haustorial encasements, all 5 cotyledons were examined by confocal microscopy. To score the number of penetration sites, host entry rate and the percentage of callose-encased haustoria, two leaves were analysed and the data were extrapolated for five cotyledon.

2. 2. 7 Isolation of haustorial complexes

Three week old plants were heavily infected with *G. orontii* and leaves were harvested 7 – 9 days past inoculation. Leaves were transferred into a beaker containing cold water. By gently shaking the beaker spores and dirt should be removed and leaves were rinsed under running tap water. Next, water was blotted off with tissue paper to weight the leaves. Leaves were placed into a pre-cooled homogenizer cup. 20 g of leaves were homogenised for 1 min in 100 ml cold Isolation Buffer (see 2. 1. 6). The homogenate was filtered through a 26 µm nylon mesh. The solid material was re-homogenised and again filtered, which was repeated once more. The pooled homogenate was then spined down at 1080 g for 15 minutes at 4°C and the pellet was resuspended in 5 ml Isolation buffer. Next the suspension was added onto 5 ml cushions of 1,085 sg Percoll and centrifuged at 720 g for 15 minutes at 4°C. The upper layer was removed and the lower Percoll layer diluted to 50 ml with Isolation buffer. The Sample was centrifuged at 1080 g for 15 minutes at 4°C. Again the supernatant was removed and the pellet resuspended in 5 ml Isolation buffer. The suspension was layered onto 5 ml cushions of

1,085 sg Percoll and centrifuged at 720 g for 15 minutes at 4°C. The upper layer was removed and the Percoll layer diluted to 50 ml with Isolation buffer. Then again centrifuged at 1080 g for 15 minutes at 4°C and the pellet was resuspended in 100 µl Isolation buffer. The quality and frequency of isolated haustoria was estimated by light microscopy using a haemocytometer.

2. 2. 8 Fixing and embedding of haustoria for Immunocytochemistry

Isolated haustoria (see 2. 2. 7) were resuspended in a glass vial containing 4% formaldehyde (w/v) and 0.5% (v/v) glutaraldehyde in sodium phosphate buffer (pH 7.2, 0.05 M). Fixation was continued at 4 °C overnight with continuous gentle agitation on a rotator. On the next morning the sample was rinsed in 0.05 M phosphate buffer (3 changes, 10 min). To facilitate further processing, the fixed, washed haustoria were embedded in 2% (w/v) low gelling temperature agarose. The haustoria were then spined down at high speed in a PCR tube and after solidification of the agarose on ice, the gel was cut into small blocks (1 mm³) and transferred into glass vials for dehydration. Dehydration was performed through increasing concentrations of ethanol in water: 25% (30 min), 50% (30 min), 70% (1h), 90% (1h), 100% ethanol dried over molecular sieve (2 changes, 1h each). Subsequent resin embedding was done slowly. LR White resin in ethanol was infiltrated in increasing concentrations as follows:

The procedure was started with 2 ml ethanol:

Add 0.5 ml resin	20%	(30 min)
Add 1 ml resin	40%	(30 min)
Add 2 ml resin	60%	(1 h)
Add 4 ml resin	80%	(1 h)

Next the solution was replaced with 100% resin (1 h), and then replaced with fresh 100% resin twice a day for 3-4 days. The single agarose cubes were transferred into empty ‘plastic pills’ and

polymerized at 50°C for 48 h in an oven. It is important that this process is performed in an oxygen free environment.

2. 2. 9 Poly-L Lysine coating of Multiwell Microscope Slides

The slides were soaked for 1 h in glassware-cleaning detergent in warm water. Afterwards, the surfaces of the slides were gently scrubbed with paper towel soaked in detergent. Then the slides were rinsed in running tap water for 5 minutes and subsequently soaked for 2 h in 5% acetic acid, after that rinsed in running tap water for 5 minutes. The slides were rinsed again in deionised water and subsequently polished dry with a tissue. Afterwards, the slides were immersed in a 0,01% aqueous solution of poly-L-lysine for 10 minutes (or place 20 µl droplets per well in multiwell slides) and finally the excess of solution was shook off and was air-dried on the bench (covered to avoid dust contamination).

2. 2. 10 Assembling of ultrathin sections

Fresh glass knives were prepared. Embedded cell blocks were sectioned with a glass knife on a Leica Ultracut R microtome into 700 nm sections. The sections were collected on Poly-L Lysine coated Multiwell Microscope Slides (see 2. 2. 9).

2. 2. 11 Immunofluorescence labeling of sections

The slides were rinsed in phosphate-buffered saline (PBS) for 2 minutes by immersion in a staining trough. Excess buffer was shaken off or blot away and immediately treated with block buffer (PBS containing 5% (v/v) normal goat serum and 6% (w/v) bovine serum albumin), 10 μ l per well for 15-30 minutes (to block non-specific binding). Afterwards excess block buffer was carefully blotted off with a tissue and replaced with 10 μ l of an appropriate dilution of the primary antibody, then incubated in a tightly sealed box lined with moist tissue paper for 60 minutes at room temperature or overnight at 4°C. Next, the slides were rinsed with a gentle stream of PBS from a Pasteur pipette, then by immersion in staining troughs (2 x 5 minutes in PBS). Afterwards the Goat anti-rabbit secondary antibody conjugated with fluorescein (GAR-FITC) was diluted 1:50 in PBS and centrifuged at 10,000 x g for 5 minutes to remove particulate contaminants, only the supernatant was taken. Then the surplus PBS was shaken off the slide treated with GAR-FITC, 10 μ l per well, for 30-60 minutes in a humid box in the dark. Afterwards again the slides were rinsed with a gentle stream of PBS from a Pasteur pipette, then by immersion in staining troughs (2 x 5 minutes in PBS). Finally, the slides were mounted under a coverslip in PBS, or preferably in antifade mountant, e.g. Vectashield or Citifluor.

2. 2. 12 EMS-Mutagenesis of *Arabidopsis* seeds

10 000 seeds were imbibe in a humid chamber and left at 4°C for 4 days. A 50 ml Falcon tube was filled with 50 ml deionised water and 0,15 ml of 0,3% methanesulfonic acid ethyl ester (EMS) solution was added and shaken until it is homogenous. Subsequently, the seeds were added and incubated for 9 h on a shaker. After mutagenesis the EMS solution was carefully decanted and the seeds were washed eight times with 45 ml water. For planting, the seeds were transferred to 1 l of 0,08% agarose solution and 5 ml were pipetted per TEKU soil pot (approximately 50 seeds per TEKU).

2. 2. 13 Confocal Laser scanning microscopy

Confocal laser scanning microscopy was performed with a Leica TCS SP2 AOBS microscope equipped with an Argon/Helium-Neon laser and diode laser of 405 nm. Detached leaves of two to three weeks old plants were mounted in 0,01% Tween20 on microscopic slides for imaging. Excitation of the samples was performed at 488 nm for GFP, at 514 nm for mYFP and 405 nm for cCFP. Emission spectra were taken from 490 to 560 nm for GFP, at 518 to 578 nm for mYFP, and 435 to 500 nm for cCFP. Aniline blue stained samples were excited using the 495 nm diode laser and the emission was taken from 410 to 480 nm. For FM4-64 stained samples the excitation was set to 561 nm and fluorescence emission was measured from 570 to 630 nm. Fluorescein in the immunofluorescence experiment was excited at 488 nm, emission was taken from 490 to 600 nm. Images were processed using the Leica Confocal Software Version 2.61 and Adobe PHOTOSHOP 7.0.

2. 2. 14 Confocal high throughput imaging

Confocal high throughput imaging was performed with the Perkin Elmer Opera microscope, which reveals four laser based excitation sources 405, 488, 561, 635 nm. Additionally, it is equipped with three 1.3 MPixel CCD cameras with a nipkov disk. Excitation of the samples was performed at 488 nm for GFP. The emission spectrum was taken from 502 to 577 nm.

2. 2. 15 Preparation of leaves for high throughput screening

For high throughput imaging the leaves were prepared in 96-well microplates. For leaf preparation a particular stamp was designed (Figure 1), which fulfilled several functions: it facilitated the leaf preparation, it fixed the leaves in the wells and it flattened the leaf during

imaging. The stamp contained 96 pins with a soft tissue out of neoprene on top to prevent damage of the leaves. A fine film of Vaseline® was distributed on the neoprene tissue to render it sticky. Detached cotyledons of two to three week old *Arabidopsis* plants were placed upside up onto the stamp. Both cotyledons of each plant were imaged. Due to technical reasons the pins at the margins were left free, resulting in 60 leaves from 30 plants on the stamp. The fully loaded stamp was then turned upside down and inserted into a water filled 96-well microplate with a optical glass bottom. Finally, the plate was ready for imaging. Since the Opera microscope is an inverted microscope the stamp could be left on the plate during imaging.

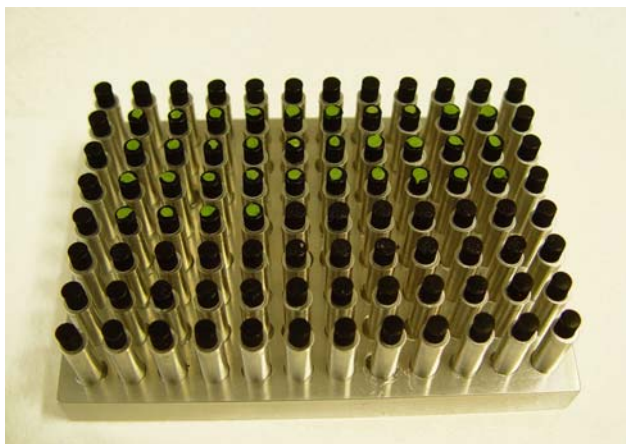


Figure 1. Stamp for *Arabidopsis* leaf preparation for high-throughput imaging with the Opera microscope.

The stamp is used to facilitate transfer of leaves to a microplate for high throughput imaging with the Opera microscope. It also serves to fix and flatten the leaf in the well during the imaging process.

2. 2. 16 Processing of high throughput images

For the high throughput imaging certain areas have to be defined for imaging. For high throughput screening (see 3.2.6) and multiparametric analysis of GFP-PEN1 FA (see 3.2.5), eight areas per leaf were defined, (Figure 2). With the usual pathogen inoculation procedure (see 2.2.3) it was expected that around 10 GFP-PEN1 FAs were recognized in one imaged area.

Because two leaves per plant were processed, around 160 GFP-PEN1 FAs were analysed per plant, which was sufficient for statistical analysis.

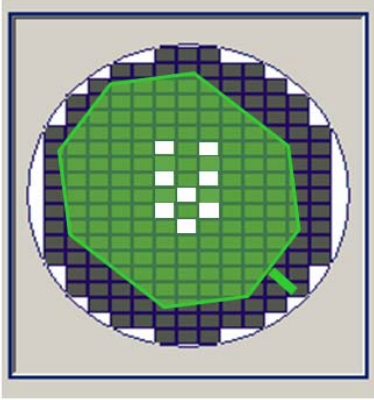


Figure 2. Schematic drawing of one well of a 96-well microplate containing one leaf for imaging.

The picture exhibits one well of a 96-well microplate. Several areas can be defined for imaging (gray boxes). In this study eight areas (white boxes) per cotyledon (depicted in green) were imaged.

Due to the natural curvature of leaves the epidermal cells, the subject of investigation, were not in the same optical plane. Thus, images of a consecutive series of 31 planes, in the z-direction (z-stack) with a distance of 1 μm were taken per area (Figure 3).

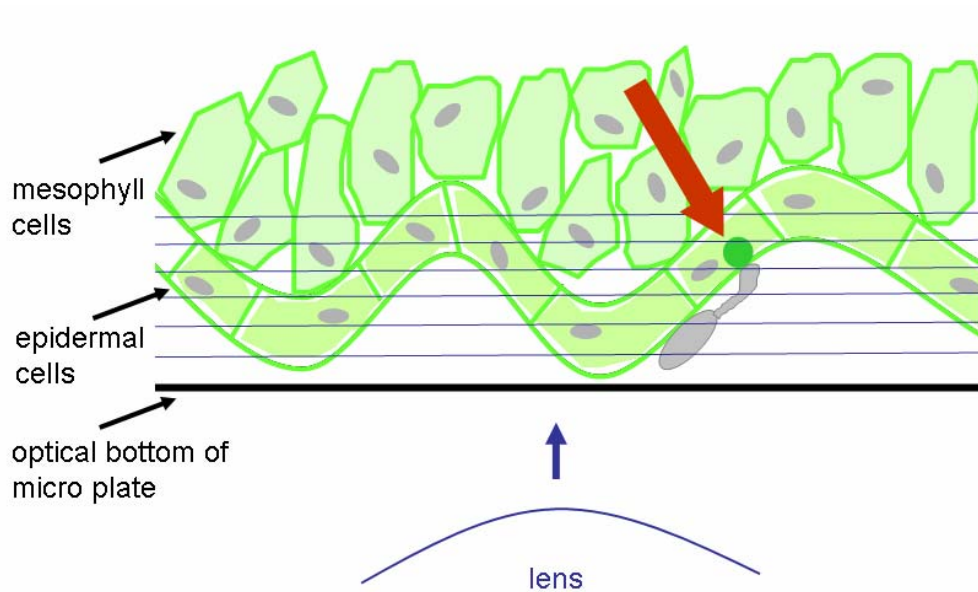


Figure 3. To capture the epidermal cells a consecutive series of optical planes in the Z-direction were imaged .

Arabidopsis plants were inoculated with fungal pathogens (germinated fungal spore on the leaf surface is depicted in grey) and detached cotyledons were imaged 24 or 48 hpi. The GFP-PEN1 FA (red arrow) can be detected in the epidermal cells. To image the epidermal cells a consecutive series of 31 optical planes per area, in z-direction was taken (optical planes are depicted as blue lines).

2. 2. 17 Image processing and automated analysis

The images were automatically analysed with the Acapella Software. To merge the three-dimensional stack of 31 optical planes, an image projection was performed, resulting in a two-dimensional ‘pseudoimage’. Subsequently, the pseudoimage was analysed with a ‘pattern recognition script’, specifically identifying GFP-PEN1 FAs. We developed the script in collaboration with Perkin Elmer. Besides the analysis of GFP-PEN1 FAs, also the numbers of epidermal leaf cells and stoma were analysed, resulting in 19 output parameters, which are listed and described in table 4. To facilitate and fasten the analysis of the output results we

generated a script for a graphical presentation of the output data with respect to the different parameters. For every parameter and microplate one graph displayed the results.

Table 4. Description of the output parameters measured in the automated high-throughput imaging

	output parameter	description
1	Number of FAs	number of GFP-PEN1 focal accumulations
2	Number of GFP-PEN1 encased haustoria	number of GFP-PEN1 encased haustoria
3	Number of FAs per analysable area	number of GFP-PEN1 focal accumulations per recognized leaf area (epidermal cell area)
4	Number of FAs per cell	number of GFP-PEN1 focal accumulations per epidermal cell
5	Total integrated FA signal per analysable area	integrated GFP signal of all GFP-PEN1 focal accumulations identified in the recognized leaf area
6	Total integrated FA signal per analysable area, background subtracted	integrated GFP signal of all GFP-PEN1 focal accumulations identified in the recognized leaf area; here the background signal was subtracted from the GFP signal
7	Average intensity of FA	average intensity of the GFP signal of all GFP-PEN1 focal accumulations
8	Average area of FA	average area of all GFP-PEN1 focal accumulations
9	Total integrated FA signal, over all FAs	integrated GFP signal of all GFP-PEN1 focal accumulations
10	Total integrated FA signal, background subtracted, over all FAs	integrated GFP signal of all GFP-PEN1 focal accumulations; here the background signal was subtracted from the GFP signal
11	Average length of FA	average length of all GFP-PEN1 focal accumulations

Table 4 continued

	output parameter	description
12	Average half width of FA	average radius of all GFP-PEN1 focal accumulations
13	Average width to length ratio of FA	average width to length ratio of all GFP-PEN1 focal accumulations
14	Average roundness of FA	average roundness of all GFP-PEN1 focal accumulations
15	Average contrast of FA compared to the background signal	average contrast between the GFP signal of the GFP-PEN1 focal accumulation and the background signal
16	Average peak intensity of FA	of all GFP-PEN1 focal accumulations the brightest pixel is taken into account, the average value of these is the average peak intensity
17	Integrated FA signal per analysable area background subtracted per FA	integrated GFP signal of all GFP-PEN1 focal accumulations identified in the recognized leaf area, divided by the number of GFP-PEN1 focal accumulations identified; here the background signal was subtracted from the GFP signal
18	Number of epidermal leaf cells	number of epidermal leaf cells
19	Number Of Stoma	number of stoma

3. Results

3.1 Specificity of GFP-PEN1 focal accumulation

3.1.1 Association of GFP-PEN1 focal accumulation with attempted host cell entry by adapted and non-adapted direct penetrating fungi

GFP-PEN1 has been shown to focally accumulate at attempted fungal penetration sites in the interaction between *Arabidopsis* and the non-adapted powdery mildew *Blumeria graminis* f. sp. *hordei* (*B. g. hordei*) (Assaad et al., 2004; Bhat et al., 2005). To reveal the specificity of the GFP-PEN1 focal accumulation (FA), diverse pathogenic interactions involving direct penetrating fungi were analysed. An *Arabidopsis* line expressing GFP-PEN1 driven by the 35S promoter in the *pen1-1* null mutant background was used. Two to three week old plants were inoculated with different pathogens, and analysed by confocal microscopy 24 hours post inoculation (hpi) (Figure 4). After germination, powdery mildews develop an appressorial germ tube. They mainly release enzymes to penetrate the cell beneath the tip of the appressorial germ tube following differentiation of the appressorium (Belanger and Bushnell, 2002). GFP-PEN1 FA can be observed at penetration entry sites in interactions of *Arabidopsis* with the non-adapted barley powdery mildew *B. g. hordei* (Figure 4 a, b) or pea powdery mildew *Erysiphe pisi* (Figure 4 c, d) and with the adapted *Arabidopsis* powdery mildew *Golovinomyces orontii* (Figure 4 e, f). Furthermore, for the powdery mildews tested, I noted the GFP-PEN1 FA in successful and non-successful interaction sites (Figure 4 e, f), suggesting that the accumulation of GFP-PEN1 at attempted fungal entry sites does not restrict entry of the invader and is not required for fungal entry.

To determine whether this phenomenon is specific for the powdery mildew interaction or whether it is also detectable at attempted penetration sites of other pathogens, I analysed the

pathogen entry sites of diverse other directly penetrating pathogens that similar to powdery mildews belong to the class of ascomycetes and show a similar mode of entry into plant cells. The pathogens tested were *Magnaporthe grisea*, causing rice blast disease, and *Colletotrichum* species causing anthracnose. In contrast to powdery mildews, they form a specialized infection structure, the melanised appressorium, which generates an enormous turgor pressure to forcefully penetrate the host cell (Bourett and Howard, 1990; Perfect et al., 1999; O'Connell et al., 2004). Interestingly, the GFP-PEN1 FA was absent from the penetration sites of the non-adapted rice blast fungus *M. grisea* (Figure 4 g, h). Furthermore, GFP-PEN1 FA was not detectable at entry sites of the non-adapted Medicago anthracnose fungus *C. destructivum* (Figure 4 i, j). For the interaction with the adapted crucifer anthracnose fungus *C. higginsianum* a GFP signal was not detectable at non-successful penetration sites (Figure 4 k, l) or at successful penetration sites (Figure 4 m, n).

Another pathogen tested was the oomycete *Hyaloperonospora parasitica*, the causal agent of downy mildew. It produces an infection hypha that forces its way into the leaf along the middle lamella between adjacent epidermal cells, penetrating epidermal and mesophyll cells (Chou, 1970). For the interaction between *Arabidopsis* and the adapted oomycete *H. parasitica* GFP-PEN1 FA was not detectable at attempted entry site (data not shown).

Negative controls with inoculated, non-GFP-expressing wild type leaves showed no fluorescent signal at papillae, demonstrating that the signal seen with GFP-PEN1 was not due to autofluorescence (data not shown). Concluding, from all pathogens tested only at interaction sites with powdery mildews the GFP-PEN1 FA was detectable.

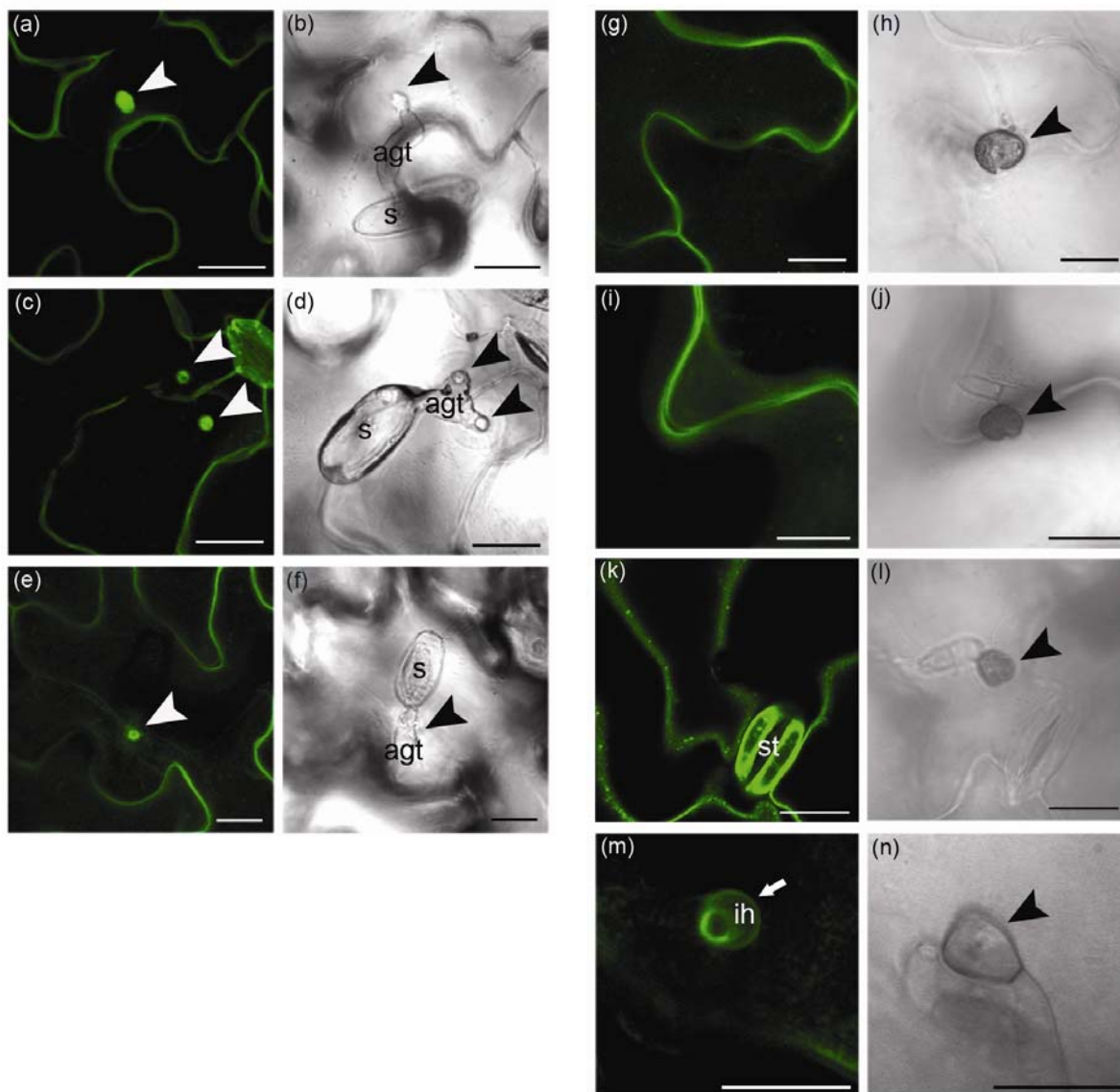


Figure 4. The focal accumulation of GFP-PEN1 in Arabidopsis epidermal cells is associated with both non-adapted and adapted powdery mildews, but does not occur in interactions with either non-adapted rice blast or adapted or non-adapted anthracnose fungi.

Arabidopsis plants expressing GFP-PEN1 were inoculated with a range of directly penetrating fungal pathogens and viewed by confocal microscopy at 24 hpi. The left column shows GFP-PEN1 fluorescence, the right column shows the corresponding bright field images. GFP-PEN1 focally accumulates at sites of attempted penetration (arrowheads) by the non-adapted powdery mildews *Blumeria graminis* f. sp. *hordei* (a, b) and *Erysiphe pisi* (c, d) and the adapted powdery mildew *Golovinomyces orontii* (e, f). Note that each spore of *E. pisi* makes one to three penetration attempts. GFP-PEN1 accumulation is not visible at attempted entry sites underneath melanized

Results

appressoria (black arrows) of the non-adapted rice blast-fungus *Magnaporthe grisea* (g, h) and Medicago anthracnose fungus *Colletotrichum destructivum* (i, j). No GFP-PEN1 focal accumulation was detectable neither at a non-successful entry site (k, l) nor at a successful entry sites (m, n) of the adapted Crucifer anthracnose fungus *C. higginsianum*, where an intracellular hypha (white arrow) has invaded the cell, although GFP-PEN1 is present at the invaginated host plasma membrane around the hypha.

agt, appressorial germ tube; ih, intracellular hypha; s, spore. Bar = 20 μm .

To prove successful entry at interaction sites with the non-adapted rice blast fungus *M. grisea* and the non-adapted anthracnose fungus *C. destructivum*, where no GFP-PEN1 FA was detectable, papillae were stained (Figure 5). Papillae are believed to play a crucial role in preventing pathogen entry, and callose is a component of papillae (Belanger and Bushnell, 2002). Callose can be stained by Sirofluor, which is a chemically defined fluorochrome, purified from Aniline blue, and visualized by its blue fluorescence under UV excitation. At attempted fungal entry sites of *M. grisea* and *C. destructivum* callose containing papillae were deposited (Figure 5 b and f), but GFP-PEN1 FA could not be detected in co-localization experiments (Figure 5 a and e).

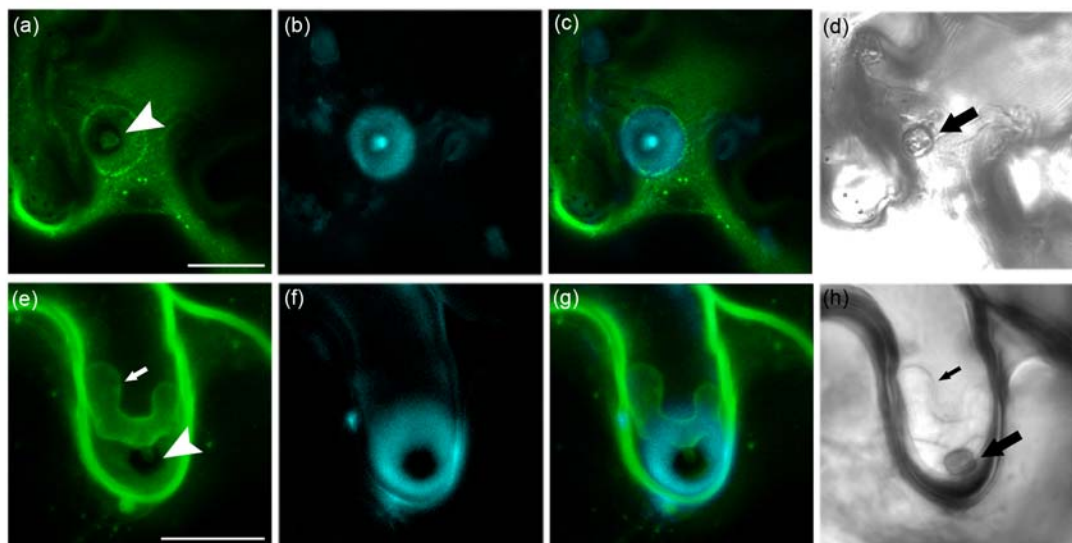


Figure 5. GFP-PEN1 focal accumulation can not be detected after successful penetration of the non-adapted rice blast-fungus *Magnaporthe grisea* or the non-adapted anthracnose fungus *Colletotrichum destructivum*.

Plants expressing GFP-PEN1 were inoculated with the non-adapted rice blast-fungus *M. grisea* (a-d) or the Medicago anthracnose fungus *C. destructivum* (e-h). The leaves were analysed by confocal microscopy at 24 hpi for *M. grisea* and at 48 hpi for *C. destructivum*. For *M. grisea* single optical sections (1 μm) are shown, while for *C. destructivum* a projection of nine optical sections (9 μm) is depicted. For simultaneous detection of callose, the leaves were vacuum infiltrated with Sirofluor. *M. grisea* penetrates the plant epidermis underneath the melanised appressorium (big arrow, d). (a) At the entry site (arrowhead) GFP-PEN1 accumulation can not be observed; a halo harbouring GFP-PEN1 is visible around the penetration site. (b) The Sirofluor staining shows a callose-containing papilla at the entry site. (c) The overlay shows that the callose precisely fills the halo outlined by GFP-PEN1. (d) brightfield. (e) An intracellular hypha of *C. destructivum* surrounded by the GFP-PEN1 labelled plant plasma membrane (small arrows, e and h) is visible, but GFP-PEN1 focal accumulation was not observed at the penetration site (arrowhead). (f) A callose-containing ring surrounds the appressorium. (g) overlay. (h) brightfield.

Bar = 10 μm .

To test a fungus belonging to the class of basidiomycetes, I examined the interaction of *Arabidopsis* with the non-adapted rust fungus *Phakopsora pachyrhizi*, the causal agent of soybean rust (Koch et al., 1983). Rust fungi usually enter their host by formation of an appressorium over a stoma and subsequent penetration of the stomatal opening. *P. pachyrhizi*

is an exception, because its appressoria directly penetrate host epidermal cells through the cuticle. A penetration hypha (PH) developing from the appressorium directly penetrates epidermal cells (Koch et al., 1983).

The penetration occurs at around 24 hpi. A papilla could be detected in 5-10% of penetration attempts, associated with the arrest of fungal growth. If the penetration is successful and the PH invades the epidermal cell, a callose encasement of the PH can be observed, leading to cell death (K. Göllner, pers. communication). I could not detect GFP-PEN1 FA at entry sites at 24 hpi, but it was visible at 48 hpi around the PH (Figure 6).

The data demonstrates a co-localization of GFP-PEN1 and callose around the PH, but not at fungal entry sites. One possible explanation could be that at the sites with no detectable GFP-PEN1 no papilla was generated. The formation of papillae was assumed when a fungal penetration peg was visible. Callose stainings would provide more definite proof. Another possibility could be that the FA is suppressed during initial papilla formation but not during later development of the PH. This is consistent with findings from Skalamera et al. (1997), who examined the interaction between cowpea (*Vigna unguiculata*) and the monokaryotic stage of the cowpea rust fungus *Uromyces vignae*. The authors found callose deposits around the tip of the invasion hypha, growing inside the epidermal cell at a much higher percentage, compared to the initial penetration site. After the fungus was killed by heat shock, callose deposition was found around the penetration region, suggesting an active suppression of papilla formation of the fungus during initial penetration.

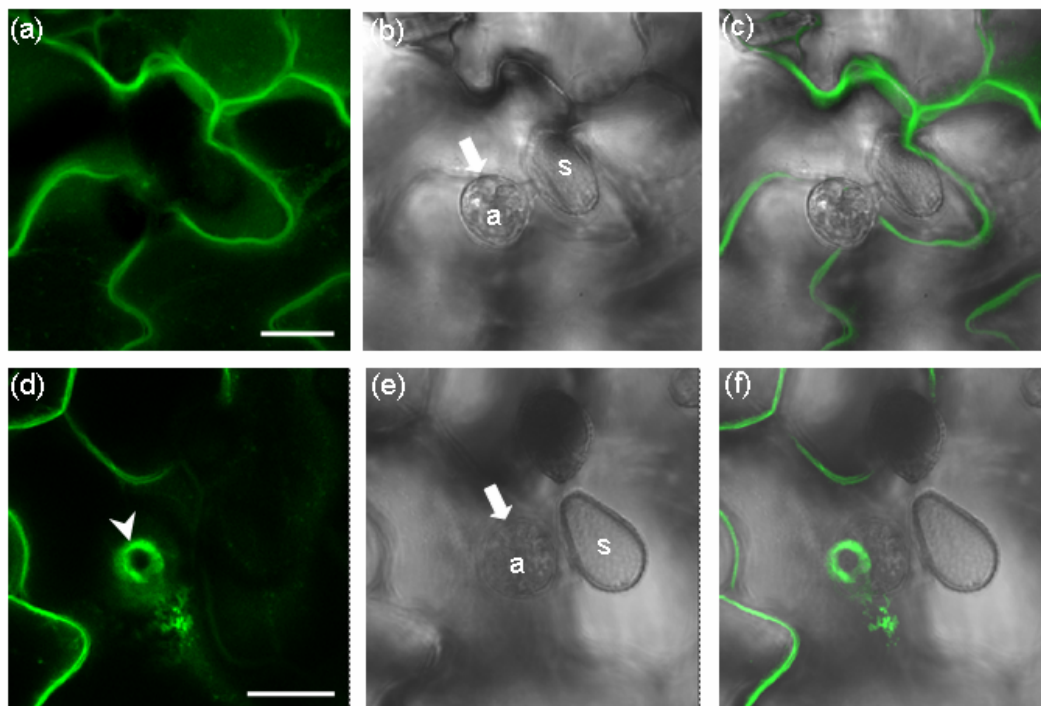


Figure 6. GFP-PEN1 accumulates around the penetration hypha of the rust fungus *Phakopsora pachyrhizi*. Plants expressing GFP-PEN1 were inoculated with the soybean rust fungus *Phakopsora pachyrhizi*. Focal accumulation of GFP-PEN1 is not detectable at the penetration site beneath the appressorium (arrow, b) at 24 hpi (a-c). However, after invasion of the fungal penetration hypha (PH) into the host epidermal cell at 48 hpi (d-f) a fluorescent signal is observed around the PH (arrowhead, d). a, appressorium; s, spore. Bar = 20 μ m.

3. 1. 2 GFP fluorescence in papillae of GFP-PEN1 plants remains stable over time

The finding that the GFP-PEN1 FA could be observed at papillae prompted me to investigate its longevity. Therefore, I examined FAs of *Arabidopsis* plants expressing GFP-PEN1 at 7, 10 and 14 days past inoculation (dpi) with *B. g. hordei*. To identify the GFP-emission spectrum and to quantify the GFP-fluorescence intensity, fluorescence emission spectrum analysis was

performed by confocal microscopy. Therefore, the leaf sample was excited with fluorescence light between 500 and 564 nm and the emission was detected. GFP specifically shows an emission peak at 509 nm and can thus be identified. GFP fluorescence was detectable at attempted penetration entry sites at 7, 10 and 14 dpi. The data shown is an example for a typical interaction site from 20 sites tested. Figure 7 shows the spectral identification of GFP and the fluorescence intensity at a typical penetration site at 14 dpi. The emission spectrum for GFP-fluorescence peaks at 510 nm, and the strongest fluorescence intensity was detected at the fungal penetration site (Figure 7 a, arrowhead, R1 and graphic d). The spectrum of this region also reveals the contribution of some autofluorescence, since a slight flattening of the signal rather than a sharp decrease was observed at wavelength higher than 509 nm. This was expected, since the accumulation of phenolics causing autofluorescence at papillae was reported previously (Nicholson and Hammerschmidt, 1992). The plant plasma membrane reveals fluorescence resulting from GFP (Figure 7 a, R2 and graphic d), indicated by the clear peak at 510 nm. Only minor background fluorescence was detectable in the epidermal cell cytoplasm, exhibited by R3 (Figure 7 a, graphic d). This could also be observed at 7 and 10 dpi (data not shown).

Together, it demonstrates that the signal at the penetration entry site is stronger compared to the signal at the plasma membrane or the background signal, hinting to the accumulation of GFP-PEN1 protein. The demonstration that a fluorescent signal is detectable at penetration sites at least 14 days, suggests that a stable, long lasting structure retain stable GFP-PEN1. Possibly, PEN1-containing vesicles accumulate inside the papilla.

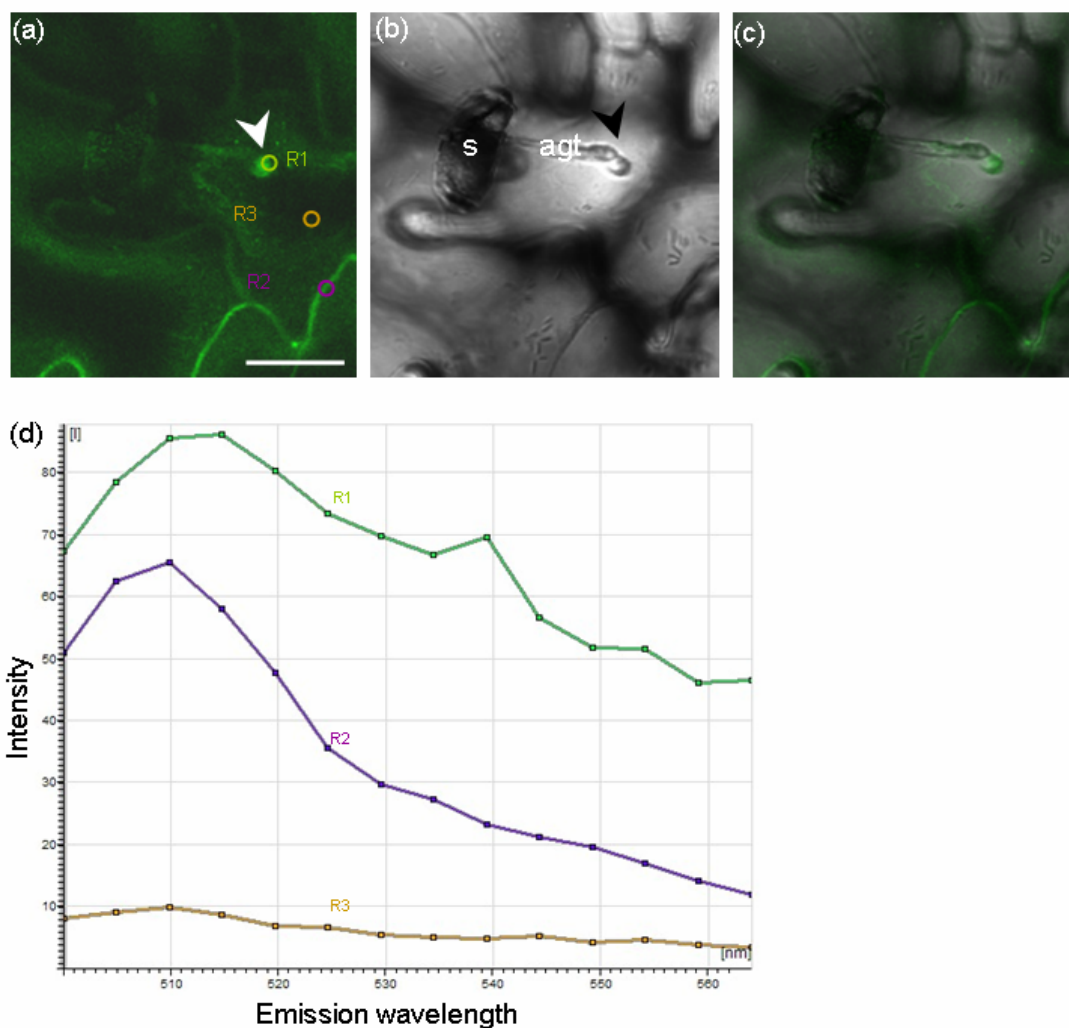


Figure 7. Spectral identification and quantification of fluorescence intensity in GFP-PEN1 focal accumulation sites.

Plants expressing GFP-PEN1 were inoculated with *Blumeria graminis* f. sp. *hordei*. Specific GFP fluorescence and fluorescence intensity of the focal accumulation of GFP-PEN1 were assessed at 14 dpi by performing a fluorescence emission spectrum with confocal microscopy. The epidermal cells were excited with a 488nm-laser-line and the spectral emission was recorded from 500nm to 564nm. (a) The image displays a single optical section (1 μ m) of the area that was measured. Three regions (R) were measured and indicated as R1 to R3. R1 is localized to the GFP-PEN1 FA of the penetration site (arrowhead), R2 is localized to the plant plasma membrane and R3 is localized to the epidermal cytoplasm. (b) A germinated spore is shown in the corresponding bright field picture. A papilla (arrowhead) is visible at the attempted penetration site. (c) Overlay of a and b. (d) The graphic shows the spectral identification and the fluorescence intensity of the regions of interest (R). agt, appressorial germ tube; R, region of interest; s, spore. Bar = 20 μ m.

Previous plasmolysis experiments have shown that after retraction of the plant plasma membrane at least a portion of the GFP fluorescence appears to be retained in papillae (pers. communication, S. Pajonk,). Moreover, Pajonk could detect a GFP-fluorescence signal located in the interior of papillae in optical cross-sections, observed by confocal microscopy. Taken together, the spectral analysis and the plasmolysis experiments indicate that the GFP-PEN1 signal is associated with cell wall appositions, outside the plant protoplast and the signal last at least for 14 days.

3. 1. 3 The GFP-signal spatially coincides with the location of callose at haustorial structures

Callose has been reported to play a host defence role by reinforcing the plant cell wall at attempted sites of parasite penetration or by providing a medium for the deposition of toxic compounds (Aist, 1976; Skou et al., 1984; Kováts et al., 1991). Callose also may contribute to host defence by impeding nutrient uptake or by delaying pathogen growth to gain time for other host defences (Allen and Friend, 1983). However, *gsl5/pmr4* callose synthase mutants show enhanced disease resistance against normally virulent powdery mildew *Golovinomyces orontii* and against the oomycete *Hyaloperonospora parasitica* (Jacobs et al., 2003) (Nishimura et al., 2003). The data demonstrates that callose deposition *per se* does not necessarily terminate pathogen growth.

After successful penetration of host epidermal cells, the fungus develops a haustorium that invaginates the plant plasma membrane. Haustoria can become encased by a callose-containing material, which can form a collar around the haustorial neck as an extension of the papilla, and can extend over the haustorial body and eventually enclose the entire haustorium (Bushnell, 1972). For oomycetes it was reported that 48% of haustoria present at 5 dpi are encased by callose in the adapted interaction between *Hyaloperonospora parasitica* and *Arabidopsis* (Donofrio and Delaney, 2001). Also, rust haustoria become encased by callose (Heath and Heath, 1971; Aist, 1976; Skalamera et al., 1997). Skalamera et al. (1997) reported

a callose encasement of the tip of the invasion hyphae of the cowpea rust *Uromyces vignae*, whereas no callose was detectable at the penetration sites. The authors performed heat treatments to kill the fungus to investigate whether the absence of callose deposition at penetration sites is due to active suppression by the fungus during initial penetration. Since a greater proportion of fully encased invasion hyphae were found after killing the fungus, they concluded that the fungus suppresses callose encasement at the initial stage. It is generally suggested that the encasement of haustoria impedes or suppresses fungal invasion. Currently not much is known about the occurrence of callose encasements of powdery mildew haustoria during interactions with *Arabidopsis*.

To investigate the localization of GFP fluorescence at haustorial structures, two to three week old *Arabidopsis* plants expressing GFP-PEN1 in the *pen1-1* mutant background were inoculated with diverse directly penetrating pathogens, and haustoria were analysed 24 hpi. At this time point the majority of the adapted powdery mildew *Erysiphe cichoracearum* haustoria are fully developed with distinct lobes emerging from the haustorial body (Koh et al., 2005). To label callose, the tissue was stained with Sirofluor and visualized by confocal fluorescence microscopy (Figure 8). The GFP-PEN1 signal was restricted to haustorial encasements in all powdery mildew interactions tested, namely the non-adapted *B. g. hordei* (Figure 8 a, b) and *E. pisi* (Figure 8 c, d) and the adapted *G. orontii* (Figure 8 e, f). Furthermore, the GFP-signal spatially coincided with the callose signal. Plasmolysis experiments showed that the GFP-signal does not originate from the plasma membrane surrounding the haustorium (extrahaustorial membrane; pers. communication, S. Pajonk.), suggesting the GFP-PEN1 localizes to the interior of the callose encasement.

In the case of *H. parasitica* haustoria, the correlation of the GFP-signal and the callose signal (Figure 8 g, h) was only partial, as seen in a high magnification view of a haustorial encasement (Figure 8 h, inset).

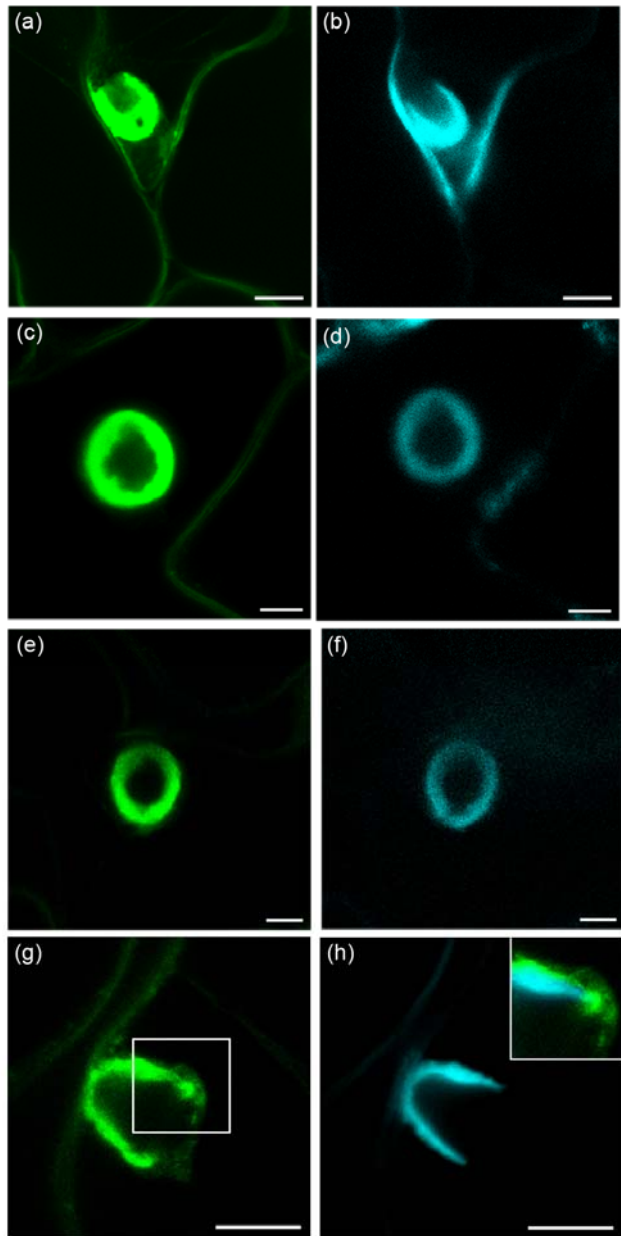


Figure 8. GFP-PEN1 and callose colocalize in the haustorial encasement.

Plants expressing GFP-PEN1 were inoculated with different haustorium-forming pathogens, and the haustorial encasements were analysed 24 hpi. To simultaneously detect callose the leaves were vacuum-infiltrated with Sirofluor, a chemically defined fluorochrome purified from Aniline blue. The left column shows GFP-PEN1 fluorescence, the right column shows blue fluorescent labeling of callose. The GFP signal spatially coincides

with the callose signal; this can be observed in interactions of *Arabidopsis* with the non-adapted *Blumeria graminis* f. sp. *hordei* (a, b) and *Erysiphe pisi* (c, d) and the adapted *Golovinomyces orontii* (e, f) powdery mildews. However, the fluorescence signals only partially colocalize in haustoria of the adapted downy mildew *Hyaloperonospora parasitica* (g, h), as seen in a high magnification view of the overlay of the green and blue channels (h, inset). Bar = 10 μ m.

Encasements of haustoria were observed in adapted as well as in non-adapted interactions between *Arabidopsis* and powdery mildews, suggesting that the encasement *per se* is not sufficient for defence. Also for rust fungi, callose encasements have been observed both in adapted and non-adapted interactions (Heath and Heath, 1971; Skalamera et al., 1997).

In the non-adapted *B. g. hordei*-*Arabidopsis* interaction haustoria became partially encased. To determine if the *B. g. hordei* haustoria get encased in the adapted interaction with barley, 7 day old barley leaves were inoculated with *B. g. hordei*. The leaves were vacuum-infiltrated with Sirofluor to label callose, and analysed by confocal microscopy. At 72 hpi clear callose-containing papillae were detectable, but the haustorial body or haustorial lobes were not encased by callose (Figure 9), suggesting that the adapted pathogen is able to fully suppress the callose deposition around haustorial structures at least for 72 hours.

Taken together, the *B. g. hordei* becomes partially encased in the non-adapted interaction with the dicotyledon *Arabidopsis* and not encased in the adapted interaction with the monocotyledon barley.

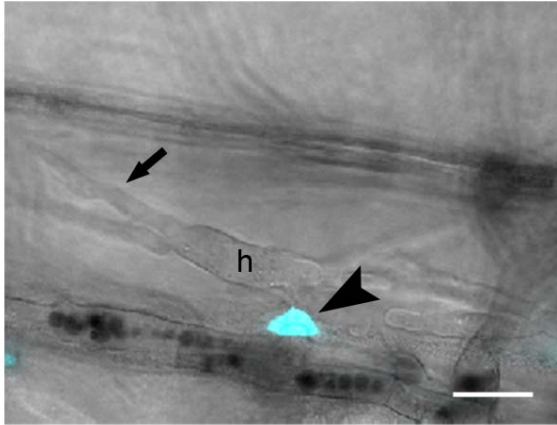


Figure 9. Fully developed haustoria of *Blumeria graminis* f. sp. *hordei* are not encased in the adapted interaction with barley.

Barley leaves were inoculated with the adapted powdery mildew *Blumeria graminis* f. sp. *hordei*. 3 dpi haustoria were analysed by confocal microscopy. To visualize callose, the leaves were vacuum infiltrated with Sirofluor. An overlay of two single optical sections (1 μm) shows a fully developed haustorium (h) with expanded lobe structures (arrow). Callose fluorescence could be detected at the penetration site (arrowhead) but not around the haustorial body or lobes.

h, haustorium. Bar = 20 μm .

3. 1. 4 Haustoria become encased by structures containing GFP-PEN1 and membrane material

Since PEN1 is a plasma membrane protein the detection of GFP-PEN1 within haustorial encasements raises the possibility that encasements contain host membrane material. Membrane structures were observed within cell wall appositions in several previous studies. From histochemical analysis, and freeze-etching electron micrographs of cabbage root hairs infected by *Plasmodiophora brassicae*, the causal agent of club root disease of crucifers, Aist reported as early as 1974 the presence of membranous, vesicular, and possibly lipoidal components embedded within papillae (Aist, 1976). More recently transmission electron microscopic studies revealed multivesicular compartments in *B. g. hordei*-induced papilla, suggesting polarized vesicle secretion of papilla building blocks and antimicrobial

compounds (An et al., 2006a). Analysing ultrathin sections by transelectron microscopy, Heath and Heath (1971) reported for the first time that rust haustoria get encased by callose, and they observed a highly convoluted host membrane around the haustorial body. Furthermore, they found portions of host cytoplasm and material of membranous appearance trapped in the encasement (Heath and Heath, 1971).

To detect membrane structures in haustorial encasements, the lipophilic styryl dye FM4-64 was used as membrane tracer. For this purpose, two to three week old *Arabidopsis* plants were challenged with different pathogens. After vacuum-infiltration of the leaf tissue with FM4-64, the haustorial complexes were analysed by confocal microscopy at 24 hpi. The labelling of haustorial encasements by GFP spatially coincided with the FM4-64 labelling, as depicted in Figure 10. This was observed with non-adapted *B. g. hordei* (Figure 10 a-c) and *E. pisi* (Figure 10 d-f) and with adapted *G. orontii* (Figure 10 g-i). Taken together, these results suggest that membranous material is trapped inside haustorial encasements. Moreover, this phenomenon is not restricted to powdery mildews, as it was also observed for fully developed haustoria of the downy mildew *Hyaloperonospora parasitica* at 72 hpi (Figure 10 j-l).

For all interactions tested the entire haustorium became encased except in the case of *B. g. hordei* haustoria, where the haustorium was only partially encased (Fig 10 c). One explanation for this could be that the encasement process is suppressed at a certain stage; alternatively the cell dies before the haustorium gets fully encased. A third possibility would be that a partially encased haustorium is sufficient to stop fungal growth.

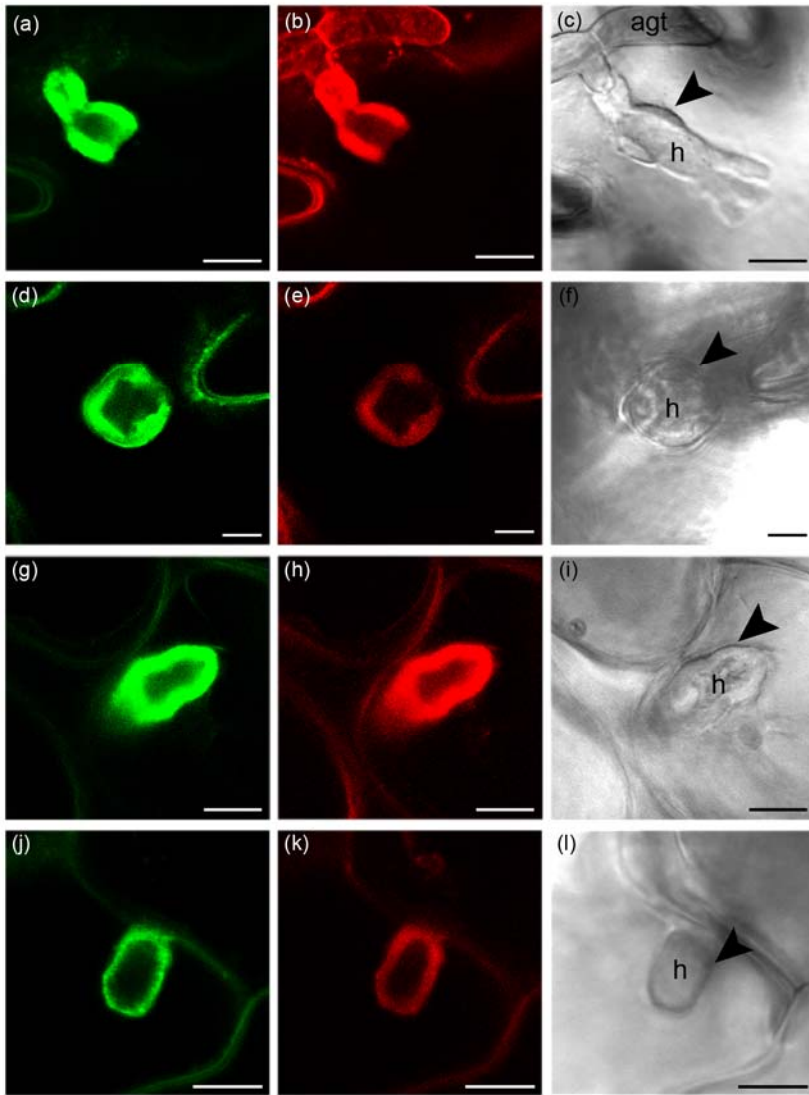


Figure 10. Haustoria become encased by structures containing GFP-PEN1 and membrane material.

Plants expressing GFP-PEN1 were infected with diverse haustorium forming pathogens and the haustorial encasements were analysed by confocal microscopy at 24 hpi for the powdery mildews and at 72 hpi for *Hyaloperonospora parasitica*. Single optical sections (1 μ m) are shown. The encasement of haustoria is observed in interactions with the non-adapted powdery mildews *Blumeria graminis* f. sp. *hordei* (*B. g. hordei*) (a-c) and *Erysiphe pisi* (d-f), the adapted powdery mildew *Golovinomyces orontii* (g-i) and the adapted downy mildew *Hyaloperonospora parasitica* (j-l). Panels in the left column show GFP-PEN1 fluorescence, panels in the middle column show the corresponding red fluorescence after staining with the membrane specific dye FM4-64 and panels in the right column show the corresponding bright field images. (a,d,g,f.) GFP-PEN1 signal is restricted to the haustorial encasement in all pathogen interactions tested. (b,e,h,k) Staining with the membrane

tracer FM4-64 reveals the presence of membranous material inside haustorial encasements. FM4-64 also labels membrane structures in the fungal and plant cells. Note that the haustorium of *B. g. hordei* is only partially encased (c). (c,f,i,l) Haustorial encasements (arrowheads) observed in the bright field channel.

agt, appressorial germ tube; h, haustorium. Bar = 10 μ m.

3. 1. 5 The haustorial encasement preferentially contains t-SNAREs

PEN1 is part of a SNARE-mediated secretion machinery involved in plant defence responses as reported by Kwon et al. (2008). The authors provide the first genetic evidence for a ternary SNARE complex function in plants. They showed that PEN1-SNAP33-VAMP721/722 complexes are required for immune responses to powdery mildew and oomycete pathogens (Kwon et al., 2008). To investigate whether SNARE proteins other than PEN1 accumulate in haustorial encasements, I tested diverse transgenic *Arabidopsis* lines, expressing fluorescent protein tagged t- or v-SNARE proteins (GFP-PEN1, CFP-Syp122, YFP-SNAP33 and GFP-VAMP722). In addition, to determine the specificity of PEN1 accumulation at haustorial structures, lines expressing fluorescent tagged plasma membrane marker proteins (PEN3-GFP, GFP-SIMIP, GFP-D41, GFP-PIP2a, GFP-29-1) were also analysed. The tested lines are listed in Material and Methods (2.1.1).

Two week old transgenic plants were inoculated with the adapted *G. orontii*. For every genotype, five plants were analysed at 24 hpi and 72 hpi. One cotyledon per plant was harvested to score GFP-PEN1-encased haustoria by confocal microscopy. The remaining cotyledon was harvested to score the number of fungal penetration sites and callose-encased haustoria by light microscopy. For this purpose, the leaves were cleared and then stained with Aniline blue.

Three different types of haustorial callose encasements were distinguished. Figure 11 shows haustoria exhibiting callose only at the haustorial neck (a), partially encased haustoria (Figure 11 b), and fully encased haustoria (Figure 11 c). For quantification both partially and fully encased haustoria were scored as 'encased', whereas haustoria with callose only at the neck were considered unencased. The same phenomenon was observed for the GFP-PEN1 labelled

Results

encasements (Figure 12), and similarly, only partially and fully encased haustoria were considered encased.

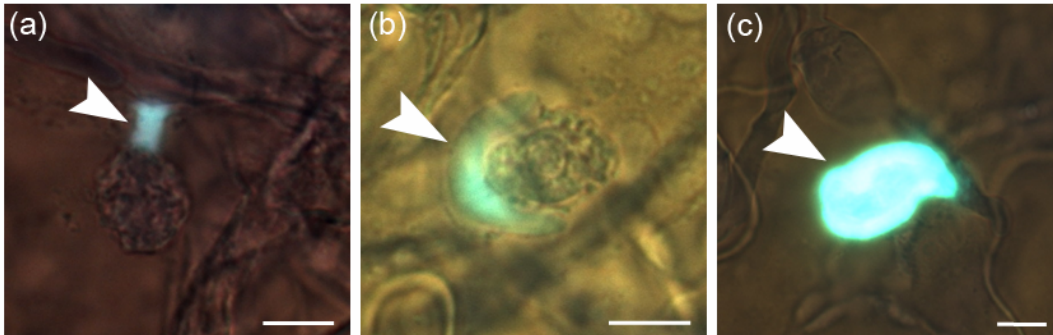


Figure 11. Haustoria become callose-encased in the adapted interaction between *Arabidopsis* and the powdery mildew *Golovinomyces orontii*.

Wild type plants were inoculated with *G. orontii*. At 3 dpi, the leaves were cleared and stained with Aniline blue to visualize callose. The haustorial structures were inspected by light microscopy. Different stages of callose encasements (arrowheads) were observed. (a) Callose can be found only at the haustorial neck. (b) Partial encasement of the haustorium. (c) The haustorium is fully encased. The images show overlays of brightfield and fluorescent images. Bar = 10 μ m.

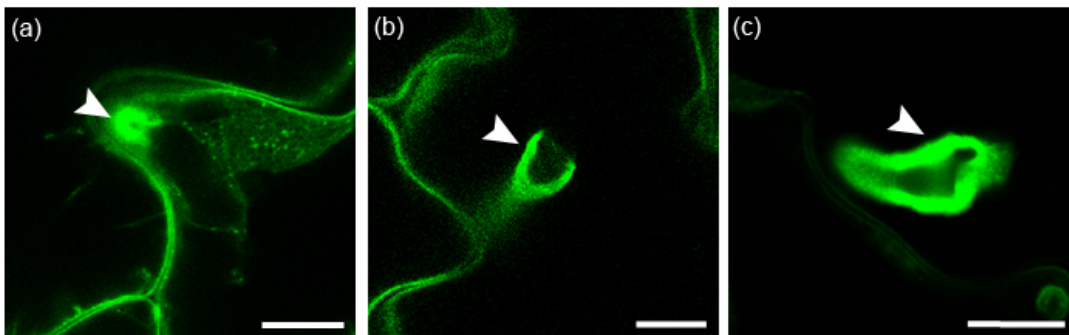
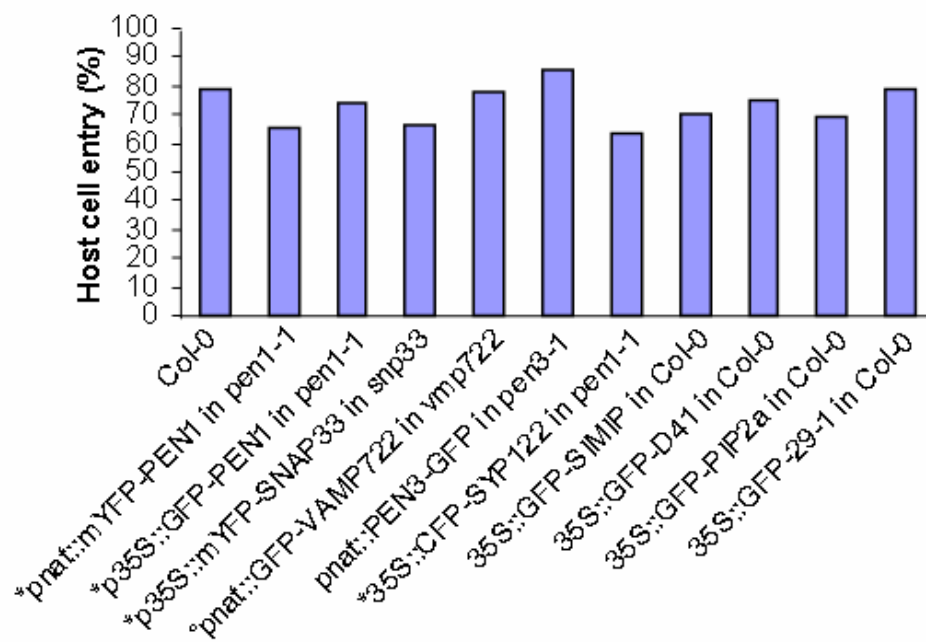


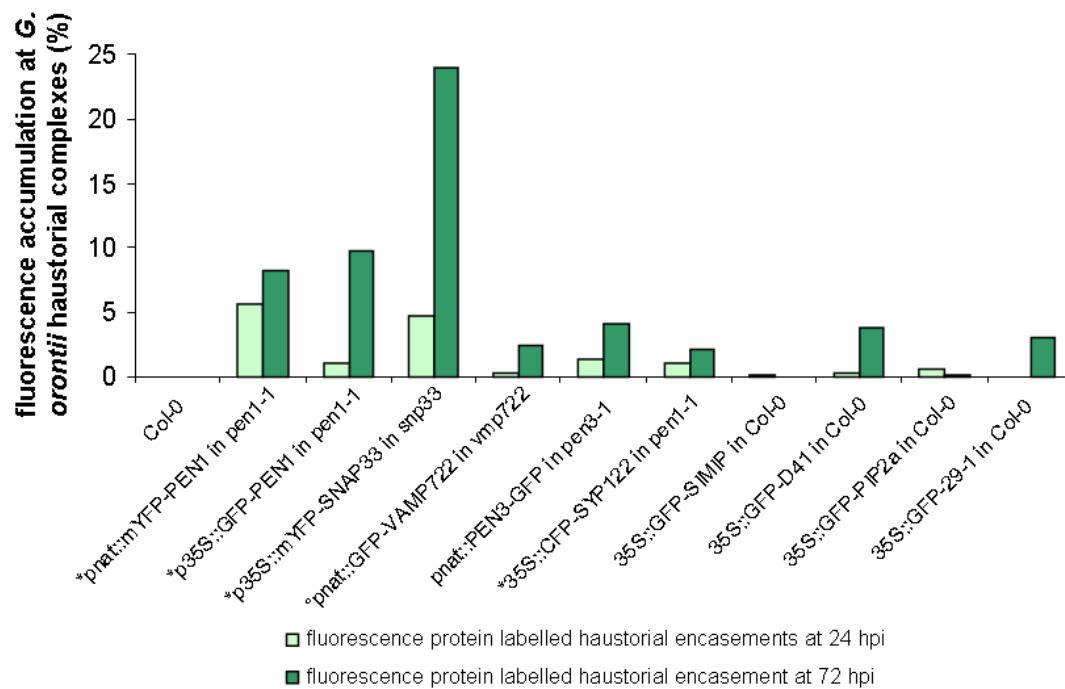
Figure 12. Haustoria become encased by GFP-PEN1 in the adapted interaction between *Arabidopsis* and the powdery mildew *Golovinomyces orontii*.

Plants expressing GFP-PEN1 were inoculated with *G. orontii*. At 3 dpi, the haustorial complexes were inspected by confocal microscopy. Different stages of GFP-PEN1 encasements (arrowheads) can be observed. (a) GFP-PEN1 focally accumulates around the haustorial neck. (b) The haustorium is partially encased by GFP-PEN1. (c) A fully encased haustorium labelled by GFP-PEN1. Bar = 10 μ m.

(a)



(b)



Results

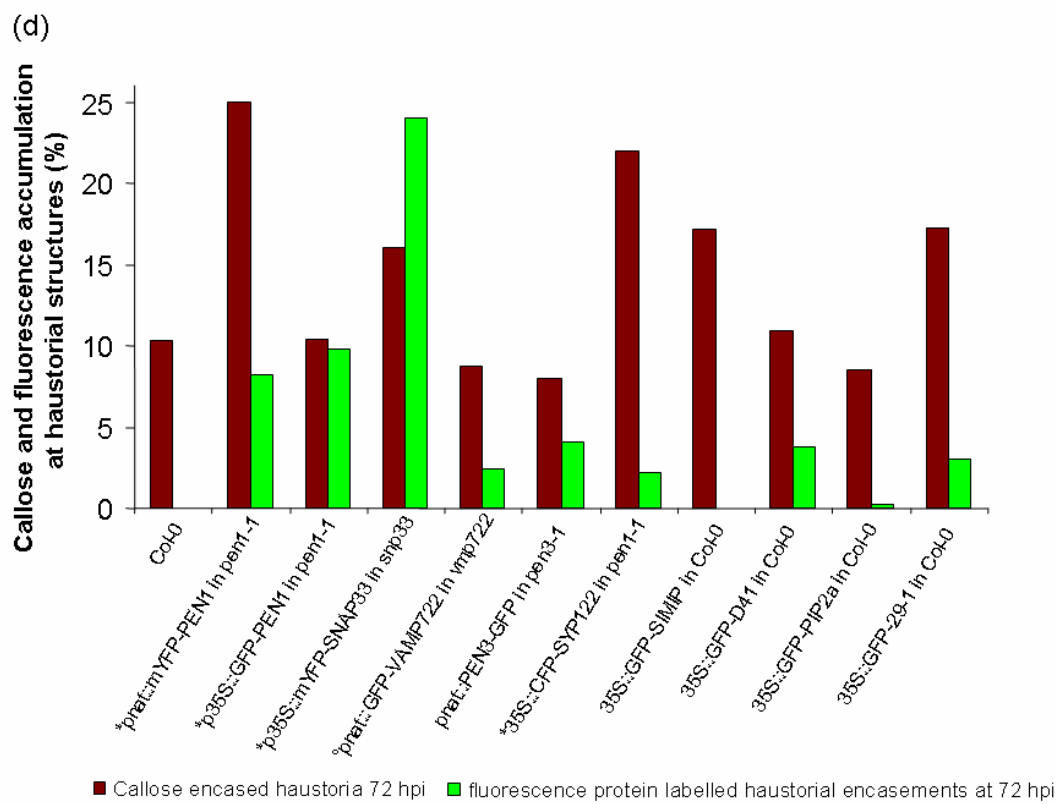
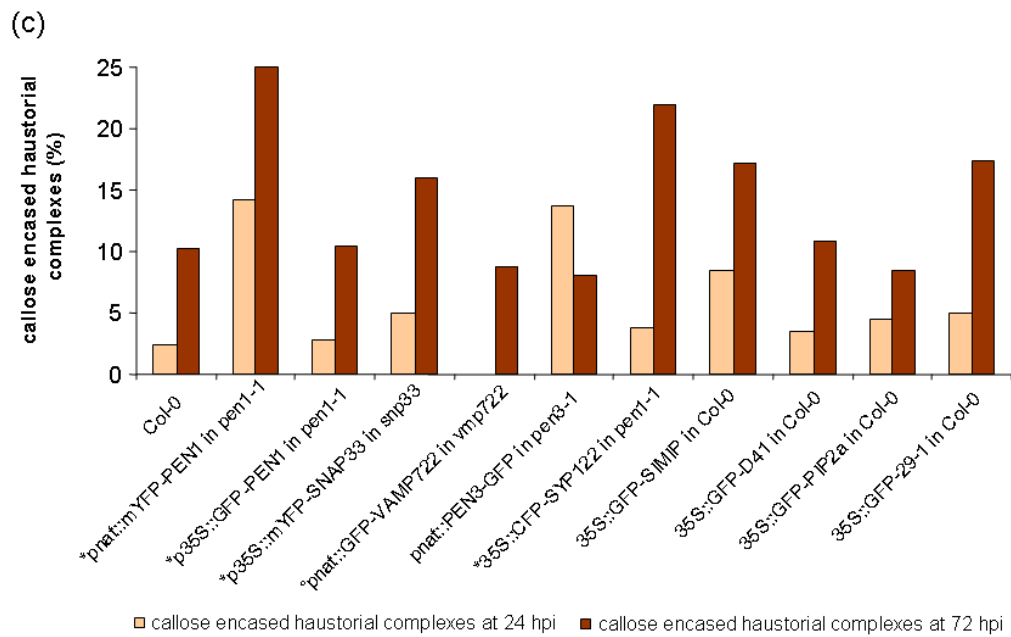


Figure 13. t-SNARES are preferentially included into haustorial encasements.

Arabidopsis genotypes expressing different fluorescent-tagged proteins were inoculated with the *Arabidopsis* powdery mildew *Golovinomyces orontii*. At 24 and 72 hpi, the haustorial complexes of five cotyledons were analysed by microscopy. (a) Leaves were stained with Aniline blue to detect callose and with Coomassie Brilliant blue to detect the fungus. Host cell entry was scored by examining individual interaction sites by light microscopy, the development of an haustorium was scored as successful entry. (b) The percentage of haustoria with encasements labelled by particular fluorescent fusion proteins was scored by confocal microscopy. (c) The leaves were stained with Aniline blue to detect callose. The frequency of callose-encased haustorial complexes was scored by light microscopy. (d) A comparison of callose and the respective fluorescent tagged protein encasing haustoria at 72 hpi is depicted. Asterisk marks t-SNAREs, circle marks v-SNARE.

To score host cell entry by the pathogen, individual interaction sites were characterized and the development of a haustorium was considered to indicate successful entry. An entry rate of around 75% is usually observed for wild type plants (Lipka and Panstruga, 2005). The individual transgenic lines showed a host cell entry rate between 63% and 86% (Figure 13 a). The slight differences can be explained by a natural variation of host cell entry.

The frequency of haustorial encasements labelled by the fluorescently tagged proteins increased between 24 hpi and 72 hpi (Figure 13 b). Either the accumulation of the proteins tested is a gradual process or is initially suppressed. A clear trend for the preferential accumulation of t-SNAREs can be seen (Figure 13, marked by asterisks). For the two fluorescently tagged PEN1 proteins, either driven by the native or by the 35S promoter fluorescent encasements were detectable at rates of 8,2% or 9,8%, respectively. 24% of haustorial structures contained fluorescently tagged SNAP33. In contrast, all other fluorescently tagged proteins showed a lower frequency of accumulation at haustorial structures (Figure 13 b). Possibly, the t-SNAREs contribute to a vesicle-mediated secretion of defence-related compounds towards haustorial complexes. Alternatively, the fungus might exploit vesicle secretion to gain nutrients. If this holds true, one would expect less SNARE protein accumulation at haustoria of non-adapted pathogens.

For the fluorescently tagged VAMP722, only a low frequency (2,4%) of encased haustoria were labelled at 72 hpi. This was unexpected, since VAMP722 was shown to build ternary SNARE complexes with PEN1 and SNAP33 *in planta* (Kwon et al., 2008). The fact that GFP-VAMP722 is driven by its own promoter, may result in a low expression level which could produce a fluorescence signal that was below the detection limit. Another possibility could be that VAMP722 gets recycled whereas the t-SNARES do not. The frequency of callose-encased haustorial structures was variable for all transgenic lines tested (Figure 13 c). In accordance with the observed increase over time in the proportion of haustoria labelled by fluorescent proteins, the frequency of callose encasements also increased over time, comparing 24 hpi and 72 hpi. However, plants expressing PEN3-GFP driven by the native promoter showed a higher frequency of callose encasement at 24 hpi compared to 72 hpi. This was unexpected, since a degradation of callose is not expected.

The line expressing mYFP-PEN1 driven by the native promoter showed a higher frequency of callose encasement compared to wild type Col-0 at both 24 hpi and 72 hpi. One possible explanation is that the fusion protein does not fully complement the *pen1-1* mutant. The callose encasement frequency of the *pen1-1* mutant was not evaluated. However, the host cell entry seemed to be complemented to wild type levels (Figure 13 a). The protein level was not measured, possibly the PEN1 protein level was enough to complement host cell entry but insufficient to complement callose encasement.

The line expressing ‘p35S::CFP-SYP122’ showed a much higher frequency of callose-encased haustoria at 72 hpi compared to the Col-0 wild type. It is possible that SYP122, the closest homologue of PEN1 (Collins et al., 2003; Assaad et al., 2004) does not fully complement the *pen1-1* mutation. Notably, this line shows the lowest host cell entry of 63% (Figure 13 a).

Figure 13 d shows the frequency of callose- and fluorescent protein-encased haustoria at 72 dpi in one graphic for better comparison. A full correspondence between the frequency of GFP-PEN1 and callose-encasements was only seen with the line ‘p35S::GFP-PEN1’, for which analysis of haustorial encasements was done (Figures 4, 5, 6, 7, 8, 10, 11, 12, 15, 16, 17). For the line in which PEN1 expression was driven by its own promoter, co-localization

was not observed. Possibly, incomplete complementation (see above), might result in more callose encasements. However, the frequency of fluorescent protein encased haustoria was similar to the overexpression line (p35S::GFP-PEN1).

More haustorial complexes were encased by YFP-SNAP33 than by callose (Figure 13 d). Possibly, SNAP33 accumulates in the extrahaustorial matrix in addition to the callose encasement. More than twice as many haustoria were encased by SNAP33 compared to PEN1 72 hpi. Three SNAP25 homologues are expressed in *Arabidopsis*, namely SNAP29, -30 and -33, but only SNAP33 transcripts were detectable in leaves (Kwon et al., 2008). Together, this suggests that SNAP33 is involved in more ternary SNARE complexes than PEN1.

Concluding, these data raise the possibility that PEN1 and VAMP722 are not the only syntaxins incorporated into haustorial encasements and there might be other syntaxins or v-SNARES which partner SNAP33. This would imply a differential recruitment of SNARE proteins in defence-related secretion around haustoria.

3. 1. 6 Deposition of callose into haustorial encasements depends on PMR4 (GSL5) callose synthase, but is independent of PEN1 syntaxin

To verify the presence of SNARE proteins inside haustorial encasements and to gain higher resolution, physical sections were produced from resin-embedded haustorial complexes, instead of optical sections obtained by confocal microscopy. *G. orontii* haustorial complexes were isolated at 7dpi from diverse plant genotypes, inoculated with *G. orontii*. Isolated haustoria were fixed and embedded in resin and thereafter cut into ultrathin sections (700 nm). However, immunofluorescence labelling with antibodies raised against PEN1 or VAMP722 was not successful due to unspecificity of the antibodies.

PMR4/GSL5 callose synthase was shown to be required for wound and papillary callose formation (Vogel and Somerville, 2000; Jacobs et al., 2003; Nishimura et al., 2003). To test whether PEN1 accumulation at haustorial encasements is dependent of callose deposition, resin sections through haustorial encasements were also stained with Sirofluor to label

callose. Haustoria grown on *pen1-1* mutant plants (Figure 14 g-i) showed callose encasements similar to wild type (Figure 14 a-c), whereas haustoria grown on the callose synthase mutant *pmr4-1* (Figure 14 d-f) did not reveal any detectable callose fluorescence, although encasements were present. The absence of callose in haustoria grown on the *pmr4-1* mutant was expected and consistent with previous reports (Jacobs et al., 2003; Nishimura et al., 2003). The fact, that haustoria grown on the *pen1-1* mutants showed callose encasements similar to wild type, gives genetic evidence that callose encasement occurs independently of PEN1. However, genetic redundancy is possible, since Assaad et al. (2004) reported an overlapping function of PEN1 and its closest homologue AtSyp122 in secretion. For haustoria grown on *pmr4-1* an encasement was still detectable, indicating that components other than callose are present in these subcellular structures as previously reported (Jacobs et al., 2003). I noticed a highly irregular shape of haustoria grown on the *pmr4-1* mutant, which was not reported before. The deformation of these haustoria suggests that callose may be needed for stability and viability of the haustorial complex. Possibly callose is needed as a physical support for fungal development, either as structural scaffold to accommodate haustorial complexes or to allow optimal nutrient uptake via this specialized feeding structure (Jacobs et al., 2003).

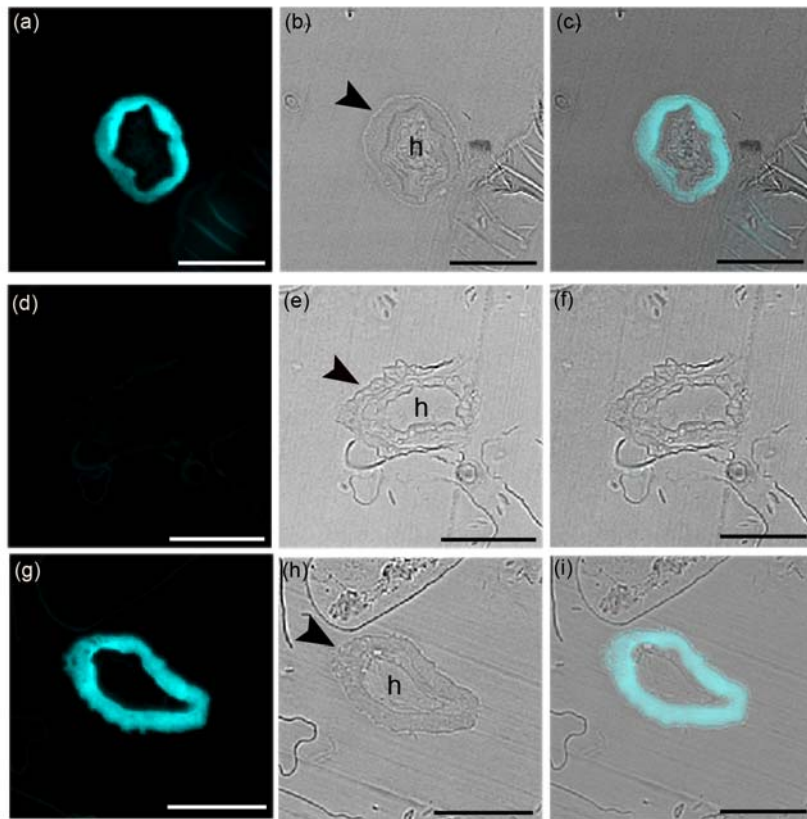


Figure 14. Deposition of callose into haustorial encasements depends on PMR4 (GSL5) callose synthase but not on PEN1 syntaxin.

Haustoria of *Golovinomyces orontii* were isolated from infected *Arabidopsis* leaves at 7 dpi. Sections (700nm thick) were prepared from fixed, resin embedded samples and stained with Sirofluor to detect callose. The left column shows callose fluorescence, the middle column shows the corresponding bright field image and the right column shows the overlay.(a-c) Haustorial complexes isolated from wild-type Col-0 plants show callose encasements (arrowhead). (d-f) Encased haustorial complexes isolated from the *pmr4-1* callose synthase mutant display an irregular surface (arrowhead), and callose was not detectable in the encasements. (g-i) Haustorial complexes isolated from *pen1-1* mutant plants exhibit normal callose encasements (arrowhead).

h, haustoria ; Bar = 20 μ m.

3. 1. 7 Time-course study of haustorial encasements

To determine when haustorial complexes become encased by GFP-PEN1 a time-course experiment was performed. Two to three week old plants expressing GFP-PEN1 in the *pen1-1* mutant background were analysed in the time-frame of 16 to 25 hpi with *G. orontii*. Previous studies on the adapted powdery mildew *E. cichoracearum* showed that fully differentiated haustoria can be observed from 16 hpi onwards (Koh et al., 2005). For every time point examined ten fully differentiated haustorial complexes were investigated. At 21 hpi fully differentiated haustoria were seen, where the haustorial body and the extrahaustorial matrix were clearly distinguishable. At that time point, labelling of the extrahaustorial membrane by GFP-PEN1 was visible (Figure 15). The first haustoria completely encased by GFP-PEN1 became visible at 23 hpi (Figure 16). At this time point hardly any secondary haustoria were detectable. A haustorium, as depicted in Figure 16 b, was scored as ‘not encased’.

There was a consistent trend that the proportion of encased haustoria increased over time. The encasement took place after the haustorium was fully differentiated. Thus, only older and mature haustoria were encased, as depicted in Figure 17, showing one spore with two haustoria at different stages of development. Here only the older haustorium is encased. This was the first formed haustorium, because it is larger in size and fully differentiated and had developed from one primary appressorium.

Concluding, this leads to the suggestion that the encasement by GFP-PEN1 is suppressed by the pathogen at earlier stages or only a fully developed haustorium can trigger the encasement. It is also possible that the accumulation of GFP-PEN1 around young haustoria is below the detection limit.

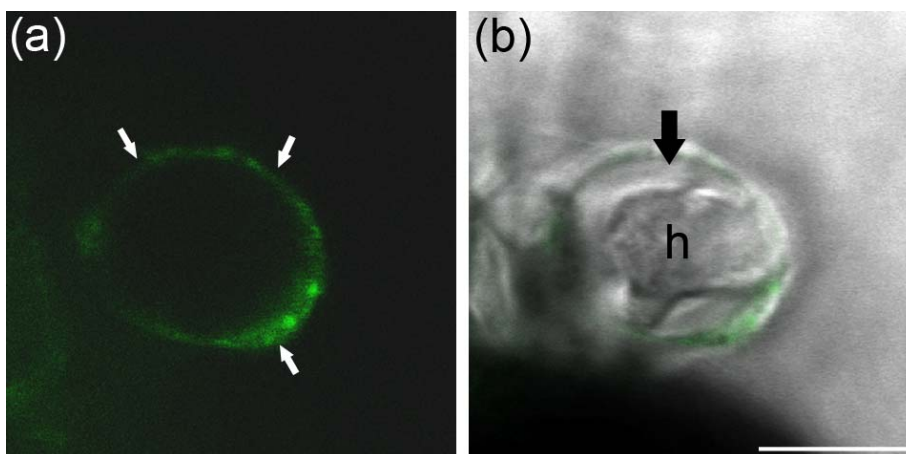


Figure 15: GFP-PEN1 is detectable in the extrahaustorial membrane

Plants expressing GFP-PEN1 were inoculated with the *Arabidopsis* powdery mildew *Golovinomyces orontii*. (a) GFP-PEN1 labels the extrahaustorial membrane (small arrows). (b) At 21 hpi the haustorial body (h) and the haustorial matrix (bold arrow) are clearly distinguishable.

h, haustorium. Bar = 10 μ m.

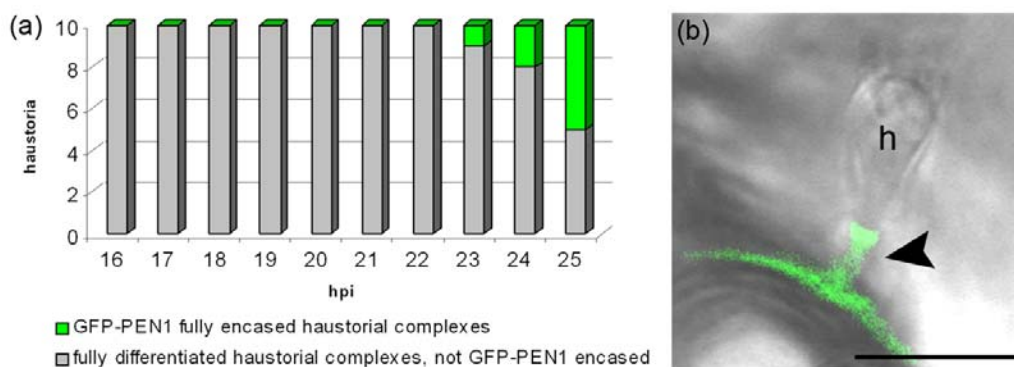


Figure 16. Accumulation of GFP-PEN1 in haustorial encasements begins at 23 hpi.

Plants expressing GFP-PEN1 were challenged with the adapted powdery mildew *Golovinomyces orontii*. In a time-course from 16 to 25 hpi, fully differentiated haustorial complexes were inspected by confocal microscopy. For each time point, 10 fully developed haustoria were examined and scored for the presence or absence of encasements containing GFP-fluorescence. Image (b) shows a fully differentiated haustorium at 19 hpi, the GFP-

Results

PEN1 focal accumulation is only visible at the haustorial neck and therefore this haustorium was scored as 'not encased'.

h, haustorium. Bar = 10 μm .

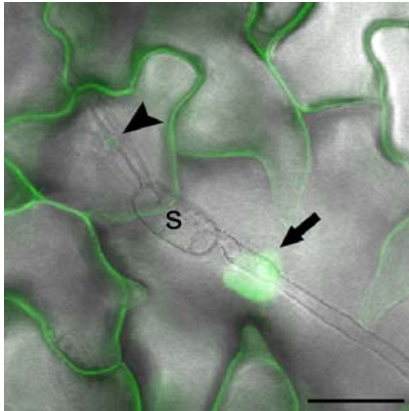


Figure 17. Mature haustoria get encased by GFP-PEN1.

Plants expressing GFP-PEN1 were inoculated with *Golovinomyces orontii*. 40 hpi the haustorial complexes were inspected by confocal microscopy. The figure shows the overlay of single optical sections (1 μm) of the green channel and the bright field image. The spore developed two haustoria, the mature haustorium is fully encased by GFP-PEN1 (arrow), whereas the young haustorium displays GFP-PEN1 accumulation only at the haustorial neck.

s, spore. Bar = 50 μm .

3. 2 Screening a chemically mutagenised plant population for mutants with altered GFP-PEN1 focal accumulation

3. 2. 1 Chemical mutagenesis of an *Arabidopsis* line expressing GFP-PEN1

To unravel mechanism(s) driving the GFP-PEN1 focal accumulation (FA) at attempted fungal entry sites, I performed an EMS-mutagenesis of an *Arabidopsis* line expressing GFP-PEN1 under the control of the 35S promoter in the *pen1-1* mutant background. The resulting M₂ population was screened for mutants showing an aberrant GFP-PEN1 FA pattern at *B. g. hordei* entry sites.

3.2.2 Evaluation of the efficiency of mutagenesis

To measure the mutation rate, the frequency of albino mutants impaired in pigment biosynthesis, was determined. 2,400 M₂ plants of 40 M₂ families were scored for an albino phenotype. Mutation frequencies for well mutagenised M₂ populations should be in the range of 2-10% (Martinez-Zapater and Salinas, 1998). In my case I observed an albino frequency of 2%, suggesting that an optimal rate of mutagenesis was achieved.

3. 2. 3. Manual screen for mutants showing an aberrant GFP-PEN1 focal accumulation phenotype

Two to three week old M₂ plants were inoculated with *B. g. hordei*. GFP-PEN1 FAs at attempted entry sites were inspected at 24 hpi by light microscopy. To image germinated spores a bright field image was taken. An Epi-fluorescence image was taken to visualize the

GFP signal originating from GFP-PEN1. One cotyledon and one primary leaf were analysed. 7700 M₂ plants were examined. In the first round 56 putative candidates were rescued. To test whether the mutation held true in the M₃ progeny, 30 plants per selfed M₂ parent were analysed. A summary of putative mutants classified for mutants with altered GFP-PEN1 FA is depicted in table 5.

Six putative mutants were identified showing no GFP-PEN1 FA. Line 45A-1-9 is one example depicted in Figure 18 c. Five putative mutants showed a weak GFP-PEN1 FA signal, the putative mutant 45A-5-1 belonged to this class and is shown in Figure 18 d. The putative mutant 37A-5-3 exhibited an excessive number of GFP-PEN1 FA, seven mutant lines were identified belonging to this class (Figure 18 e). Ten mutant lines showed more GFP-PEN1 encased haustoria than wild type. Figure 18 f shows the putative mutant 32B-8-4 as an example of this mutant class. Since the GFP-PEN1 FA at haustorial structures is a novel finding (see 3. 1. 3), this mutant class was of special interest. The other mutant classes ‘reduced number of GFP-PEN1 FA’, ‘increased number of GFP-PEN1 FA’ or ‘GFP-PEN1 FA with an aberrant pattern’ (e.g. bigger in size, different shape or a lot of small aggregated vesicle-like structures) showed only subtle phenotypes and were not further analysed.

Table 5. Summary of putative EMS-mutants that were identified by light microscopy.

The putative mutants showing an aberrant GFP-PEN1 focal accumulation pattern were arranged in seven classes based on the phenotype of focal accumulation. FA, focal accumulation of GFP-PEN1.

mutant class	M ₂ phenotype					M ₃ phenotype			
	total	lethal	seed set	no seed set	dwarf	WT	M ₂ -like	no seed germination	no data
no or single FA	6	3	2	1	0	1	0	0	1
weak FA signal	5	1	4	0	2	3	0	1	0
excessive number of FA	7	5	2	0	2	2	0	0	0
reduced number of FA	5	0	4	1	1	2	0	0	2
increased number of FA	10	0	9	1	0	7	2	0	0
FA with aberrant pattern	13	0	13	0	0	11	1	0	1
enhanced number of GFP-PEN1 encased haustoria	9	0	9	0	0	7	1	0	1
total	56	9	44	3	5	34	4	1	5

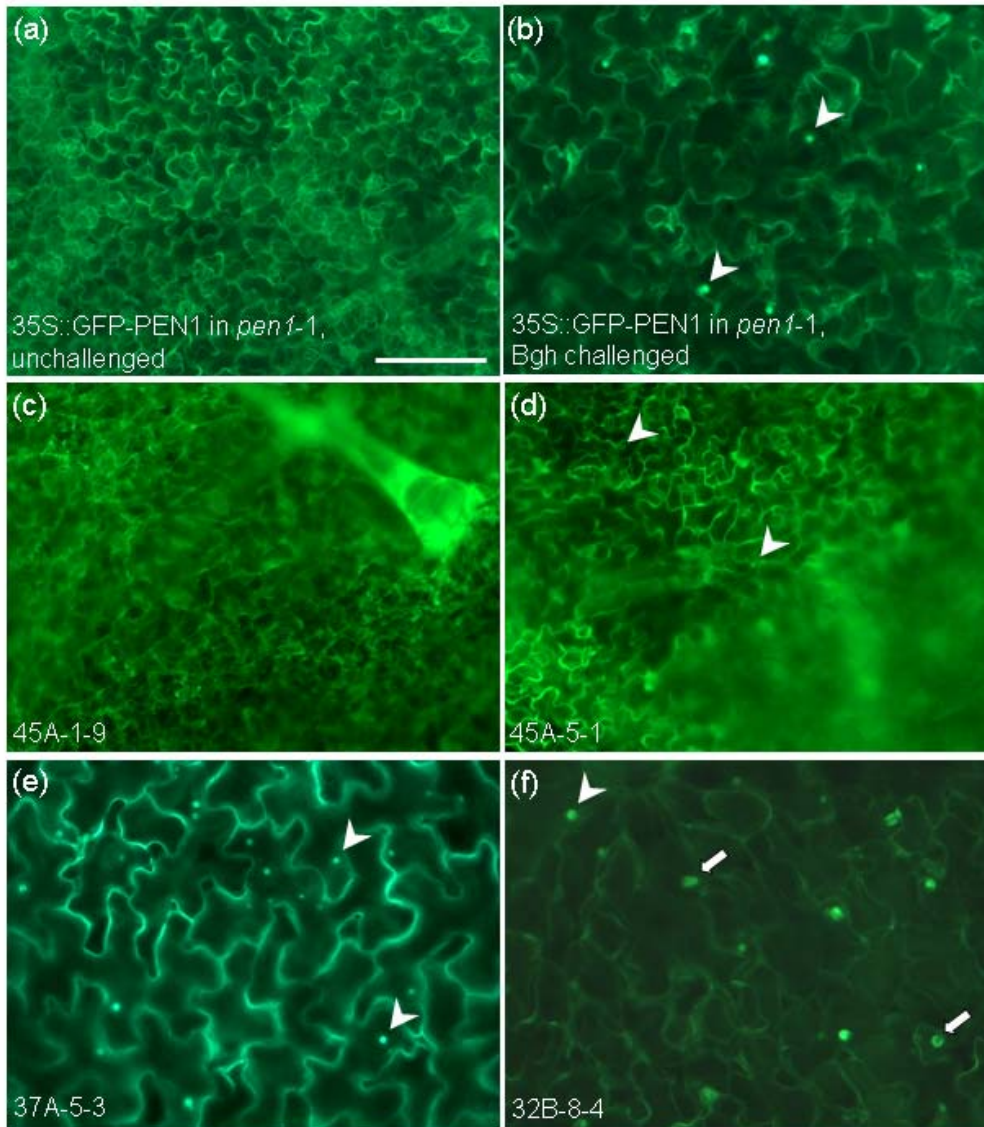


Figure 18. Putative mutants showing an aberrant GFP-PEN1 focal accumulation.

M₂ plants were inoculated with *Blumeria graminis* f. sp. *hordei* (*B. g. hordei*) and leaves were analysed at 24 hpi by light microscopy. (a) Epidermal *Arabidopsis* cells expressing GFP-PEN1 in the *pen1-1* mutant background. (b) GFP-PEN1 focally accumulates (arrowheads) at attempted penetration entry sites of *B. g. hordei*. (c) The putative mutant 45A-1-9 shows no GFP-PEN1 focal accumulation. (d) The putative mutant 45A-5-1 exhibits weak GFP-PEN1 focal accumulation signals (arrowheads). (e) The putative mutant 37A-5-3 shows an excessive number of GFP-PEN1 focal accumulations. (f) The putative mutant 32B-8-4 exhibits an enhanced number of GFP-PEN1 encased haustoria (arrows) besides GFP-PEN1 focal accumulations (arrowhead). Bar = 100µm.

From the 56 putative candidates, 34 could not be confirmed in the subsequent generation. However, for four mutants the phenotype was validated in the M₂ progeny. These mutants showed a very subtle phenotype which might give rise to too many misscorings in a mapping population.

For the three mutant classes with the strongest phenotype ('no or a single FA', 'weak FA signal' or 'excessive number of FA'), 18 putative mutants were found, but 9 of these mutants (50%) exhibited juvenile lethality. These plants were able to germinate and I was able to analyse cotyledons, but the plants died while they were still in the juvenile stage. The high number of lethal putative mutants indicates that the corresponding wild type genes are also important for proper plant development.

3. 2. 4 Development of a fully automated confocal high-throughput imaging method to image living plant tissue at sub-cellular resolution

The original manual screen was extremely time consuming and predisposed for the identification of mutants with a severe phenotype. Thus, the screening method that was available at the beginning of my work needed to be improved to yield quantitative data about the GFP-PEN1 FA in an unbiased manner.

The manual screen showed that mutants with a strong phenotype were lethal, suggesting that mutations in the genes of interest lead to lethality and are therefore important in plant development. However, a mutation in a weak allele showing a weak phenotype might be viable and could nevertheless help to unravel the mechanism underlying GFP-PEN1 FA at pathogen entry sites. A more sensitive method would allow the identification of mutants with a weak microscopic phenotype, which would be impossible to score by eye. For this reasons, In parallel to the manual screen, I developed a high-throughput imaging system for living plant tissue. I used a confocal micro imaging reader, named OPERA (Perkin Elmer). The Opera system is a confocal microscope for high-throughput imaging normally used for animal or human cell cultures. I adapted the system to image *Arabidopsis* leaves. This was the first

demonstration of high-throughput confocal imaging in living plant tissue at a subcellular level.

I developed a system for preparing leaves in 96-well plates. Therefore, a particular stamp was generated, which fulfilled several functions: it facilitated the leaf preparation, it helped to fix the leaves in the wells and finally, it flattened the leaf during the imaging. Furthermore, a procedure for imaging the leaf tissue was developed. Together with Perkin Elmer, we developed a pattern recognition script for fully automated recognition and analysis of the GFP-PEN1 FA (for procedure in detail see Material and Methods, 2. 2. 14-17). Together with a bioinformatician, Kurt Stüber, I developed a method for the analysis of the huge amount of data. Therefore, we designed a graphical output for quantitative image analysis.

One experimental hurdle was the curvature of the leaves. Since the epidermal cells, which were of interest for my work, were not all in the same optical plane, consecutive series of images in the z-direction (z-stack) were taken. An image projection was made of the z-stack which was analysed by the Opera software ‘Acapella’ with the generated pattern recognition and analysis script. To characterize the recognized GFP-PEN1 FAs, several parameters were generated (a list of recognized output parameter can be found in the Material and Methods, 2. 2. 17).

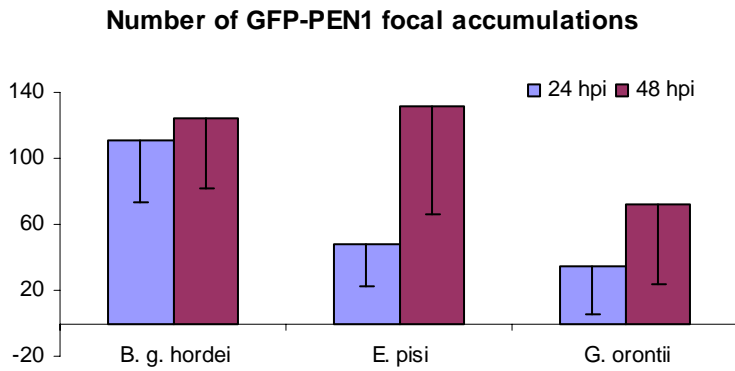
Taken together, it was the first time that high-throughput confocal imaging in living plant tissue was made possible. A multiparametric analysis of pattern changes at subcellular resolution became realistic. Furthermore, the new approach was unbiased, gave reliable quantitative data and was much faster than the manual screening method. I was able to screen 150 plants per day with the automated approach, in contrast to around 80 plants per day with the manual screen.

3. 2. 5 Multiparametric analysis of GFP-PEN1 focal accumulation sites triggered by adapted and non-adapted powdery mildews

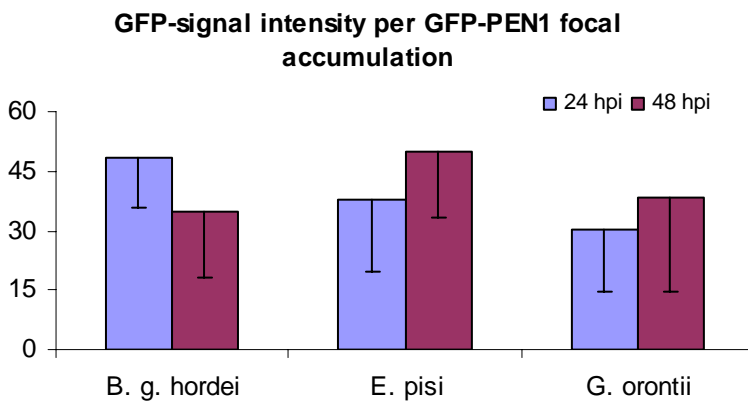
With the new automated screening approach a characterization of the GFP-PEN1 FA was possible. Initially, I determined whether there are quantitative differences in the GFP-PEN1 FA, triggered by adapted and non-adapted powdery mildews. The GFP-PEN1 FA was only

detected at fungal entry sites of powdery mildews but not at entry sites of other tested directly penetrating fungi, thus GFP-PEN1 FA is either only triggered by powdery mildews or suppressed by the other fungi tested (see 3.1.1). Thus, it might be a counter defence mechanism of the powdery mildews. The fungus possibly manipulates PEN1 FA to protect itself. If so, I would expect a different GFP-PEN1 FA pattern triggered by adapted or non-adapted powdery mildews. This prompted me to carry out a multiparametric analysis of the GFP-PEN1 FA after inoculation with three different powdery mildew species. Plants expressing GFP-PEN1 in the *pen1-1* mutant background were inoculated with the non-adapted *B. g. hordei* or *E. pisi* or with the adapted *G. orontii*. The leaves were analysed at 24 hpi and at 48 hpi. For each pathogen and time point, 300 plants were analysed in three independent experiments. The analysis was performed with the automated OPERA microscope. Eight defined areas per leaf were imaged (for details see 2.2.16 and Figure 2). The results are summarized in table SD1 (Supplementary data).

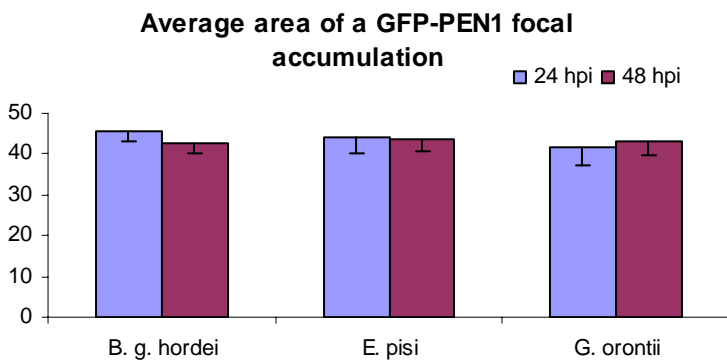
(a)



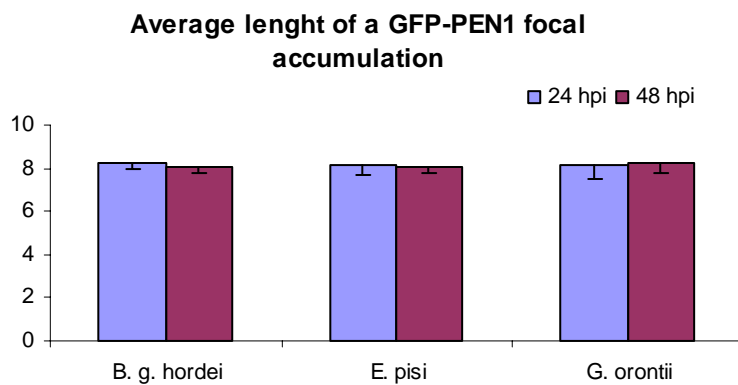
(b)



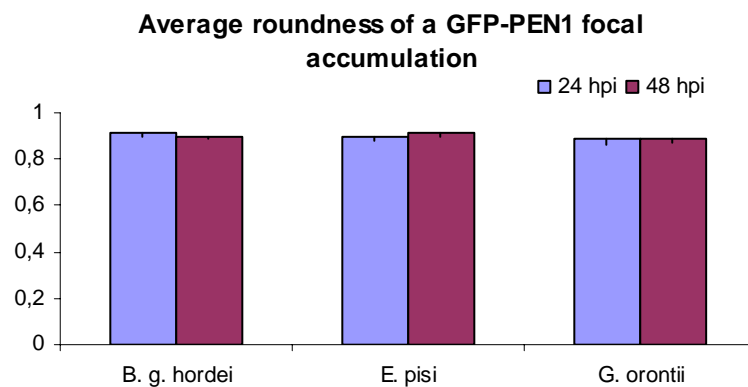
(c)



(d)



(e)



(f)

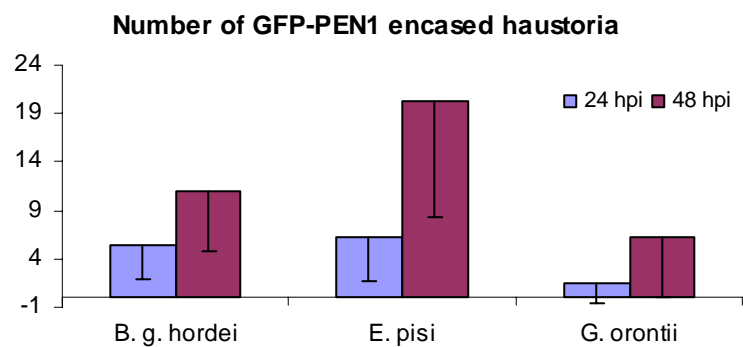


Figure 19. Multiparametric analysis of GFP-PEN1 FA triggered by non-adapted and adapted powdery mildews.

Plants expressing GFP-PEN1 in the *pen1-1* mutant background were inoculated with the non-adapted *Blumeria graminis* f. sp. *hordei* and *Erysiphe pisi* and with the adapted *Golovinomyces orontii*. The leaves were analysed at 24 hpi and at 48 hpi. The analysis was done with the automated OPERA microscope, providing several output parameters. The different output parameters are displayed in the graphs. Error bars show the standard deviation.

From all analysed parameters the largest difference was detected in the number of GFP-PEN1 FAs (Figure 19 a). The number of GFP-PEN1 FAs for *B. g. hordei* (111 +/- 38) and *E. pisi* (48 +/- 25) at 24 hpi ($p < 0,05$) and for *B. g. hordei* and *G. orontii* (35 +/- 29) at 24hpi ($p < 0,05$) differed significantly. At 24 hpi the leaves inoculated with the adapted *G. orontii* showed the lowest number of GFP-PEN1 FAs. Assuming that GFP-PEN1 FAs are involved in fungal counter defence, one would expect to see more GFP-PEN1 FAs in the adapted than in the non-adapted interaction. By contrast, both tested non-adapted powdery mildews *B. g. hordei* and *E. pisi* revealed a higher number of GFP-PEN1 FAs, suggesting that the GFP-PEN1 FA is a plant defence mechanism which the adapted *G. orontii* is able to suppress. At 48 hpi the *G. orontii* interaction still yields a lower frequency of GFP-PEN1 FA than the non-adapted species (*B. g. hordei* 124 +/- 42; *E. pisi* 132 +/- 66; *G. orontii* 72 +/- 48; $p < 0,05$, except for the difference between *B. g. hordei* - *E. pisi* where $p = 0,06$).

Due to more frequent penetration sites of the adapted *G. orontii*, more GFP-PEN1 FAs were expected at 48 hpi compared to 24 hpi, which is in accordance with the data. Since the non-adapted *B. g. hordei* is not able to grow on *Arabidopsis* it was expected that the fungus stopped growing after the first penetration attempt, accounting for the rather low difference in GFP-PEN1 FA frequencies between 24 hpi and 48 hpi. The increased number of GFP-PEN1 FA in the *E. pisi* interaction at 48 hpi compared to 24 hpi can be accounted by the fact that *E. pisi* makes up to three penetration attempts (Figure 19 b). It is also possible that the altered GFP-PEN1 FA frequency observed with diverse powdery mildew species is based on the different inoculation methods used.

The GFP signal intensity of the GFP-PEN1 FAs at 24 hpi in the adapted *G. orontii* interaction were lower (30,43 +/- 15,73) than for the non-adapted *B. g. hordei* (48,5 +/- 12,53) and *E. pisi* (38,06 +/- 18,41; Figure 19 b), suggesting that PEN1 FA is a plant defence mechanism and can be suppressed to a certain level by the adapted powdery mildew fungus. The fluorescence signal for *G. orontii* GFP-PEN1 FA was stronger at 48 hpi (38,46 +/- 23,63), compared to 24 hpi, suggesting that at later time points the fungus was not able to suppress the GFP-PEN1 accumulation efficiently. In the *B. g. hordei* interaction, the signal intensity was lower at 48 hpi (34,66 +/- 16,36) compared to 24 hpi. Possibly at 'old' GFP-PEN1 FAs the SNARE protein PEN1 gets recycled. In the *E. pisi* interaction, the signal was stronger at 48 hpi (49,93 +/- 16,64) compared to 24 hpi, suggesting that at 48 hpi more GFP-PEN1 protein accumulation occurred at fungal entry sites. For all interactions tested, the data showed a significant difference for the measured GFP-signal intensity.

The average area, length and roundness of the GFP-PEN1 FA in response to the adapted and the non-adapted powdery mildew species were comparable, as depicted in figure 19 c, d and e. It appears that GFP-PEN1 FA reached a certain size and shape, independently of whether triggered by an adapted or non-adapted pathogen. Thus, the adapted fungus might be able to manipulate the frequency and intensity of the GFP-PEN1 FA, but once initiated not the size and shape.

At 24 hpi, the frequency of GFP-PEN1 encased haustoria of both non-adapted powdery mildew species were similar and comparably higher than the GFP-PEN1 encased haustoria observed for the adapted fungus (Figure 19 f). Overall, the frequency of encased haustoria was low at 24 hpi. This was expected since I could show that the first haustoria completely encased became visible at 23 hpi (see 3. 1. 7).

Interestingly, *E. pisi* haustoria show a very high GFP-PEN1 encasement frequency at 48 hpi. This is in accordance to the also observed high frequency of GFP-PEN1 FAs at that time point. The data suggest that the non-adapted *E. pisi* makes more penetration attempts (see Figure 20 a-c) and also more haustoria are developed compared to the non-adapted *B. g. hordei*. At 48 hpi the lowest frequency of GFP-PEN1 encased haustoria was observed in the adapted interaction. It is assumed that the haustorial encasement causes impairment of

nutrient transfer from the plant cell to the haustorium to terminate fungal growth (Heath and Heath, 1971). Thus, it is possible that the adapted powdery mildew suppresses haustorial encasements, at least for the time until a new haustorium has developed.

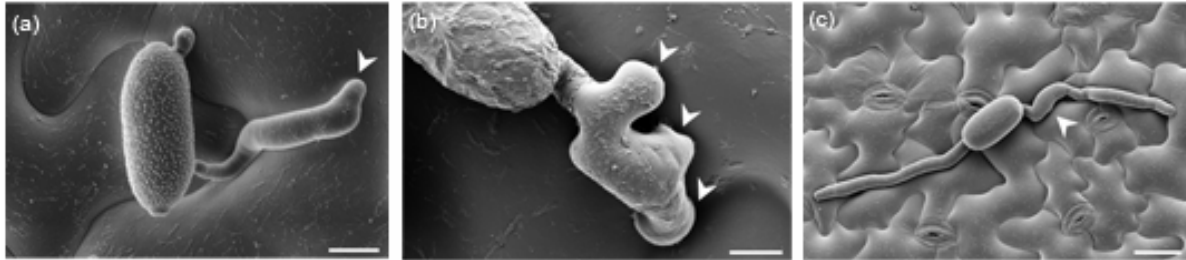


Figure 20. Electron microscopically pictures of germinated powdery mildew spores.

(a) *Blumeria graminis* f. sp. *hordei* makes mostly one penetration attempt (arrowhead) per appressorium. Bar = 10 μm . (b) *Erysiphe pisi* can make up to three penetration attempts (arrowheads) per appressorium. Bar = 5 μm . (c) *Golovinomyces orontii* makes one penetration attempt (arrowhead) per appressorium. Bar = 20 μm .

3. 2. 6 A fully automated screen for mutants showing aberrant GFP-PEN1 focal accumulation at *B. g. hordei* entry sites

Two to three week old M_2 plants were inoculated with *B. g. hordei* and analysed 24 hpi with the Opera microscope. A total of 3000 M_2 plants were inspected and 28 putative mutants were identified. More putative mutants were found by this approach than by the manual screen. This was expected since the new approach also identified candidates with more subtle phenotypes.

Data from the multiparametric analysis of GFP-PEN1 FA served as control data, and output results were compared to these data. Results from the measurement of 24 hpi with *B. g. hordei* were taken as average wild type and putative mutants revealing altered parameters were rescued. Table 6 summarizes the putative candidates that were identified in the first round and placed in different classes according to the GFP-PEN1 FA phenotype. Figure 21

shows some examples of putative mutants identified. The graphical output result of the parameter for which the putative mutant showed an aberrant phenotype is shown. Furthermore, it illustrates the easy identification of a putative mutant at a glance. Diverse output parameters identified mutants revealing different features.

Of the 28 identified putative mutants, seven candidates were showing ‘no or a single GFP-PEN1 FA’. This is a higher number compared to the manual screen. A disadvantage of the high-throughput automated screening method is that certain areas are preset to image and it is possible that by chance no spores had landed in that area during inoculation. The M₃ progeny has to be re-tested and this will show if there are true mutants in this phenotype class. Figure 21 a shows two examples of putative mutants belonging to the mutant class ‘no or single GFP-PEN1 FA’. Both, 68A-4-2 and 68A-4-8, did not show any GFP-PEN1 FA. Although the output results show either 31 or 6 GFP-PEN1 FAs, after manual check of the images taken, the recognized GFP-PEN1 FAs turned out to be false positives. 68A-4-2 was seedling lethal, 68A-4-8 revealed a dwarf phenotype but was fertile and set seed. Since these putative mutants are from the same pool of M₁ plants, it is likely that they are siblings from the same M₁ mother.

For two candidate mutants the recognized GFP-PEN1 FA revealed a weak GFP-signal. Figure 21 b displays mutant candidate 63B-2-12, belonging to the mutant class ‘weak GFP-PEN1 FA signal’. The measured signal intensity was 1149, whereas the average wild type GFP-PEN1 intensity was 1735 (see table SD1 in supplementary data). The plant was fertile and set seed. Putative mutant 71B-2-6, depicted in Figure 21 c, exhibited an example for the mutant class ‘reduced number of GFP-PEN1 FA’, for this plant 15 GFP-PEN1 FAs were observed, while the average wild type frequency was 111 (see table SD1 in supplementary data). The plant was fertile and set seed. Eleven putative mutants were identified in this class. Four putative mutants were identified showing an ‘increased number of GFP-PEN1 FA’ compared to the wild type plants. The putative mutant 74B-5-13, displayed in Figure 21 d, showed 247 GFP-PEN1 FAs. This was more than twice as many as was for the wild type plants. Two putative mutants were identified revealing an aberrant pattern from wild type. The average area for the

Results

wild type GFP-PEN1 FA was 45,67 +/- 2,45 (see table SD1 in supplementary data), whereas candidate 57A-1-8 reveals an average area of 57 (Figure 21 e).

Two mutant lines were identified showing an 'increased number of GFP-PEN1 encased haustoria'. The wild type average showed five haustoria per plant (see table SD1 in supplementary data), whereas the putative mutant 74B-5-8 revealed 46 GFP-PEN1 encased haustoria (Figure 21 f).

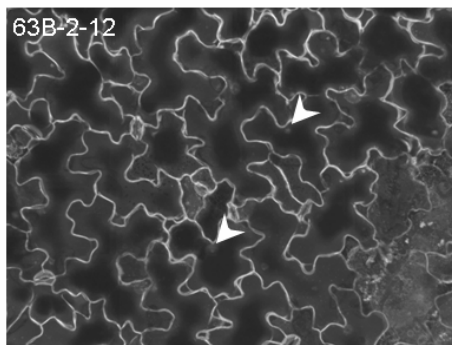
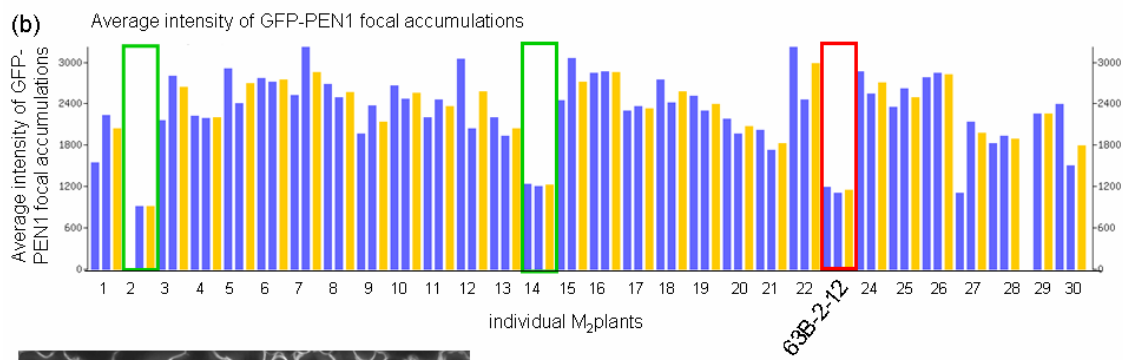
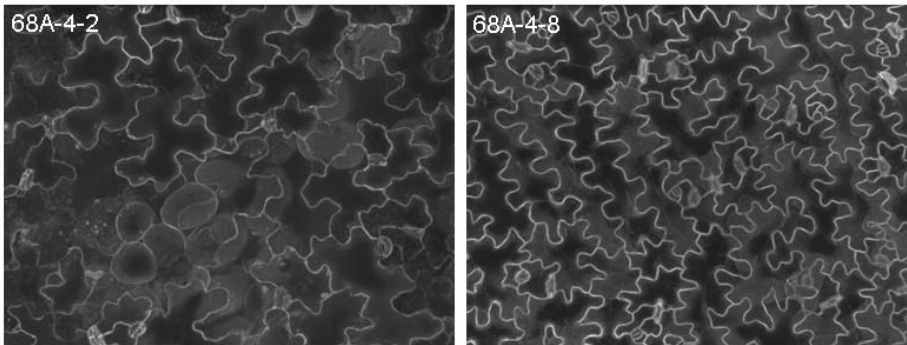
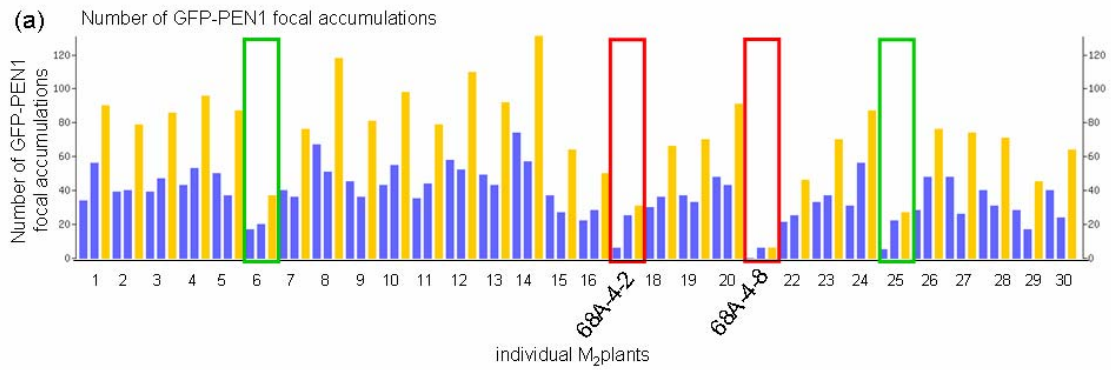
From the overall identified 28 putative mutants, nine (32%) were identified belonging to the three mutant classes with the strongest phenotype (no or a single FA, weak FA signal or an excessive number of FA). In the manual screen only 16% of the identified putative mutants belonged to these mutant classes, indicating that more putative mutants can be identified with the automated approach. Apparently, this screening method is more reliable and subsequent mapping procedures are maybe more promising.

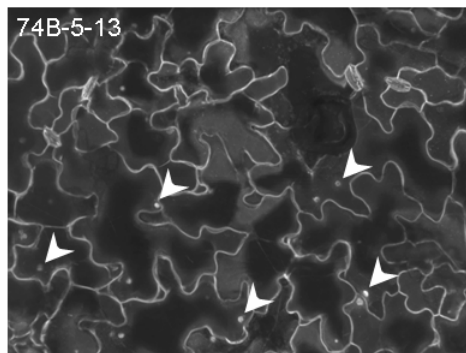
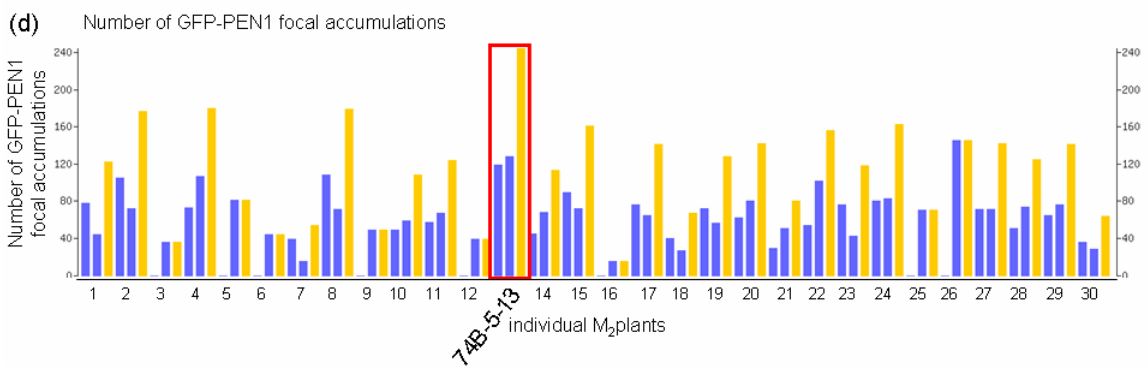
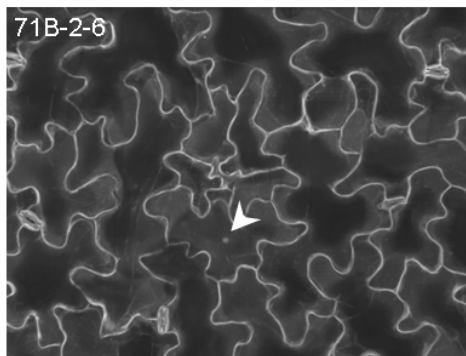
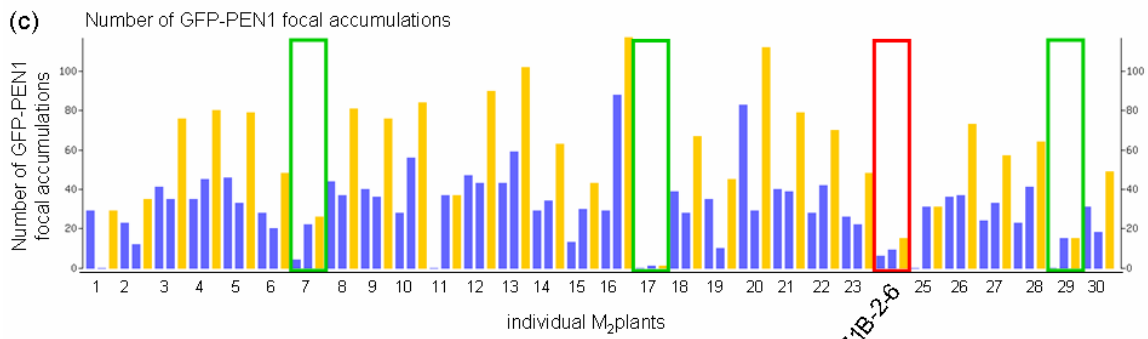
Table 6. Summary of putative mutants that were analysed by fully automated screening.

M₂ plants were inoculated with the non-adapted powdery mildew *Blumeria graminis* f. sp. *hordei* and at 24 hpi screened for mutants showing an altered pattern of the GFP-PEN1 focal accumulation with the fully automated high-throughput confocal microscope Opera. The putative mutants showing an aberrant GFP-PEN1 focal accumulation pattern were classified as indicated. M₃ progeny were not yet inspected. FA, focal accumulation of GFP-PEN1.

mutant class	M ₂ phenotype					M ₃ phenotype			
	total	lethal	seed set	no set	seed dwarf	WT	M ₂ -like	no seed germination	no data
no or single FA	7	2	5	0	4	0	0	0	5
weak FA signal	2	0	2	0	0	0	0	0	2
excessive number of FA	0	0	0	0	0	0	0	0	0
reduced number of FA	11	2	9	0	4	0	0	0	9
increased number of FA	4	1	3	0	0	0	0	0	3
FA with aberrant pattern	2	1	1	0	0	0	0	0	1
increased number of GFP-PEN1 encased haustoria	2	0	2	0	0	0	0	0	2
total	28	6	22	0	8	0	0	0	22

Results





Results

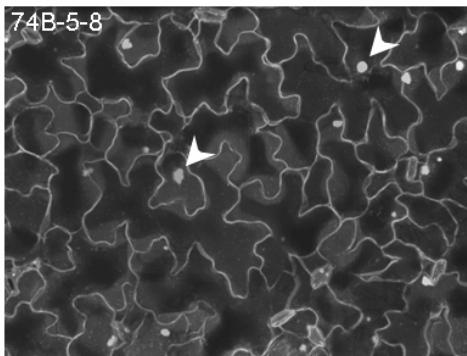
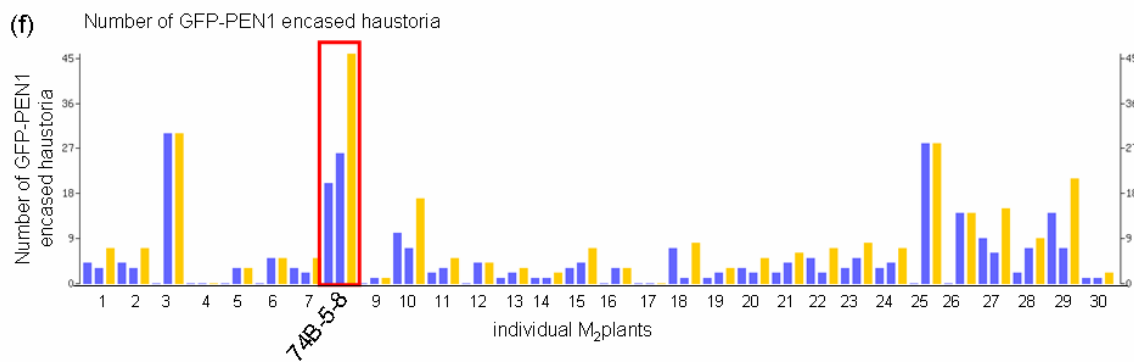
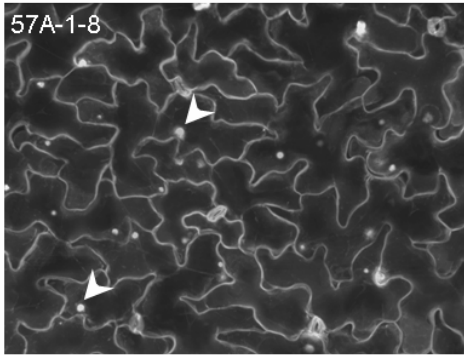
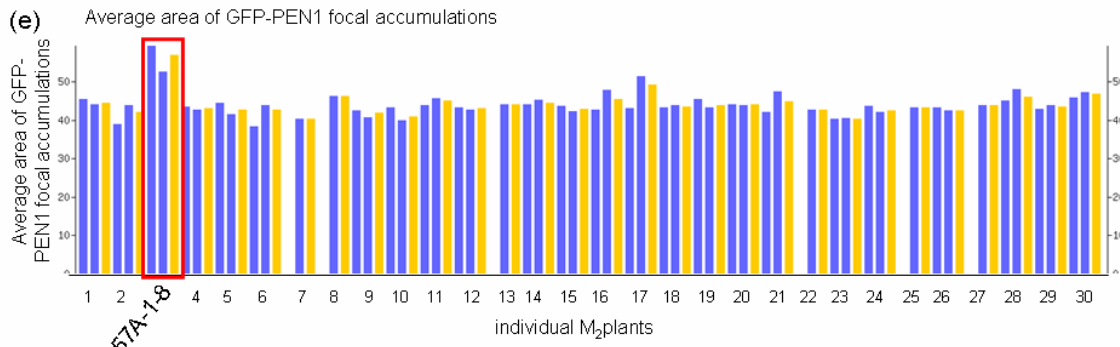


Figure 21. Output results of the automated screening, showing putative candidates with an altered GFP-PEN1 FA.

M₂ plants were inoculated with the non-adapted powdery mildew *Blumeria graminis* f. sp. *hordei* and analysed at 24 hpi by the fully automated confocal microscope for high-throughput screening OPERA. 30 M₂ plants were inspected per micro plate. 19 different parameters were analysed. Putative mutants revealing an aberrant output parameter compared to wild type were identified. The results of the corresponding output parameter for which the mutant was identified is displayed in the graphic. X-axis reveals individual M₂ plants. Two cotyledons per plant were analysed. Three bars are displayed per plant. The first blue bar represents the value scored for the corresponding output result for leaf number one, the second blue bar the value for leaf number two and the yellow bar the value for both leaves together. Red rectangles mark putative mutants, green rectangles mark plants that were found to be false positives after subsequent inspection of the corresponding images that were analysed. For every putative mutant displayed one image out of 16 imaged and analysed areas is shown as an example for the microscopic phenotype. Examples of identified putative mutants are displayed. (a) Putative mutants showing no GFP-PEN1 FA. (b) Putative mutant exhibiting weak GFP-PEN1 FA signal. (c) Putative mutant with a reduced number of GFP-PEN1 FAs. (d) Putative mutant with an increased number of GFP-PEN1 FAs. (e) Putative mutant revealing GFP-PEN1 FAs that are bigger in size. (f) Putative mutant with an increased number of GFP-PEN1 encased haustoria. FA, focal accumulation of GFP-PEN1.

3. 2. 7 Validation of candidate mutants identified in the manual screen in the M₃ generation

The automated mutant screen was expected to be more sensitive than the manual screen, because several parameters that were impossible to score by eye were now detectable. For example, ‘GFP signal intensity of GFP-PEN1 FA’ or ‘average area of the GFP-PEN1 FA’. As a proof of principle, 13 putative mutants found in the manual screen and scored as false positives were verified using the automated approach. Therefore, the plants were inoculated with *B. g. hordei* and analysed 24 hpi. For the analysis of every putative mutant, 30 M₃ siblings of selfed M₂, and at the same time 30 wild-type like plants (p35S::GFP-PEN1 in *pen1-1*) were inoculated and analysed. The average data of 30 plants were compared. For all but one candidate a wild-type-like phenotype was observed in the M₃ progeny, confirming that they were indeed false positives.

Results

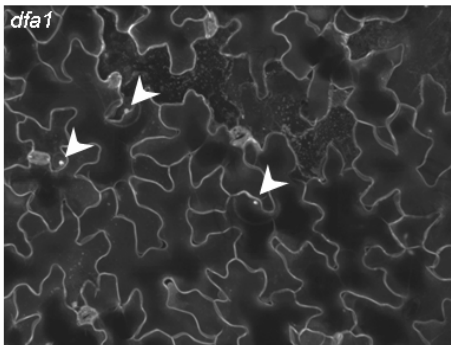
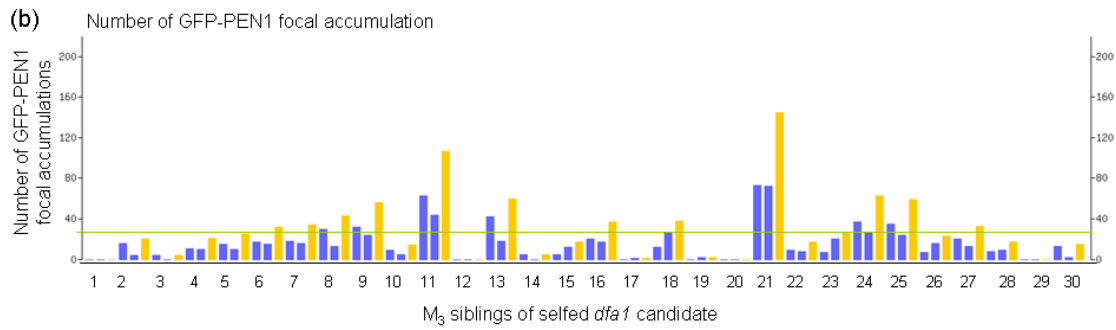
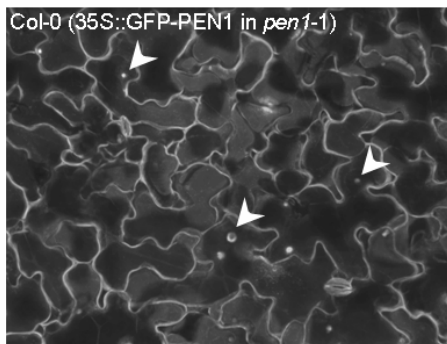
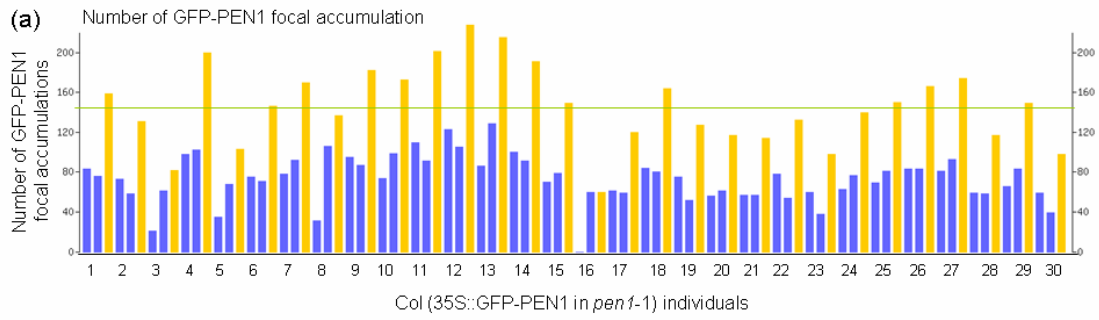


Figure 22. Comparison between the number of GFP-PEN1 focal accumulations in wild-type plants and the *dfal* mutant.

Plants were inoculated with *Blumeria graminis* f. sp. *hordei* (*B. g. hordei*) and leaves were imaged at 24 hpi by the fully automated confocal microscope for high-throughput screening by the Opera microscope. (a) *Arabidopsis* plants expressing GFP-PEN1 in *pen1-1* mutant background behaved like wild type in terms of *B. g. hordei* penetration phenotype. The graphic displays the number of GFP-PEN1 FA of 30 imaged Col-0 (p35S::GFP-PEN1 in *pen1-1*) individuals, it shows an average of 146 GFP-PEN1 FAs per individual plant (green line). The image displays the microscopic phenotype of the wild type GFP-PEN1 FA pattern. The arrowheads mark the GFP-PEN1 FAs. (b) The graphic exhibits the number of GFP-PEN1 FA of 30 M₃ siblings of selfed *dfal* mutant. It shows an average number of 30 GFP-PEN1 FAs per individuum (green line). The image displays the microscopic phenotype of the mutant. GFP-PEN1 FAs are marked by arrowheads. FA, GFP-PEN1 focal accumulation.

For one candidate, named hereafter *dfal* (*defect in focal accumulation*), the phenotype was confirmed in the M₃ progeny. As shown in Figure 22 b, *dfal* exhibited a significantly reduced number of GFP-PEN1 FAs (31 +/- 33) compared to wild type (146 +/- 40; $p < 0,05$; Figure 22 a). Some *dfal* individuals (e.g. *dfal* individual number 11 with 107 scored GFP-PEN1 FAs or number 21 with 145 scored GFP-PEN1 FAs in Figure 22 b) displayed a higher frequency of GFP-PEN1 FA compared to some wild type plants (e.g. number 3 with 82 scored GFP-PEN1 FAs or 23 with 98 scored GFP-PEN1 FAs in Figure 22 a). Possibly, this distribution illustrates the variation of the phenotype. Alternatively, the fungal spore density is not equal on every plant leaf and could explain the variation in GFP-PEN1 FA frequency. A current disadvantage in the automated screen is that it is not possible to search for areas with desired spore density.

With respect to the other output parameters; size, shape and signal intensity of the GFP-PEN1 FAs; wild type and *dfal* mutant plants behaved similarly (data not shown). The only difference was a lower number of GFP-PEN1 encased haustoria found in the *dfal* mutant compared to wild type. An average of 16 (+/-7) GFP-PEN1 encased haustoria per individual plant were observed in wild type plants, whereas only 2 (+/-2) GFP-PEN1 encased haustoria per individual plant were found for the *dfal* mutant. This discrepancy was expected, since *dfal* also displayed a reduced frequency of GFP-PEN1 FA, suggesting that the same secretory

Results

pathway is involved in PEN1 FA at papillae and haustorial structures (see also chapter 3. 1. 1 and 3. 1. 3).

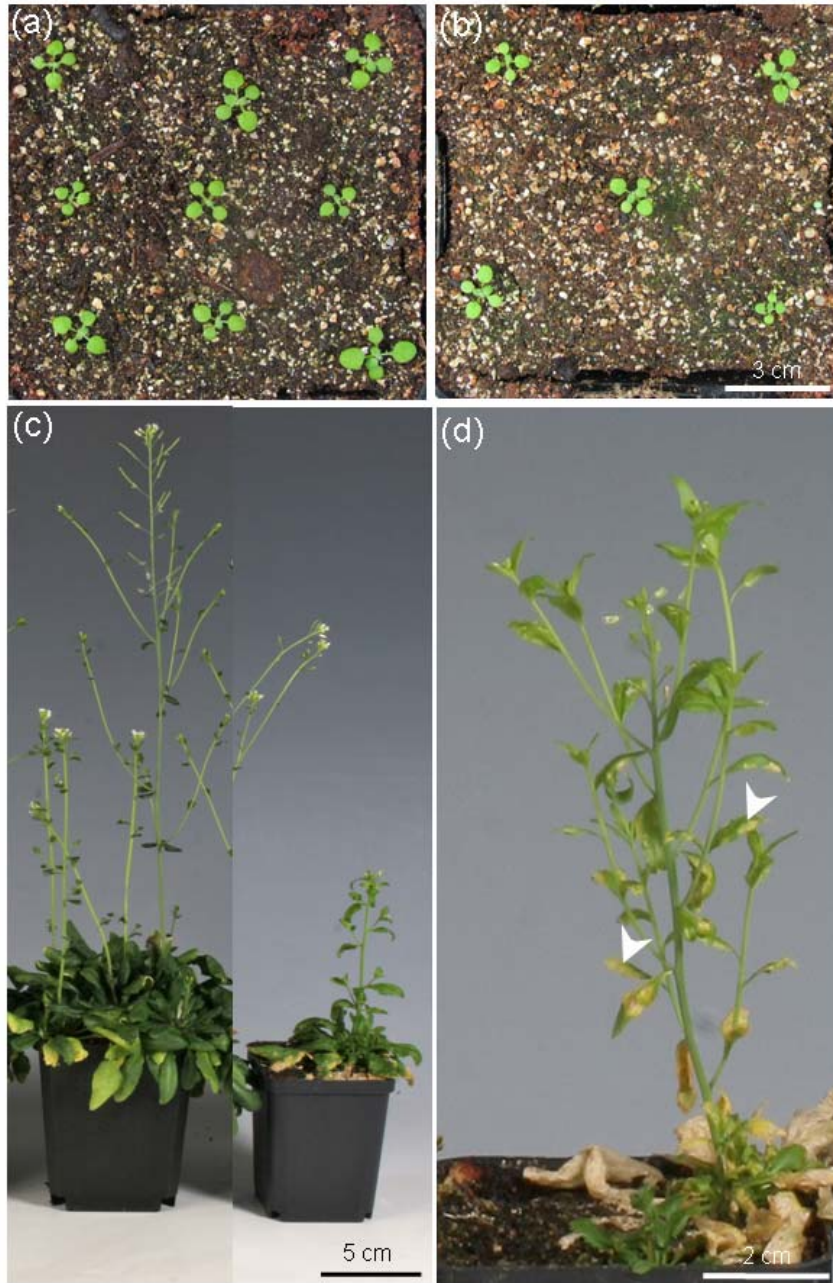


Figure 23. *dfa1* mutants display a developmental-dependent phenotype.

(a) Two weeks old *Arabidopsis* plants expressing GFP-PEN1 in *pen1-1*. (b) Two weeks old *dfa1* mutant. A difference in macroscopic phenotype, compared to wild type plants is not visible. (c) Ten weeks old *Arabidopsis*

plants. The plant on the left expresses GFP-PEN1 in the *pen1-1* mutant background. The *dfa1* plant is shown on the right. (d) Close-up view of *dfa1*. The mutant displays in addition to dwarfism, spontaneous lesions on the leaves (arrowheads).

The *dfa1* mutant was also analysed during its entire life cycle. Notably, the analysis was confined to the M₃ progeny originating from selfed M₂ *dfa1*. No backcrosses with eliminated other chemically induced mutations have been analysed. The *dfa1* mutant revealed a wild-type like macroscopic phenotype in two week old plants, which was used for microscopy of *B. g. hordei* infected leaves (Fig 23 b), indicating no recognizable pleiotropic effects at this developmental stage. However, ten weeks old *dfa1* plants were dwarf and exhibited spontaneous lesion formation. Inoculation experiments showed that *dfa1* is resistant to the adapted powdery mildew *G. orontii*, as depicted in Figure 24.

Together, the dwarf phenotype and the resistance to an adapted pathogen is reminiscent of mutants with a constitutive active defence response. One example of a mutant with constitutive active defence response, is the *cpr5* (*constitutive expression of pathogenesis-related proteins*) mutant (Bowling et al., 1997). Systemic acquired resistance is defined as a plant defence response that occurs after infection by an adapted pathogen and results in long-lasting, non-specific, systemic resistance to subsequent pathogen infection. It is characterized by activation of pathogenesis-related genes and dependent on SA (Ross, 1961). *cpr5* was identified in a screen for constitutive expression of systemic acquired resistance. The mutant is significantly smaller than wild type plants and shows spontaneous lesions. In addition it is constitutively resistant to two adapted pathogens (Bowling et al., 1997).



Figure 24. *dfa1* mutant plants are resistant to the adapted powdery mildew *Golovinomyces orontii*.

Three weeks old plants were inoculated with the adapted powdery mildew *Golovinomyces orontii*. The macroscopic phenotype was checked at 19 dpi. (a) The line p35S::GFP-PEN1 in *pen1-1* shows sporulation of the *G. orontii*. (b) *dfa1* mutant plants reveal a resistant phenotype.

Bar = 2 cm.

4. Discussion

4. 1 PEN1 focal accumulation might be suppressed by adapted powdery mildews

Polarised secretory processes are likely to contribute to defence responses in a variety of pathosystems. Diverse studies report the accumulation of vesicles and vesicle-like structures at plant pathogen interaction sites (Collins et al., 2003; Schulze-Lefert, 2004; An et al., 2006b; Hüchelhoven, 2007). H₂O₂-containing vesicles were frequently detected at sites of attempted pathogen entry. Interestingly, the incidence of H₂O₂-containing vesicles appears to correlate with a successful resistance response, since more H₂O₂-containing vesicles are observed at attempted entry sites of non-adapted than of adapted interaction sites (Thordal-Christensen et al., 1997; Collins et al., 2003; Hüchelhoven, 2007). Onion cells react with the accumulation of diverse phenolic compounds at infection sites of *Botrytis allii* (Stewart and Mansfield, 1985). In addition, in epidermal cells of sorghum leaves, at attempted entry sites of the hemibiotroph *Colletotrichum graminicola*, a focal accumulation of phytoalexins is detectable (Snyder and Nicholson, 1990).

SNARE proteins in yeast and animals are involved in controlling vesicle traffic and bulk transport of cargo in cells. Formation of a ternary SNARE complex consisting of syntaxin, SNAP25-like protein and v-SNARE, drives membrane fusion (Bock et al., 2001). Recently, the syntaxin *AtPEN1* was found to be required for preinvasion resistance in *Arabidopsis* to the non-adapted powdery mildew *Blumeria graminis* f. sp. *hordei* and is suggested to have a secretory function in the defence process (Collins et al., 2003; Schulze-Lefert, 2004). In addition, the SNAP25-homolog *AtSNAP33* was shown to form a binary SNARE complex with *AtPEN1* and to be required for preinvasion resistance (Collins et al., 2003). Evidence for the third binding partner of a ternary SNARE complex to mediate membrane fusion was recently reported by Kwon et al. (2008). The authors showed that PEN1-SNAP33-VAMP721/722 complexes are required for immune responses to powdery mildew and

oomycete pathogens, and provided the first biochemical and genetic evidence for ternary SNARE complex functions in plants.

An additional syntaxin other than *AtPEN1* was shown to be involved in SNARE-mediated defence responses of plants against bacteria. Transgenic tobacco leaves expressing the tomato resistance gene *Pto* show a visible resistance response, when inoculated with *Pseudomonas syringae* pv *tabaci* expressing the corresponding avirulence gene *AvrPto* (Kalde et al., 2007). Virus-induced-gene silencing of the *NbSYP132* syntaxin did not alter bacterial growth in the compatible interaction, but compromised *Pto*-mediated resistance in the incompatible interaction. Possibly, virulent bacteria already interfere with *NbSYP132*-mediated secretion and thus loss of the syntaxin caused no further effect. Secretion of PR1a, a defence marker protein, was detectable in the plant cell wall in the incompatible interaction, and less PR1 secretion was detectable in silenced plants, indicating a role for *NbSYP132* in secretion of antimicrobial compounds and/or defence-related proteins. Silencing of *NbSyp121*, the ortholog of the *AtPEN1* syntaxin, did not alter the *Pto*-mediated resistance response in the incompatible interaction, demonstrating that *NbSYP121* is dispensable for resistance against bacteria, whereas *NbSYP132* contributed significantly. The data indicate a potential specificity for particular syntaxins in secretion of defence-related cargo (Kalde et al., 2007). Thus, different pathogens might trigger secretion that is mediated by different subsets of SNARE proteins, thereby determining specific antimicrobial cargo.

Subcellular localisation studies of fluorescently tagged SNARE proteins in response to fungal attack demonstrated a focal accumulation of GFP-PEN1, YFP-SNAP33 and GFP-VAMP722 at attempted fungal entry sites of the non-adapted powdery mildew *B. g. hordei* (Assaad et al., 2004; Bhat et al., 2005; Kwon et al., 2008). Thus, the localization of the SNAREs is consistent with the presumed focal secretory process in defence responses at pathogen entry sites. It remains to be shown, however, whether the focal accumulation of SNARE proteins is essential for resistance responses.

Herein, I addressed two aspects of SNARE activity in defence responses. First, I explored the importance of PEN1 focal accumulation at pathogen entry sites of adapted and non-adapted

pathogens. Second, I characterized the specificity and appearance of this focal accumulation in response to these pathogens. For this purpose, I used an *Arabidopsis* transgenic line expressing GFP-PEN1.

Specifically, I analysed GFP-PEN1 focal accumulation (FA) at attempted entry sites of different directly penetrating pathogens by confocal microscopy (see 3.1.1). I could detect GFP-PEN1 FA at attempted entry sites of all three powdery mildew species tested, the non-adapted *B. g. hordei* and *E. pisi* and the adapted *G. orontii* (Figure 4). The finding that GFP-PEN1 FA is also detectable in the adapted interaction indicates that PEN1 FA is not restricted to non-adapted interaction sites and that PEN1 FA *per se* is not sufficient to terminate fungal entry. Thus, PEN1 FA is not a marker for resistance responses to powdery mildews.

As previously reported, GFP-PEN1 FA was not detectable at attempted penetration sites of both hemibiotrophic *Colletotrichum* species tested, the adapted *C. higginsianum*, and the non-adapted *C. lagenarium* (Shimada et al., 2006). Consistent with these results, I could not observe a GFP-PEN1 signal at attempted penetration entry sites of adapted *C. higginsianum* and non-adapted *C. destructivum*. Likewise, GFP-PEN1 FA was not recognisable at attempted fungal entry sites of the hemibiotrophic fungus, *Magnaporthe grisea*, or at entry sites of the non-adapted rust fungus *Phakopsora pachyrhizi*. Thus, PEN1 FA appears to be specific for powdery mildews. Possibly, only powdery mildews trigger PEN1 FA. This could involve the release of a powdery mildew-specific PAMP, recognised by the plant to trigger PEN1-mediated focal secretion.

It is conceivable that recognition of pathogens other than powdery mildews operates *via* a different preinvasion resistance pathway. Another PAMP may be recognised by triggering a different signalling pathway that is absent in powdery mildews. This might trigger altered PEN1-independent vesicle secretion with possible different antimicrobial cargo. This is in accordance with the finding that in bacteria defence-related secretion is mediated by *NbSYP132* and is independent of *NbSYP121*, the tobacco homolog of PEN1 (Kalde et al., 2007). However, in powdery mildews preinvasion resistance is dependent on *AtPEN1* in *Arabidopsis* and on its orthologue *HvROR2* in barley (Collins et al., 2003). Together, the data indicate a potential specificity for particular syntaxins in the secretion of defence-related

cargo (Kalde et al., 2007). It is also conceivable that pathogens other than powdery mildews are able to manipulate a potential PEN1-mediated secretory pathway. Possible suppression or absence of initiation of GFP-PEN1 FA by non-adapted pathogens, correlate well with the finding that PEN1 is not required for preinvasion resistance to *Colletotrichum* species and that GFP-PEN1 does not accumulate at attempted entry sites of all non-powdery mildews tested (Shimada et al., 2006) (and this study).

Colletotrichum and *Magnaporthe* species show different host cell entry strategies in comparison to powdery mildew. *Colletotrichum* and *Magnaporthe* form a specialised infection structure, the melanised appressorium. The structural reinforcement provided by the melanin allows the generation of enormous turgor pressure within the appressorium, which drives the emerging penetration peg forcefully through the plant cuticle (Bourett and Howard, 1990; Perfect et al., 1999; O'Connell et al., 2004). Furthermore, enzymes including cutinases, are involved in the penetration process (Skamnioti and Gurr, 2007). In contrast, powdery mildews build a lower turgor pressure in mature appressorial germ tubes, relying instead mainly on release of enzymes to penetrate epidermal cells (Belanger and Bushnell, 2002). Based on the findings presented here, it appears that powdery mildew specific enzymes or small molecules may induce GFP-PEN1 FA. Such secreted compounds might be absent from other fungal species tested. Alternatively, *Colletotrichum* and *Magnaporthe* species initially trigger PEN1 FA, but at the same time release molecules to interfere with the signalling pathway and suppress it.

4. 2 GFP-PEN1 FA is located inside papillae

During pathogen infections, callosic papillae are formed beneath the pathogen entry site between cell wall and plasma membrane. Callose has been suggested to provide a medium for the deposition of toxic compounds (Aist, 1976). Besides callose, also phenolics,

polysaccharides, reactive oxygen species and hydrolases were found to accumulate in papillae and are likely to constitute effective barriers to fungal penetration (Belanger and Bushnell, 2002). In addition, membrane-like structures have been frequently found in papillae (Aist, 1976; An et al., 2006a; Zeyen and Bushnell, 1979; Assaad et al., 2004), suggesting the presence of vesicles inside papillae. The papilla is deposited in the apoplast. The apoplastic environment is important as primary site of interaction between plant and pathogen since many biotrophic pathogens do not cross the host plasma membrane barrier. Based on cell culture experimental systems, the apoplastic pH optimizes both membrane transport and enzyme activities: a Ca^{2+} influx into the cytoplasm and a K^{+} efflux are common to most defence elicitation response systems and lead to an extracellular alkalinisation, as found in French bean cells treated with a cell wall elicitor from *Colletotrichum lindemuthanum* (Bolwell et al., 2002). By the use of ion-selective microprobes in barley, a strong alkalinisation of the apoplast is detectable in resistant interactions with powdery mildews, whereas alkalinisation is less obvious in susceptible barley (Felle et al., 2004). The authors concluded that a low pH might maximize the activity of fungal cell wall degrading enzymes and might have a role in fungus-induced host cell wall loosening. Thus, the apoplastic proton environment might be pivotal for both elicitor signal transduction and for the success of fungal penetration (Felle et al., 2004; Hückelhoven, 2007).

The GFP-PEN1 signal was found inside papillae in optical cross-sections by confocal microscopy analysing GFP-PEN1-expressing *Arabidopsis* at 17-24 hpi with non-adapted *B. g. hordei* or adapted *Erisiphe cichoracearum* (Assaad et al., 2004). Genetic evidence for *AtPEN1* involvement in papillae formation was found by observing a delay in papillae formation in *pen1-1* mutant plants. In addition, membrane-like entities were detectable in papillae by TEM analysis, suggesting that *AtPEN1* accumulates inside papillae. This led to the suggestion that PEN1 plays an active role in polarised secretion events that give rise to the formation of papillae during fungal attack (Assaad et al., 2004). These data correlate well with plasmolysis experiments in GFP-PEN1-expressing *Arabidopsis* showing that after retraction of the plasma membrane at least a proportion of GFP fluorescence appears to be in the interior of the papilla at 12 hpi after *B. g. hordei* inoculation (pers. communication, S.

Pajonk). In contrast, Bhat et al. (2005) observed that GFP-PEN1 FA at attempted entry sites of *B. g. hordei* remained in the plasma membrane after plasmolysis. The authors suggest that the GFP-PEN1 FA is separable from papillae by forming a pathogen-triggered plasma membrane microdomain.

To examine the accumulation of PEN1 at FA sites more closely, I analysed the longevity of GFP-PEN1 FA triggered by *B. g. hordei* at 7, 10, and 14 dpi (see 3.2.1). Acquisition of spectra between 500 to 564 nm in optical cross sections through FA sites of GFP-PEN1 expressing transgenic plants revealed an authentic GFP signal even at 14 dpi (Figure 7), demonstrating that GFP remains functional and that GFP-PEN1 might be protected inside papillae against degradation. Alternatively, the GFP-signal in the interior of papillae represents a cleavage product of the GFP-PEN1 fusion protein. This latter possibility appears less likely since transient assays in barley revealed no focal accumulation of similar fluorescently tagged plasma membrane fusion proteins, such as two aquaporin isoforms or a lipid transfer protein (Bhat et al., 2005). To my knowledge, little is known about the longevity of pathogen induced cell wall appositions. Leaf growth comprises *de novo* synthesis and elongation of the cell wall, a process that involves many enzymes for remodelling. Therefore, it is possible that the GFP-PEN1 FA disappears at later time points during the process of intrinsic cell wall remodelling. Taken together, the reported data from optical cross-sections of the GFP-PEN1 FA (Assaad et al., 2004), plasmolysis experiments (pers. communication, S. Pajonk) and data from spectral analysis in this study, suggest the localisation of GFP-PEN1 in the interior of the papilla.

The mechanisms by which PEN1 becomes localised to papillae is currently unclear. One potential mechanism might involve outward budding of multi vesicular bodies (MVB), which release their internal vesicles into the apoplast. This is reminiscent of animal exosome secretion (An et al., 2006a; Li et al., 2006; van Niel et al., 2006). Unusual trafficking and fusion events, involving fusion of large vesicles at papillae, have been reported during papillae formation in barley (Zeyen and Bushnell, 1979). Vesicles retaining PEN1 in the vesicle membrane, harbouring cargo with antimicrobial compounds or compounds required for papilla formation may be secreted into the apoplast and accumulate inside the papilla to

directly defend the intruder. This correlates with the frequent occurrence of vesicles and membrane-like material and the co-localisation of GFP-PEN1 and callose in papillae (Aist, 1976; Assaad et al., 2004; An et al., 2006a) (Zeyen and Bushnell, 1979). Identification of mutants impaired in GFP-PEN1 FA could shed light on this mechanism and help to unravel underlying processes.

The apoplastic proton environment was suggested to be important for both elicitor signal transduction and for the success of fungal penetration (Felle et al., 2004; Hückelhoven, 2007). At least GFP originating from GFP-PEN1 fusion protein remains functional in the interior of papillae (see 3.2.1).

An independent method to examine whether PEN1 localises to the interior of papillae could be immunolabeling of papillae of inoculated plant tissue with a PEN1 antibody. To address this point, initial immunolocalisation of native PEN1 to papillae in wild type plants with a PEN1 antibody was attempted on resin-embedded isolated haustorial complexes (see 3.1.6). However, due to low specificity of the antibody no conclusion could be drawn on PEN1 localisation. These experiments require further optimisation. Alternatively, papillae or haustoria microdissection followed by western blotting with PEN1 antibody may also clarify this question.

4. 3 Mature haustorial complexes contain GFP-PEN1 and membranous material

The callose-containing haustorial encasement of plant pathogens forms a collar around the haustorial neck as an extension of the papilla, and can extend to the haustorial body and enclose the entire haustorium (Bushnell, 1972). Several studies report a potential suppression of haustorial encasements by pathogens. In a non-adapted interaction of cowpea and rust, the formation of an encasement was suggested to terminate fungal growth (Heath and Heath, 1971). In rust-infected roots of chrysanthemum plants the haustoria were encased after

treatment with a fungicide, also suggesting that death of haustoria is accompanied by encasement (Aist, 1976). This is in accordance with Skalamera et al. (1997), who observed that heat-shock treatment of rust-infected leaves killed the fungus and resulted in callose encasements of intracellular structures in both resistant and susceptible cultivars. In the adapted interaction wheat - *Erysiphe graminis* f. sp. *tritici* (*E. g. tritici*), an increase of haustorial encasements was detected after treatment with the fungicide Bromuconazole (Mangin-Peyrard and Pépin, 1996).

In different plant-pathogen interactions, different frequencies of haustorial encasements were reported. In the adapted interaction wheat - *E. g. tritici* only 2% of haustorial complexes are encased at 7 dpi (Mangin-Peyrard and Pépin, 1996). In the adapted interaction *Arabidopsis* - *Hyaloperonospora parasitica*, 48% of fully developed haustoria are encased at 5 dpi (Donofrio and Delaney, 2001). In the adapted interaction of cowpea and the rust *Uromyces vignae*, 45% – 55% of haustoria are encased already at 1 dpi. A higher frequency of encasements in non-adapted versus a lower frequency in adapted interactions, points towards a role in defence for haustorial encasements. An encasement would presumably block or decrease nutrient uptake and/or virulence factor delivery to and from the host.

The encasement is deposited after the haustorium has been formed and the mode of growth is through localised addition of material to the callose-containing deposit formed on the host cell wall at the time of penetration (Heath and Heath, 1971). Membranous material accumulates inside the haustorial encasement (Heath and Heath, 1971; Bushnell, 1972). Analysis of ultrathin sections by electron microscopy revealed a highly convoluted host plasma membrane adjacent to the encasement. Also, irregular membrane portions became trapped between the developing encasement and the haustorial wall in a cowpea resistant to the cowpea rust *Uromyces phaseoli* var. *vignae*. The trapped membrane material might have been derived from sequestration of excess membrane (Heath and Heath, 1971).

Taken together, the mechanisms behind haustorial encasement formation are unclear. Furthermore, the role of haustorial encasements in defence responses is still unknown. The reported data point to a function of encasement in plant defence, but it is also conceivable that the encasement or at least gene-products needed for the encasement are required for pathogen

growth. This is reminiscent of findings about the plant GSL5/PMR4 callose-synthase that is responsible for callose deposition in response to biotic and abiotic stress. Interestingly, *gsl5/pmr4* mutants are resistant rather than susceptible to adapted powdery mildew, indicating that either callose or callose synthase may have differential roles in pathogenesis (Jacobs et al., 2003; Nishimura et al., 2003). Callose might be needed by some fungi for successful pathogenesis, maybe as physical support for fungal development as structural scaffold to accommodate haustorial complexes. Although, this seems unlikely since haustorium differentiation was not detectable in *gsl5/pmr4* mutant plants compared to wild type plants at least at light microscopic level. Alternatively, the callose might serve as protection barrier preventing recognition of pathogen-derived molecules by the host, e.g. lack of callose might expose fungal cell wall polysaccharides or secreted proteins (Jacobs et al., 2003).

This study characterized haustorial encasements by callose and GFP-PEN1 of three powdery mildews and of the oomycete *H. parasitica* in the interaction with *Arabidopsis* plants (see 3.1.3 and Figure 8). In addition, haustorial complexes in the adapted interaction of *B. g. hordei* and barley were analysed by callose staining (see 3.1.3 and Figure 9). I wanted to explore whether callose and PEN1 are part of the same structures and have similar dynamics of deposition and maintenance.

I detected a GFP-PEN1 FA restricted to the encased portion of haustorial complexes in the interaction between the powdery mildews and *Arabidopsis*. Since the GFP-PEN1 encasement was observed in the adapted and non-adapted powdery mildew interaction, it is conceivable that the encasement phenomenon is a component of basal defence. Alternatively, the encasement is a consequence of haustorial aging. This would correlate with reported data that only mature haustoria become encased by callose (Heath and Heath, 1971). This is consistent with my finding that only mature haustoria were encased by GFP-PEN1 (see 3.1.7 and Figure 17). Interestingly, labelling of GFP-PEN1 spatially coincides with FM4-64 labelling, suggesting membranous material in the interior of the encasement. This is in agreement with former TEM analysis in which membranous material was detected in encasements (Heath and Heath, 1971; Bushnell, 1972), suggesting the potential presence of vesicles inside papillae.

Since *pen1-1* mutants showed a delay in papillae formation in the non-adapted interaction with *B. g. hordei* and PEN1 focally accumulated inside papillae, it was suggested that PEN1 is involved in papilla formation (Assaad et al., 2004). Given that papillae formation is delayed but not abolished in *pen1-1* mutants points to redundancy on the level of plasma membrane syntaxins, but also to the resilience of non-host resistance (Assaad et al., 2004). Maybe, PEN1-mediated vesicle secretion is involved in papillae as well as in haustorial encasement formation. If so, a delay in development of haustorial encasements would be expected in *pen1-1* mutant plants. In this study the GFP-signal at haustorial encasements spatially coincided with the callose signal for all powdery mildews tested, but for *H. parasitica* encasements the correlation was only partial (Figure 8). It is conceivable that vesicle secretion and encasement formation are temporally separated in this interaction. Maybe, GFP-PEN1 containing vesicles accumulate at the tip of the callose encasement and the vesicles may not be completely incorporated in the callosic structure at the tip. This could be evidence for tip growth of the encasement. Since a GFP-PEN1 FA was not detectable at entry sites of *H. parasitica*, it is possible that the PEN1 accumulation at penetration sites is initially suppressed by the oomycete. As the phenomenon was observed at several interaction sites tested, it is highly unlikely to be due to incomplete staining of callose.

Callose encasement of haustorial complexes was not detectable in the adapted interaction between *B. g. hordei* and the monocotyledon barley (see 3.1.3 and Figure 9), whereas a partial callose and GFP-PEN1 encasement was detectable in the non-adapted interaction between *B. g. hordei* and the dicotyledon *Arabidopsis* (Figure 10 c). At least regarding the callose encasement, *B. g. hordei* might be able to fully suppress encasements in the adapted barley interaction and thus is able to grow and propagate on barley. In contrast, in the non-adapted interaction between *Arabidopsis* and *B. g. hordei* the fungus is only partially able to suppress the callose encasement. Alternatively, monocotyledons are missing a specific PAMP receptor, recognising the pathogen and trigger the encasement to terminate fungal growth. As papilla formation was observed, this potential receptor and signalling pathway must be independent from papilla formation pathway. To investigate whether PEN1 encasements at haustorial

complexes is actively suppressed by pathogens, heat-shock experiments or fungicide treatments could be performed. If more encasements are observed after killing of a pathogen, this hints to an active suppression of PEN1 in encasements by the fungus. However, these experiments are critical since they can also affect the plant.

To test whether PEN1 accumulation is dependent on callose accumulation, ultrathin sections of embedded *G. orontii* haustorial complexes that were isolated from different plant genotypes, were analysed by confocal microscopy (see 3.1.6). Callose staining showed PMR4/GSL5-mediated callose deposition at haustorial complexes grown on *pen1-1* mutants (Figure 14). The results indicate that PMR4/GSL5-mediated callose deposition is an independent process from GFP-PEN1 FA. This is in accordance with the finding that GFP-PEN1 FA is independent of the cytoskeleton (Bhat et al., 2005), whereas the callose accumulation is cytoskeleton-dependent (Schmelzer, 2002). Since *pen1-1* null mutant plants exhibit a delay but not an exclusion of papillary callose against a broad range of fungal pathogens (Assaad et al., 2004; Shimada et al., 2006), it is possible that due to genetic redundancy callosic haustorial encasements developed in *pen1-1* mutant plants.

Taken together, it was a novel finding that GFP-PEN1 FA was not confined to papillae, but was also detectable in haustorial encasements. The detected membranous material in the interior of haustorial encasements and PEN1-vesicles potentially incorporated in the encasement point to a function of SNARE proteins in the postinvasive stage.

4. 4 Haustorial complexes preferentially contain t-SNAREs

To examine whether SNARE proteins other than PEN1 accumulate in haustorial encasements, different transgenic *Arabidopsis* lines, expressing fluorescently tagged t- or v-SNARE proteins, were inspected (see 3.1.5). Haustorial complexes were analysed after *G. orontii* inoculation. In addition, lines expressing fluorescently tagged plasma membrane marker

proteins were analysed to determine specificity. GFP-PEN1 and callose encasements were observed and quantified by confocal microscopy (see 2.2.6).

The data revealed a preferential FA of the t-SNARES GFP-PEN1 and YFP-SNAP33 at sites of haustorial encasements (Figure 13 b). Notably, the frequency of YFP-SNAP33-encased haustoria was higher than the frequency of callose-encased haustoria scored (Figure 13 d). Possibly, the YFP-SNAP33 accumulation around some haustoria was not localised to the interior of the callose encasement. This suggests that SNAP33 accumulates in the extrahaustorial matrix surrounding the haustorium as well as in the encasement. Presumably, SNAP33 loses its membrane anchor and becomes secreted into the extrahaustorial matrix during potential secretion of PEN1- and SNAP33-membrane-containing vesicles, whereas PEN1 remains in the extrahaustorial membrane. This would also explain the detected PEN1 in the extrahaustorial membrane (Figure 15).

24% of haustoria were encased by YFP-SNAP33, which was the highest frequency found for all lines tested. It was more than twice as much as for PEN1 and ten times more than found for VAMP722-containing encasements. Since SNAP33 is the only SNAP25-like protein transcribed in *Arabidopsis* leaves (Kwon et al., 2008), it is likely that SNAP33 is involved in all ternary SNARE complexes built in leaf tissue. A relatively low percentage of haustoria was encased by GFP-VAMP722, compared to GFP-PEN1 or YFP-SNAP33 encasements (Figure 13 b). The quantitative data for these three SNAREs were expected to be more equal, since VAMP722 was shown to form a ternary SNARE complex with PEN1 and SNAP33 *in vitro* and *in planta* and is involved in defence responses to *G. orontii* (Kwon et al., 2008). Possibly, GFP-VAMP722 accumulation was below the detection limit, as it was driven by its own promoter and was microscopically only visible in attacked cells (Kwon et al., 2008). Alternatively, differential recycling of SNAREs led to the unequal distribution detected. Presumably, VAMP722, but not PEN1 or SNAP33 are recycled after vesicle fusion at the extrahaustorial membrane. This could explain VAMP722 involvement in defence response to *G. orontii*, although it is not always detectable in the interior of haustorial encasements. It is also conceivable that VAMPs other than VAMP722 are involved in vesicle secretion

processes. Together, the data indicate that PEN1 and VAMP722 are not the only syntaxins and v-SNARES respectively, involved in defence-related secretion towards haustoria.

Concluding, the SNARE machinery leading to PEN1-SNAP33-VAMP722 accumulation at pathogen entry sites in preinvasion resistance might also be involved in postinvasion resistance at the level of haustorium development. So far, genetic evidence for this hypothesis is missing. Possibly, characterization of timely haustorial callose encasement formation in *pen1-1* mutants and VAMP haplo-insufficient mutant lines, could help to demonstrate a genetic evidence for SNAREs in postinvasive immunity. Since *vamp721/vamp722* double mutants are lethal, haplo-insufficient lines would have to be used, which are lines homozygous for *vamp721* and heterozygous for *vamp722* or lines homozygous for *vamp722* and heterozygous for *vamp721* (Kwon et al., 2008).

4. 5 Development of a high-throughput screening method for living plant tissue

I developed a new automated, high-throughput microscopic screening method (see 3.2.4) that collects quantitative data to characterise the GFP-PEN1 FA in an unbiased manner. It is far less labour-intensive than conventional microscopy and the analysis can be carried out in a reasonable timeframe by a standardised evaluation procedure. The developed script for GFP-PEN1 FA recognition can be easily adjusted to other patterns, but a fluorescently tagged fusion protein of the protein of interest is prerequisite. Through the possibility to score different parameters, mutants showing abnormalities in diverse microscopically features can now be scored. Most of the new features are impossible to score by eye, for example the size or signal intensity of GFP-PEN1 FA. This also explains why more mutants were identified in the automated screening approach compared to the initial manual screen (see 3.2.6). Moreover, the multiparametric analysis of GFP-PEN1 FA triggered by adapted and non-adapted powdery mildews revealed more differences and similarities than did the detection by

eye (see 3.2.5). Already the manual screen (see 3.2.3) revealed that mutants showing no GFP-PEN1 FAs were juvenile lethal, indicating that the genes of interest are also important for some stages of plant development. With the new approach it is possible to identify mutants with reliable but more subtle phenotypes, probably harbouring weak alleles of the genes of interest. Evidence for advantages of the automated method is provided by the identification of the *dfa1* mutant (see 3.2.7).

Concluding, this was the first demonstration of high-throughput confocal imaging in living plant tissue at subcellular resolution. The method might help to recover mutant plants containing weakly defective alleles showing subtle changes in GFP-PEN1 frequency or intensity, which would be missed in a manual screen. Null mutations, likely due to complete loss of GFP-PEN1 FA, in these genes might be lethal.

4. 6 Multiparametric analysis of the GFP-PEN1 focal accumulation

To further investigate GFP-PEN1 FA, the Opera microscope was applied for detailed analysis. Only with the new automated imaging approach it was possible to characterize different features of the GFP-PEN1 FA triggered by different fungi. As already discussed, GFP-PEN1 FA is triggered by adapted and non-adapted powdery mildews. The multiparametric analysis of GFP-PEN1 FAs revealed less frequent and weaker GFP-PEN1 FAs at adapted than at non-adapted interaction sites. This might indicate a suppression of GFP-PEN1 FA by the adapted powdery mildew and suggests that PEN1 FA is not a fungal counter defence mechanism. It is conceivable that adapted, but not non-adapted powdery mildews are able to suppress PEN1-mediated vesicle secretion to a certain level. This is consistent with the finding that PEN1 is required for preinvasion resistance to the non-adapted powdery mildew *B. g. hordei*, but is not required for penetration entry of the adapted powdery mildew *G. orontii* (Collins et al., 2003; Lipka and Panstruga, 2005).

The potential suppression of PEN1 FA by adapted powdery mildews is not complete; there is still GFP-PEN1 FA detectable though not as frequent and with a weaker GFP fluorescent signal compared to the GFP-PEN1 FA in the non-adapted interaction. It would be interesting to analyse if there is a delay in GFP-PEN1 FA for the adapted compared to non-adapted powdery mildew interaction. If that is the case, it is conceivable that the fungus suppresses the GFP-PEN1 FA for a certain time period during early infection and thus gains time for invasion. A potentially localised manipulation at the plasma membrane is in accordance with findings reported for rust. In a study by Mellersh et al. (2001), rust fungi locally manipulated plasma membrane cell-wall adhesions, namely Hecht threads, at attempted fungal entry sites. The authors suggested that the adapted fungus disrupts Hecht threads and thereby the cell-wall associated defence response (Mellersh and Heath, 2001).

4. 7 A number of juvenile lethal mutants were identified

A SNARE-mediated secretory pathway restricts in *Arabidopsis* entry of the non-adapted *B. g. hordei* (Collins et al., 2003; Assaad et al., 2004; Schulze-Lefert, 2004; Lipka et al., 2007; Kwon et al., 2008). SNARES as key players in vesicle fusion also play a crucial role in developmental processes. Loss-of-function mutants are often associated with severe morphological aberrations or lethality (Lipka et al., 2007).

In the manual (see 3.2.3) and in the automated screen (see 3.2.6) of this study a striking number of putative mutants were either juvenile lethal or showing a dwarf phenotype (see table 5 and table 6). These observations suggest that a mutation that leads to impairment in PEN1 FA also impairs development, indicating that the mutated gene may harbour two functions, one in development and one in defence. Notably, the putative mutants stayed alive until they reached the juvenile phase, suggesting that a gene not required until the juvenile phase in development, but required to confer PEN1 FA, is impaired in function. Alternatively,

there might be genetic redundancy for the function of these genes until the juvenile stage, but not thereafter.

4. 8 The *dfa1* mutant shows an altered GFP-PEN1 focal accumulation pattern

In this study, an EMS-mutagenised population expressing GFP-PEN1 was screened to identify mutants showing an altered GFP-PEN1 FA. One mutant line, designated *dfa1* (*defect in focal accumulation*) was identified (see 3.2.7; Figure 22 b). The *dfa1* mutant exhibits a reduced number of GFP-PEN1 FAs and a reduced number of GFP-PEN1-encased haustorial structures. It is conceivable that the same PEN1-dependent secretory pathway is involved in both processes, secretion towards papillae and encasements. *dfa1* confers resistance to the adapted *G. orontii* (Figure 24). Ten week old *dfa1* mutant plants display a dwarf phenotype with spontaneous lesions in the selfed progeny M₃ generation of the identified M₂ mutant line (Figure 23). The dwarf phenotype was observed as early as four weeks (preliminary observation). The phenotype might be dependent on the developmental stage. Notably, these plants might harbour secondary site mutations, since they were not yet backcrossed to eliminate other chemically induced mutations. However, it is important that *dfa1* at the time point of analysis in two week old plants had a wild-type-like phenotype, which likely excludes pleiotropic effects at that time point.

The *dfa1* macroscopic phenotype is reminiscent of mutants with a constitutive active defence response. For example, the *ssi4* (*suppressor of salicylic acid insensitivity of npr1-5*) mutant, was identified in a screen for suppressors of *npr1-5*-based salicylic acid (SA) insensitivity. Mutation of the *NPR1* gene causes SA insensitivity and SA sensitivity is recovered in *ssi4* mutant plants. Moreover, *ssi4* confers constitutive expression of several pathogenesis-related (PR) genes and induces SA-accumulation. It exhibits several morphological abnormalities, including stunted growth, severe chlorosis, and the development of spontaneous lesions. It also reveals enhanced resistance to bacterial and oomycete pathogens. *SSI4* encodes an R

protein, belonging to the TIR-NB-LRR class (Shirano et al., 2002). Another example of a mutant with constitutively active defence responses is the *cpr5* (*constitutive expression of pathogenesis-related proteins*) mutant. Systemic acquired resistance is defined as a plant defence response that occurs after infection by an adapted pathogen and results in long-lasting, non-specific, systemic resistance to subsequent pathogen infection. It is characterised by activation of pathogenesis-related genes and dependency on SA (Ross, 1961). *cpr5* was identified in a screen for constitutive expression of systemic acquired resistance (Bowling et al., 1997). The authors used a line expressing the promoter region of the *PR* gene β -1,3-glucanase 2 fused to the β -glucuronidase (*GUS*) and screened for constitutive expression of *GUS* (Bowling et al., 1997). The resulting *cpr5* mutant is significantly smaller than wild type plants and shows spontaneous lesions. In addition it is constitutively resistant to two virulent pathogens (Bowling et al., 1997).

Taken together, the *dfal* macroscopic and penetration phenotype is reminiscent of mutants showing constitutively active defence responses. It has to be shown whether *dfal* after backcrosses with Col-0 wild type retains all phenotypes seen in the M₃ generation. Isolation of the *DFAI* gene should help to understand the mechanism behind PEN1 FA and reveal its potential involvement in SNARE-mediated vesicle secretion at attempted pathogen entry sites. Possibly, it could also provide new insights into the process of pathogen induced cell polarity.

5. Supplementary data

Output parameters	<i>B. g. hordei</i>				<i>E. pisi</i>				<i>G. orontii</i>			
	24hpi		48hpi		24hpi		48hpi		24hpi		48hpi	
	mean value	STD	mean value	STD	mean value	STD	mean value	STD	mean value	STD	mean value	STD
Number of FA	111	38	124	42	48	25	132	66	35	29	72	48
Number of epidermal leaf cells	354	63	361	91	427	85	390	81	418	84	403	84
Number of GFP-PEN1 encased haustoria	5,48	3,62	11,06	6,2	6,2	4,46	20,22	11,97	1,5	2	6,14	6,14
Number of stoma	35	10	37	16	31	12	38	11	32	12	36	14
Number of FA per analysable area (orig *1000000)	22,68	7,45	27,6	8,36	10,7	5,3	28,33	13,1	7,94	6,77	15,46	10,23
Number of FA per cell	0,33	0,13	0,36	0,16	0,19	0,07	0,36	0,2	0,1	0,1	0,2	0,16
Total integrated FA signal per analysable area	1,88	0,77	1,41	0,48	0,6	0,36	2,07	1	0,41	0,37	0,95	0,68
Total integrated FA signal per analysable area, background subtracted	1,33	0,58	0,96	0,34	0,42	0,26	1,53	0,76	0,28	0,27	0,65	0,48
Average intensity of FA	1735	283	1188	190	1156	311	1607	265	1175	418	1395	433
Average area of FA	45,67	2,45	42,72	2,56	44,08	4,04	43,84	2,95	41,79	4,7	43,3	3,67
Total integrated FA signal, over all FAs (orig /1000)	9257	3932	6400	2447	2672	1597	9712	5075	1850	1698	4467	3291
Total integrated FA signal, background subtracted, over all FAs (orig /1000)	6519	2938	4314	1727	1915	1223	7189	3890	1262	1238	3031	2330
Average length of FA	8,23	0,27	8,09	0,31	8,17	0,47	8,07	0,3	8,16	0,67	8,23	0,45
Average half width of FA	2,66	0,08	2,53	0,07	2,58	0,11	2,59	0,09	2,48	0,12	2,54	0,1
Average width to length ratio of FA	0,66	0,02	0,64	0,01	0,65	0,03	0,66	0,01	0,63	0,04	0,63	0,02
Average roundness of FA	0,91	0,01	0,9	0,01	0,9	0,02	0,91	0,01	0,89	0,03	0,89	0,02
Average contrast of FA compared to the background signal	0,48	0,03	0,45	0,03	0,46	0,05	0,5	0,04	0,43	0,05	0,44	0,04
Average peak intensity of FA	2588	393	1816	286	1764	468	2424	371	1815	634	2135	630
Integrated FA signal per analysable area background subtracted per FA (orig * 1000)	48,5	12,53	34,66	16,36	38,06	18,41	49,93	16,64	30,43	15,73	38,46	23,63

Table SD 1. Multiparametric analysis of the GFP-PEN1 focal accumulation triggered by adapted and non-adapted powdery mildews. In some cases the original values were multiplied (orig*) or divided (orig/) by a number for simple representation

6 References

- Aist, J.R.** (1976). Papillae and Related Wound Plugs of Plant Cells. *Annual Review of Phytopathology* **14**, 145-163.
- Allen, F., and Friend, J.** (1983). Resistance of potato tubers to infection by *Phytophthora infestans*: A structural study of haustorial development. *Physiological and Molecular Plant Pathology* **22**, 285-292.
- An, Q., Huckelhoven, R., Kogel, K.-H., and van Bel, A.J.E.** (2006a). Multivesicular bodies participate in a cell wall-associated defence response in barley leaves attacked by the pathogenic powdery mildew fungus. *Cellular Microbiology* **8**, 1009-1019.
- An, Q., Ehlers, K., Kogel, K.-H., van Bel, A.J.E., and Huckelhoven, R.** (2006b). Multivesicular compartments proliferate in susceptible and resistant MLA12-barley leaves in response to infection by the biotrophic powdery mildew fungus. *New Phytologist* **172**, 563-576.
- Asai, T., Tena, G., Plotnikova, J., Willmann, M.R., Chiu, W.-L., Gomez-Gomez, L., Boller, T., Ausubel, F.M., and Sheen, J.** (2002). MAP kinase signalling cascade in *Arabidopsis* innate immunity. *Nature* **415**, 977-983.
- Assaad, F., Qiu, J.-L., Youngs, H., Ehrhardt, D., Zimmerli, L., Kalde, M., Wanner, G., Peck, S., Edwards, H., Ramonell, K., Somerville, C., and Thordal-Christensen, H.** (2004). The PEN1 Syntaxin Defines a Novel Cellular Compartment upon Fungal Attack and Is Required for the Timely Assembly of Papillae. *Mol Biol Cell* **15**, 5118-5129.
- Belanger, R.R., and Bushnell, W.R.** (2002). *The Powdery Mildews: A Comprehensive Treatise*. St. Paul, MN: APS Press.
- Bennett, M.K., Calakos, N., and Scheller, R.H.** (1992). Syntaxin: A Synaptic Protein Implicated in Docking of Synaptic Vesicles at Presynaptic Active Zones. *Science* **257**, 255-259.
- Bhat, R.A., Miklis, M., Schmelzer, E., Schulze-Lefert, P., and Panstruga, R.** (2005). Recruitment and interaction dynamics of plant penetration resistance components in a plasma membrane microdomain. *PNAS*, 0500012102.
- Bhattacharjee, S., Hiller, N.L., Liolios, K., Win, J., Kanneganti, T.-D., Young, C., Kamoun, S., and Haldar, K.** (2006). The Malarial Host-Targeting Signal Is Conserved in the Irish Potato Famine Pathogen. *PLoS Pathogens* **2**, e50.
- Biemelt, S., and Sonnewald, U.** (2006). Plant-microbe interactions to probe regulation of plant carbon metabolism. *Journal of Plant Physiology* **163**, 307-318.
- Billadeau, D.D., Nolz, J.C., and Gomez, T.S.** (2007). Regulation of T-cell activation by the cytoskeleton. *Nat Rev Immunol* **7**, 131-143.
- Bock, J.B., Matern, H.T., Peden, A.A., and Scheller, R.H.** (2001). A genomic perspective on membrane compartment organization. *Nature* **409**, 839-841.

- Bolwell, G.P., Bindschedler, L.V., Blee, K.A., Butt, V.S., Davies, D.R., Gardner, S.L., Gerrish, C., and Minibayeva, F.** (2002). The apoplastic oxidative burst in response to biotic stress in plants: a three-component system. *J. Exp. Bot.* **53**, 1367-1376.
- Bonifacino, J.S., and Glick, a.B.S.** (2004). The Mechanisms of Vesicle Budding and Fusion. *Cell* **116**, 153-166.
- Bourett, T.M., and Howard, R.J.** (1990). In vitro development of penetration structures in the rice blast fungus *Magnaporthe grisea*. *Canadian Journal of Botany* **68**, 329-342.
- Bowling, S.A., Clarke, J.D., Liu, Y., Klessig, D.F., and Dong, X.** (1997). The *cpr5* Mutant of *Arabidopsis* Expresses Both NPR1-Dependent and NPR1-Independent Resistance. *Plant Cell* **9**, 1573-1584.
- Brisson, L.F., Tenhaken, R., and Lamb, C.** (1994). Function of Oxidative Cross-Linking of Cell Wall Structural Proteins in Plant Disease Resistance. *Plant Cell* **6**, 1703-1712.
- Bromley, S.K., Burack, W.R., Johnson, K.G., Somersalo, K., Sims, T.N., Sumen, C., Davis, M.M., Shaw, A.S., Allen, P.M., and Dustin, M.L.** (2001). The Immunological Synapse. *Annual Review of Immunology* **19**, 375-396.
- Bushnell, W.R.** (1971). The haustorium of *Erysiphe graminis*: An experimental study by light microscopy. Morphological and Biochemical events in plant-parasite interaction, 229-254.
- Bushnell, W.R.** (1972). Physiology of Fungal Haustoria. *Annual Review of Phytopathology* **10**, 151-176.
- Chisholm, S.T., Coaker, G., Day, B., and Staskawicz, B.J.** (2006). Host-Microbe Interactions: Shaping the Evolution of the Plant Immune Response. *Cell* **124**, 803-814.
- Chou, C.K.** (1970). An Electron-Microscope Study of Host Penetration and Early Stages of Haustorium Formation of *Peronospora parasitica* (Fr.) Tul. on Cabbage Cotyledons. *Ann Bot* **34**, 189-204.
- Collins, N.C., Thordal-Christensen, H., Lipka, V., Bau, S., Kombrink, E., Qiu, J.-L., Huckelhoven, R., Stein, M., Freialdenhoven, A., Somerville, S.C., and Schulze-Lefert, P.** (2003). SNARE-protein-mediated disease resistance at the plant cell wall. *Nature* **425**, 973-977.
- Dangl, J.L., and Jones, J.D.G.** (2001). Plant pathogens and integrated defence responses to infection. *Nature* **411**, 826-833.
- Dangl, J.L., Ritter, C., Gibbon, M.J., Mur, L.A.J., Wood, J.R., Goss, S., Mansfield, J., Taylor, J.D., and Vivian, A.** (1992). Functional Homologs of the *Arabidopsis* RPM1 Disease Resistance Gene in Bean and Pea. *Plant Cell* **4**, 1359-1369.
- Das, V., Nal, B., Dujeancourt, A., Thoulouze, M.-I., Galli, T., Roux, P., Dautry-Varsat, A., and Alcover, A.** (2004). Activation-Induced Polarized Recycling Targets T Cell Antigen Receptors to the Immunological Synapse: Involvement of SNARE Complexes. *Immunity* **20**, 577-588.

- Davison, E.M.** (1968). Cytochemistry and Ultrastructure of Hyphae and Haustoria of *Peronospora parasitica* (Pers. ex Fr.) Fr. *Ann Bot* **32**, 613-621.
- DebRoy, S., Thilmony, R., Kwack, Y.-B., Nomura, K., and He, S.Y.** (2004). A family of conserved bacterial effectors inhibits salicylic acid-mediated basal immunity and promotes disease necrosis in plants. *Proceedings of the National Academy of Sciences* **101**, 9927-9932.
- Dhonukshe, P., Kleine-Vehn, J., and Friml, J.** (2005). Cell polarity, auxin transport, and cytoskeleton-mediated division planes: who comes first? *Protoplasma* **226**, 67-73.
- Dodds, P.N., Lawrence, G.J., Catanzariti, A.-M., Teh, T., Wang, C.-I.A., Ayliffe, M.A., Kobe, B., and Ellis, J.G.** (2006). Direct protein interaction underlies gene-for-gene specificity and coevolution of the flax resistance genes and flax rust avirulence genes. *Proceedings of the National Academy of Sciences* **103**, 8888-8893.
- Donofrio, N.M., and Delaney, T.P.** (2001). Abnormal Callose Response Phenotype and Hypersusceptibility to *Peronospora parasitica* in Defense-Compromised *Arabidopsis* *nim1-1* and Salicylate Hydroxylase-Expressing Plants. *Molecular Plant-Microbe Interactions* **14**, 439-450.
- Dow, M., Newman, M.-A., and von Roepenack, E.** (2000). The induction and modulation of plant defense responses by bacterial lipopolysaccharides. *Annual Review of Phytopathology* **38**, 241-261.
- Fasshauer, D., Sutton, R.B., Brunger, A.T., and Jahn, R.** (1998). Conserved structural features of the synaptic fusion complex: SNARE proteins reclassified as Q- and R-SNAREs. *PNAS* **95**, 15781-15786.
- Fasshauer, D., Bruns, D., Shen, B., Jahn, R., and Brunger, A.** (1997). A Structural Change Occurs upon Binding of Syntaxin to SNAP-25. *J. Biol. Chem.* **272**, 4582-4590.
- Felix, G., Duran, J.D., Volko, S., and Boller, T.** (1999). Plants have a sensitive perception system for the most conserved domain of bacterial flagellin. *Plant J* **18**, 265-276.
- Felle, H.H., Herrmann, A., Hanstein, S., Huckelhoven, R., and Kogel, K.-H.** (2004). Apoplastic pH Signaling in Barley Leaves Attacked by the Powdery Mildew Fungus *Blumeria graminis* f. sp. *hordei*. *Molecular Plant-Microbe Interactions* **17**, 118-123.
- Flor, H.H.** (1971). Current status of the gene-for-gene concept. *Annu Rev Phytopathol* **9**, 275-296.
- Gay, J.L., Salzberg, A., and Woods, A.M.** (1987). Dynamic experimental evidence for the plasma membrane ATPase domain hypothesis of haustorial transport and for ionic coupling of the haustorium of *Erysiphe graminis* to the host cell (*Hordeum vulgare*). *New Phytologist* **107**, 541-548.
- Geldner, N., and Jurgens, G.** (2006). Endocytosis in signalling and development. *Current Opinion in Plant Biology* **9**, 589-594.

- Gil, F., and Gay, J.L.** (1977). Ultrastructural and physiological properties of the host interfacial components of haustoria of *Erysiphe pisi* in vivo and in vitro. *Physiological Plant Pathology* **10**, 1-12.
- Gomez-Gomez, L., and Boller, T.** (2002). Flagellin perception: a paradigm for innate immunity. *Trends in Plant Science* **7**, 251-256.
- Green, J.R., Pain, N.A., Cannell, M.E., Jones, G.L., P, L.C., McCready, S., Mendgen, K., Mitchell, A.J., Callow, J.A., and O'Connell, R.** (1994). Analysis of differentiation and development of the specialized infection structures formed by biotrophic fungal plant pathogens using monoclonal antibodies. *Canadian Journal of Botany* **73(Suppl.1)**, S408-417.
- Gus-Mayer, S., Naton, B., Hahlbrock, K., and Schmelzer, E.** (1998). Local mechanical stimulation induces components of the pathogen defense response in parsley. *PNAS* **95**, 8398-8403.
- Hanson, P.I., Heuser, J.E., and Jahn, R.** (1997). Neurotransmitter release -- four years of SNARE complexes. *Current Opinion in Neurobiology* **7**, 310-315.
- He, P., Shan, L., Lin, N.-C., Martin, G.B., Kemmerling, B., Nurnberger, T., and Sheen, J.** (2006). Specific Bacterial Suppressors of MAMP Signaling Upstream of MAPKKK in Arabidopsis Innate Immunity. *Cell* **125**, 563-575.
- Heath, M.C., and Heath, I.B.** (1971). Ultrastructure of an immune and susceptible reaction of cowpea leaves to rust infection. *Physiological and Molecular Plant Pathology* **277-287**.
- Hückelhoven, R.** (2007). Cell Wall-Associated Mechanisms of Disease Resistance and Susceptibility. *Annual Review of Phytopathology* **45**.
- Jacobs, A.K., Lipka, V., Burton, R.A., Panstruga, R., Strizhov, N., Schulze-Lefert, P., and Fincher, G.B.** (2003). An Arabidopsis Callose Synthase, GSL5, Is Required for Wound and Papillary Callose Formation. *Plant Cell* **15**, 2503-2513.
- Jaenicke-Despres, V., Buckler, E.S., Smith, B.D., Gilbert, M.T.P., Cooper, A., Doebley, J., and Paabo, S.** (2003). Early Allelic Selection in Maize as Revealed by Ancient DNA. *Science* **302**, 1206-1208.
- Jahn, R., and Scheller, R.H.** (2006). SNAREs - engines for membrane fusion. *Nat Rev Mol Cell Biol* **7**, 631-643.
- Jahn, R., Lang, T., and Südhof, T.C.** (2003). Membrane Fusion. *Cell* **112**, 519-533.
- Jasinski, M., Stukkens, Y., Degand, H., Purnelle, B., Marchand-Brynaert, J., and Boutry, M.** (2001). A Plant Plasma Membrane ATP Binding Cassette-Type Transporter Is Involved in Antifungal Terpenoid Secretion. *Plant Cell* **13**, 1095-1107.
- Jia Y, Sean A. McAdams, Gregory T. Bryan, and, H.P.H., and Valent, B.** (2000). Direct interaction of resistance gene and avirulence gene products confers rice blast resistance. *The EMBO Journal* **19**, 4004-4014.
- Jones, J.D.G., and Dangl, J.L.** (2006). The plant immune system. *Nature* **444**, 323-329.

- Kalde, M., Nuhse, T.S., Findlay, K., and Peck, S.C.** (2007). The syntaxin SYP132 contributes to plant resistance against bacteria and secretion of pathogenesis-related protein 1. *Proceedings of the National Academy of Sciences* **104**, 11850-11855.
- Kim, S.-H., Lechman, E.R., Bianco, N., Menon, R., Keravala, A., Nash, J., Mi, Z., Watkins, S.C., Gambotto, A., and Robbins, P.D.** (2005). Exosomes Derived from IL-10-Treated Dendritic Cells Can Suppress Inflammation and Collagen-Induced Arthritis. *J Immunol* **174**, 6440-6448.
- Kobayashi, I., Murdoch, L.J., Kunoh, H., and R, H.A.** (1995). Cell biology of early events in the plant resistance response to infection by pathogenic fungi. *Canadian Journal of Botany* **73**, 418-425.
- Kobayashi, Y., Kobayashi, I., Funaki, Y., Fujimoto, S., Takemoto, T., and Kunoh, H.** (1997). Dynamic reorganization of microfilaments and microtubules is necessary for the expression of non-host resistance in barley coleoptile cells. *The Plant Journal* **11**, 525-537.
- Koch, E., Ebrahim-Nesbat, F., and H, H.H.** (1983). Light and Electron Microscopic Studies on the Development of Soybean Rust (*Phakopsora pachyrhizi* Syd.) in Susceptible Soybean Leaves. *Phytopathologische Zeitung* **106**, 302-320.
- Koh, S., Andre, A., Edwards, H., Ehrhardt, D., and Somerville, S.** (2005). *Arabidopsis thaliana* subcellular responses to compatible *Erysiphe cichoracearum* infections. *The Plant Journal* **44**, 516-529.
- Kováts, K., Binder, A., and Hohl, H.R.** (1991). Cytology of induced systemic resistance of tomato to *Phytophthora infestans*. *Planta* **183**, 491-496.
- Kwon, C., Panstruga, R., and Schulze-Lefert, P.** Les liaisons dangereuses: immunological synapse formation in animals and plants. *Trends in Immunology* **29**, 159-166.
- Kwon, C., Neu, C., Pajonk, S., Yun, H.S., Lipka, U., Humphry, M., Bau, S., Straus, M., Kwaaitaal, M., Rampelt, H., Kasmi, F.E., Jurgens, G., Parker, J., Panstruga, R., Lipka, V., and Schulze-Lefert, P.** (2008). Co-option of a default secretory pathway for plant immune responses. *Nature* **451**, 835-840.
- Li, X.-B.L., Zhang, Z.-R., Schluesener, H.J., and Xu, S.-Q.** (2006). Role of exosomes in immune regulation *JCMM* **10**, 374-375.
- Lipka, V., and Panstruga, R.** (2005). Dynamic cellular responses in plant-microbe interactions. *Current Opinion in Plant Biology* **8**, 625-631.
- Lipka, V., Kwon, C., and Panstruga, R.** (2007). SNARE-Ware: The Role of SNARE-Domain Proteins in Plant Biology. *Annual Review of Cell and Developmental Biology* **23**, 147-174.
- Lipka, V., Dittgen, J., Bednarek, P., Bhat, R., Wiermer, M., Stein, M., Landtag, J., Brandt, W., Rosahl, S., Scheel, D., Llorente, F., Molina, A., Parker, J., Somerville, S., and Schulze-Lefert, P.** (2005). Pre- and Postinvasion Defenses Both Contribute to Nonhost Resistance in *Arabidopsis*. *Science* **310**, 1180-1183.

- Mackey , D., Holt, B.F., Wiig , A.a., and Dangl, J.L.** (2002). RIN4 Interacts with *Pseudomonas syringae* Type III Effector Molecules and Is Required for RPM1-Mediated Resistance in *Arabidopsis*. *Cell* **108**, 743-754.
- Mangin-Peyrard M., and Pépin, R.** (1996). Encasement of *Erysiphe graminis* haustoria after treatment with bromuconazole. *Pesticide Science* **46**, 121-130.
- Martinez-Zapater, J.M., and Salinas, J.** (1998). *Arabidopsis* Protocols. Humana Press.
- Mathur, R.S., Barnett, H.L., and Lilly, V.G.** (1950). Sporulation of *Colletotrichum lindemuthianum* in culture. *Phytopathology* **40**, 104-114.
- May, A.P., Whiteheart, S.W., and Weis, W.I.** (2001). Unraveling the Mechanism of the Vesicle Transport ATPase NSF, the N-Ethylmaleimide-sensitive Factor. *J. Biol. Chem.* **276**, 21991-21994.
- Mellersh, D.G., and Heath, M.C.** (2001). Plasma Membrane-Cell Wall Adhesion Is Required for Expression of Plant Defense Responses during Fungal Penetration. *Plant Cell* **13**, 413.
- Mellersh, D.G., and Heath, M.C.** (2003). An Investigation into the Involvement of Defense Signaling Pathways in Components of the Nonhost Resistance of *Arabidopsis thaliana* to Rust Fungi Also Reveals a Model System for Studying Rust Fungal Compatibility. *Molecular Plant-Microbe Interactions* **16**, 398-404.
- Nicholson, R.L., and Hammerschmidt, R.** (1992). Phenolic Compounds and Their Role in Disease Resistance. *Annual Review of Phytopathology* **30**, 369-389.
- Nishimura, M.T., Stein, M., Hou, B.-H., Vogel, J.P., Edwards, H., and Somerville, S.C.** (2003). Loss of a Callose Synthase Results in Salicylic Acid-Dependent Disease Resistance. *Science* **301**, 969-972.
- Nomura, K., Melotto, M., and He, S.-Y.** (2005). Suppression of host defense in compatible plant-*Pseudomonas syringae* interactions. *Current Opinion in Plant Biology* **8**, 361-368.
- Nomura, K., DebRoy, S., Lee, Y.H., Pumphlin, N., Jones, J., and He, S.Y.** (2006). A Bacterial Virulence Protein Suppresses Host Innate Immunity to Cause Plant Disease. *Science* **313**, 220-223.
- Nurnberger, T., Brunner, F., Kemmerling, B., and Piater, L.** (2004). Innate immunity in plants and animals: striking similarities and obvious differences. *Immunological Reviews* **198**, 249-266.
- O'Connell, R., Herbert, C., Sreenivasaprasad, S., Khatib, M., Esquerre-Tugaye, M.-T., and Dumas, B.** (2004). A Novel *Arabidopsis*-*Colletotrichum* Pathosystem for the Molecular Dissection of Plant-Fungal Interactions. *Molecular Plant-Microbe Interactions* **17**, 272-282.
- Perfect, S.E., Hughes, H.B., O'Connell, R.J., and Green, J.R.** (1999). *Colletotrichum*: A Model Genus for Studies on Pathology and Fungal-Plant Interactions. *Fungal Genetics and Biology* **27**, 186-198.
- Robatzek, S.** (2007). Vesicle trafficking in plant immune responses. *Cellular Microbiology* **9**, 1-8.

- Ross, A.F.** (1961). Systemic acquired resistance induced by localized virus infections in plants. *Virology* **14**, 340-358.
- Sánchez-Madrid, F.a., and Angel del Pozo, M.** (1999). Leukocyte polarization in cell migration and immune interactions. *The EMBO Journal* **18**, 501-511.
- Sanderfoot, A.A., and Raikhel, N.V.** (2003). The Secretory System of Arabidopsis. *The Arabidopsis Book*, American Society of Plant Biologists.
- Sasabe, M., Toyoda, K., Shiraishi, T., Inagaki, Y., and Ichinose, Y.** (2002). cDNA cloning and characterization of tobacco ABC transporter: NtPDR1 is a novel elicitor-responsive gene. *FEBS Letters* **518**, 164-168.
- Schmelzer, E.** (2002). Cell polarization, a crucial process in fungal defence. *Trends in Plant Science* **7**, 411-415.
- Schulze-Lefert, P.** (2004). Knocking on the heaven's wall: pathogenesis of and resistance to biotrophic fungi at the cell wall. *Current Opinion in Plant Biology* **7**, 377-383.
- Sherriff, C., Whelan, M.J., Arnold, G.M., R, L.J., Brygoo, Y., and Bailey, J.** (1994). Ribosomal DNA sequence analysis reveals new species groupings in the genus *Colletotrichum*. *Experimental Mycology* **18**, 121-138.
- Shimada, C., Lipka, V., O'Connell, R., Okuno, T., Schulze-Lefert, P., and Takano, Y.** (2006). Nonhost Resistance in Arabidopsis-Colletotrichum Interactions Acts at the Cell Periphery and Requires Actin Filament Function. *MPMI* **19**, 270-279.
- Shirano, Y., Kachroo, P., Shah, J., and Klessig, D.F.** (2002). A Gain-of-Function Mutation in an Arabidopsis Toll Interleukin1 Receptor-Nucleotide Binding Site-Leucine-Rich Repeat Type R Gene Triggers Defense Responses and Results in Enhanced Disease Resistance. *Plant Cell* **14**, 3149-3162.
- Skalamera, D., and Heath, M.C.** (1998). Changes in the cytoskeleton accompanying infection-induced nuclear movements and the hypersensitive response in plant cells invaded by rust fungi. *The Plant Journal* **16**, 191-200.
- Skalamera, D., Jibodh, S., and Heath, M.C.** (1997). Callose deposition during the interaction between cowpea (*Vigna unguiculata*) and the monokaryotic stage of the cowpea rust fungus (*Uromyces vignae*). *New Phytologist* **136**, 511-524.
- Skamnioti, P., and Gurr, S.J.** (2007). Magnaporthe grisea Cutinase2 Mediates Appressorium Differentiation and Host Penetration and Is Required for Full Virulence. *Plant Cell* **19**, 2674-2689.
- Skou, J.P., Jorgensen, J.H., and Lilholt, U.** (1984). Comparative studies on callose formation in powdery mildew compatible and incompatible barley *Hordeum vulgare*. *Phytopathologische Zeitung* **109**, 147-168.
- Snyder, B.A., and Nicholson, R.L.** (1990). Synthesis of Phytoalexins in Sorghum as a Site-Specific Response to Fungal Ingress. *Science* **248**, 1637-1639.
- Söllner, T.e.a.** (1993). SNAP receptors implicated in vesicle targeting and fusion. *Nature* **362**, 318-324.

- Spencer-Phillips, P.T.N., and Gay, J.L.** (1981). Domains of ATPase in plasma membranes and transport through infected plant cells. *New Phytologist* **89**, 393-400.
- Staskawicz, B.J., Mudgett, M.B., Dangl, J.L., and Galan, J.E.** (2001). Common and Contrasting Themes of Plant and Animal Diseases. *Science* **292**, 2285-2289.
- Stein, M., Dittgen, J., Sanchez-Rodriguez, C., Hou, B.-H., Molina, A., Schulze-Lefert, P., Lipka, V., and Somerville, S.** (2006). Arabidopsis PEN3/PDR8, an ATP Binding Cassette Transporter, Contributes to Nonhost Resistance to Inappropriate Pathogens That Enter by Direct Penetration. *THE PLANT CELL* **18**, 731-746.
- Stewart, A., and Mansfield, J.W.** (1985). The composition of wall alterations and appositions (reaction material) and their role in the resistance of onion bulb scale epidermis to colonization by *Botrytis allii*. *Plant Pathology* **34**, 25-37.
- Stoorvogel, W., Kleijmeer, M.J., Geuze, H.J., and Raposo, G.** (2002). The Biogenesis and Functions of Exosomes. *Traffic* **3**, 321-330.
- Sutton, R.B., Fasshauer, D., Jahn, R., and Brunger, A.T.** (1998). Crystal structure of a SNARE complex involved in synaptic exocytosis at 2.4 Å resolution. *Nature* **395**, 347 - 353.
- Talbot, N.J.** (2004). Emerging themes in plant-pathogen interactions. *Annual Plant Reviews*; Blackwell Publishing **11**.
- Thomma, B.P.H.J., Penninckx, I.A.M.A., Cammue, B.P.A., and Broekaert, W.F.** (2001). The complexity of disease signaling in Arabidopsis. *Current Opinion in Immunology* **13**, 63-68.
- Thordal-Christensen, H., Gregersen, P.L., and Collinge, D.B.** (2000). in *Mechanisms of Resistance to Plant Disease*. Kluwer Academic Publishers., 77-100.
- Thordal-Christensen, H., Zhang, Z., Wei, Y., and Collinge, D.B.** (1997). Subcellular localization of H₂O₂ in plants. H₂O₂ accumulation in papillae and hypersensitive response during the barley-powdery mildew interaction. *Plant J* **11**, 1187-1194.
- Uemura, T., Ueda, T., Ohniwa, R., Nakano A, T.K., and Sato, M.** (2004). Systematic analysis of SNARE molecules in Arabidopsis: dissection of the post-Golgi network in plant cells. *Cell Struct Funct.* **29**, 49-65.
- van Niel, G., Porto-Carreiro, I., Simoes, S., and Raposo, G.** (2006). Exosomes: A Common Pathway for a Specialized Function. *J Biochem (Tokyo)* **140**, 13-21.
- Vogel, J., and Somerville, S.** (2000). Isolation and characterization of powdery mildew-resistant Arabidopsis mutants. *PNAS* **97**, 1897-1902.
- Whisson, S.C., Boevink, P.C., Moleleki, L., Avrova, A.O., Morales, J.G., Gilroy, E.M., Armstrong, M.R., Grouffaud, S., van West, P., Chapman, S., Hein, I., Toth, I.K., Pritchard, L., and Birch, P.R.J.** (2007). A translocation signal for delivery of oomycete effector proteins into host plant cells. *Nature* **450**, 115-118.

- Zeidler, D., Zahringer, U., Gerber, I., Dubery, I., Hartung, T., Bors, W., Hutzler, P., and Durner, J.** (2004). Innate immunity in *Arabidopsis thaliana*: Lipopolysaccharides activate nitric oxide synthase (NOS) and induce defense genes. *Proceedings of the National Academy of Sciences* **101**, 15811-15816.
- Zeyen, R.J., and Bushnell, W.R.** (1979). Papilla response of barley epidermal cells caused by *Erysiphe graminis*: rate and method of deposition determined by microcinematography and transmission electron microscopy. *Can J Botany* **57**, 898-913.
- Zipfel, C., and Felix, G.** (2005). Plants and animals: a different taste for microbes? *Current Opinion in Plant Biology* **8**, 353-360.

References

V Acknowledgements

Diese Arbeit wurde am Max-Planck-Institut für Züchtungsforschung in der Arbeitsgruppe von Prof. Dr. Paul Schulze-Lefert angefertigt. Ich möchte mich bei allen bedanken, die mich während der Anfertigung dieser Doktorarbeit unterstützt haben, insbesondere bei:

Paul Schulze-Lefert für die Möglichkeit zur Promotion in seiner Gruppe, für intensive und motivierende Gespräche und für die Freiheiten die er mir gelassen hat.

Prof. Dr. Martin Hülskamp für die Übernahme des Korreferats und Prof. Dr. Ulf Ingo Flüge für die Übernahme des Prüfungsvorsitzes.

Richard O'Connell for his supervision, for very helpful discussions and for provided pathogen species and plant lines.

Katharina Göllner für die gute Kooperation mit dem Rostpilz *Phakopsora pachyrhizi*.

Kurt Stüber für die große Hilfe bei der Script Entwicklung und bei jeglichen Software technischen Schwierigkeiten.

Elmon Schmelzer für all seine Hilfe mit diversen Mikroskopen und dafür, dass er immer ein offenes Ohr hatte.

Olavi Ollikainen, Kurt Herrenknecht und Norbert Garbow für eine fruchtbare Kooperation mit Perkin Elmer (ehemals Evotec Technologies).

Georg Mancel für seine sehr große und konstruktive Hilfe bei der Stempelentwicklung für die Hochdurchsatz Mikroskopie.

Special thanks to Cristina, Corina, Chiara, Aurelie, Doris, Imre and Mark for very, very fruitful discussions and proof-reading of this thesis. Johannes and Matt for help with editing and formatting.

Einen lieben Dank an all meine Kollegen für die super nette Arbeitsatmosphäre und die schönen Aktivitäten außerhalb des Labores; besonders an die Panstruga/PSL crew: Anja, Sandra, Shen, Nana, Yuske, Ralph, Matt, Chian, XinLi, Chiara, Sarah, Cristina, HyeSup, Mark K., Mark H., Armin, Mario, Martha, Mariola, Pawel, Nico und Phillip.

Allen Kollegen im gemischten Kombrink-Somssich-PSL Labor für jegliche Hilfe, besonders bei Rainer und Elke.

Ein großes Dankeschön geht an Simone, für all die aufmunternden Worte, die sehr hilfreichen Diskussionen und so mach eine Laufrunde.

Acknowledgements

Ein riesen Dank geht an die Kontainer Besatzung Doris, Aurelie, Ana, Armin, Takaki, Enrico, Simone und Stefan für die Rücksichtnahme, die vielen aufmunternden Worte und die angenehme Atmosphäre.

Super lieben Dank an Doris: M... wir kommen!!!

Ein besonders großes Dankeschön an Joachim für jegliche Unterstützung, Rücksichtnahme und Geduld. Zu guter Letzt möchte ich mich bei meiner gesamten Familie bedanken, besonders bei Mum für die große Unterstützung und die aufmunternden Gespräche.

VI Erklärung

„Ich versichere, dass ich die von mir vorgelegte Dissertation selbstständig angefertigt, die benutzten Quellen und Hilfsmittel vollständig angegeben und die Stellen der Arbeit – einschließlich Tabellen, Karten und Abbildungen –, die anderen Werken im Wortlaut oder dem Sinn nach entnommen sind, in jedem Einzelfall als Entlehnung kenntlich gemacht habe; dass diese Dissertation noch keiner anderen Fakultät oder Universität zur Prüfung vorgelegen hat; dass sie – abgesehen von unten angegebenen Teilpublikationen – noch nicht veröffentlicht worden ist sowie, dass ich eine solche Veröffentlichung vor Abschluss des Promotionsverfahrens nicht vornehmen werde. Die Bestimmungen dieser Promotionsordnung sind mir bekannt. Die von mir vorgelegte Dissertation ist von Prof. Dr. Paul Schulze-Lefert betreut worden.“

Köln, im April 2008

Dorit Meyer

Dorit Meyer

Curriculum Vitae

Angaben zur Person

Geburtsdatum und -ort	15. März 1977, Emsdetten
Staatsangehörigkeit	Deutsch
Familienstand	ledig

Ausbildung

Seit 06/2004	Dissertation am Max-Planck Institut für Züchtungsforschung in Köln, Abteilung Molekulare Phytopathologie unter der Leitung von Prof. Dr. Paul Schulze-Lefert Titel: "Molecular characterization of pathogen triggered cell polarity. "
01/2003 – 01/2004	Diplomarbeit an der Westfälischen Wilhelms-Universität Münster, Institut für Biochemie und Biotechnologie, unter der Leitung von Prof. Dr. Bruno Moerschbacher Titel: "Molekularbiologische Untersuchung zur Genexpression in elicitierten Weizenpflanzen."
04/1997 – 12/2003	Diplomstudium an der Westfälischen Wilhelms-Universität Münster
08/ 1996	Abitur, Arnold-Jansen-Gymnasium, Neuenkirchen

Köln, 22. April 2007, _____